SAPIENZA
UNIVERSITÀ DI ROMA

Development and applications of an innovative wearable system based on time-of-flight technology for the measurement of the human movement

Department of Computer, Control, and Management Engineering 'Antonio Ruberti'

Research Doctorate in Automatic Control, **Bioengineering** and Operation Research (ABRO) – XXXI Cycle

Candidate:

Stefano BERTULETTI

Student ID: 1700043

Thesis Supervisor:

Prof. Ugo Della Croce

Co-Supervisor:

Prof. Andrea Cereatti

31/10/2018

Thesis defended on 26/02/2019
in front of a Board of Examiners composed by:

Prof. Giancarlo Bigi (chairman)

Prof. Giovanni Sparacino

Prof. Giovanni Ulivi

Development and applications of an innovative wearable system based on time-of-flight technology for the measurement of the human movement
Ph.D. thesis. Sapienza – University of Rome

This thesis has been typeset by LaTeX and the Sapthesis class.

Author's email: stefano.bertuletti@uniroma1.it

Abstract

The analysis of the human movement is the subject of many research projects. Recently, thanks to the advancement in the development of high performance and low-power electronic components, wearable sensors have given rise to devices and techniques which allow an objective evaluation of different human movement quantities both inside and outside the laboratory setting (e.g. during activities of daily living).

The objectives of the research conducted and reported in this Ph.D. thesis regard the devise, development, validation and applications of an innovative wearable system, named SWING, for the human movement monitoring and analysis.

The SWING system is the result of a design aimed at providing a wireless system-on-board processing capabilities integrating a magneto-inertial measurement unit and a Bluetooth module (main board) and up to three infrared time-of-flight distance sensors (satellite boards). It was specifically devised to take advantage of the positive points of magneto-inertial measurement units, which are capable of measuring the human movement for a long period of time and also during daily life activities with a good level of accuracy, but also to overcome some of their limitations (e.g. drift, ferromagnetic interferences, etc.). Moreover, the SWING system allow the direct measurement of quantities, such as the inter-foot distance and the step width, that magneto-inertial measurement units can only obtained indirectly (high estimation errors).

The advantages of using the infrared time-of-flight technology over other technologies, such as ultrasound and light intensity infrared which have been already investigated in the literature, are that the same or higher performance can be obtained with a simpler experimental setup (only one foot instrumented) and with a higher robustness to the changing of the experimental/environmental conditions (e.g. colour of the shoe, ambient light).

First, a thorough testing protocol for evaluating the infrared time-of-flight distance sensor performances was performed under experimental conditions resembling those encountered during gait.

Second, the SWING system was validated for the inter-foot distance estimation and step detection during walk on sixteen healthy subjects.

Third, the SWING system was tested and validated on a group of subjects characterised by highly abnormal gait patterns (e.g. low speed walks, foot dragging walks, use of walking aids) while performing a six-minute walking test.

Finally, by exploiting the Bluetooth low energy as an alternative solution for indoor-localisation and proximity sensing, a thorough characterisation of the received signal strength indicator and distance relationship under controlled conditions was provided.

The findings of this Ph.D. thesis lead to the conclusion that the SWING system and the proposed methods could be reliably applied to both normal and abnormal gaits obtaining a high level of accuracy while maintaining a very simple experimental setup (only one lower limb instrumented).

Indeed, the mean absolute errors obtained for the measurement of the inter-foot distance on healthy subjects were in the range of 9.3–12.4 mm.

The results of the validation of the SWING system, as step counter, showed an accuracy of 100 % on healthy and between 94.6 % and 98 % on pathological subjects (i.e. multiple sclerosis).

Lastly, the findings of the characterisation of the Bluetooth low energy technology for the inter-distance estimation showed an average percentage error of 25.7 % (0.4 m). Therefore, Bluetooth low energy can be a solution for indoor positioning applications, but cannot be used for proximity sensing applications which require very high accuracy (resolution down to 0.1 m).

Acknowledgments

I would like to express my sincere gratitude to my supervisor Prof. Ugo Della Croce and my co-supervisor Prof. Andrea Cereatti for all teachings, continuous support and constructive criticism during my Ph.D. experience.

I want also to thank Prof. Claudia Mazzà and people from the INSIGNEO Institute for all the support, kindness and friendship they showed me in Sheffield.

I am also deeply grateful to my loving family for encouraging me to start the doctorate and for supporting me.

I want also to thank my lab mates and my friends in Bergamo, Sassari, Turin and Sheffield.

List of Publications and Patents

International Peer-Reviewed Journals

- S. Bertuletti, U. Della Croce, and A. Cereatti, "A wearable solution for accurate step detection based on the direct measurement of the inter-foot distance", *Journal of Biomechanics*, vol. 84, pp. 274 –277, 2019, ISSN: 0021-9290. DOI: https://doi.org/10.1016/j.jbiomech.2018.12.039. [Online]. Available: http://www.sciencedirect.com/science/article/pii/S0021929018309382.

- S. Bertuletti, A. Cereatti, D. Comotti, M. Caldara, and U. Della Croce, "Static and dynamic accuracy of an innovative miniaturized wearable platform for short range distance measurements for human movement applications", *Sensors*, vol. 17, no. 7, 2017, ISSN: 1424–8220. DOI: 10.3390/s17071492. [Online]. Available: http://www.mdpi.com/1424-8220/17/7/1492.

Conference Proceedings published on International Journals

- S. Bertuletti, F. Salis, A. Cereatti, L. Angelini, E. Buckley, K. Nair, C. Mazzà, and U. Della Croce, "Inter-leg distance measurement as a tool for accurate step counting in patients with multiple sclerosis", *IEEE Engineering in Medicine and Biology Magazine (under review)*, 2019.

- S. Bertuletti, A. Cereatti, and U. Della Croce, "Development of a novel wearable system for real-time measurement of the inter-foot distance during gait", *Gait & Posture*, vol. 57, pp. 6–7, 2017, SIAMOC, ISSN: 0966–6362. DOI: 10.1016/j.gaitpost.2017.07.054. [Online]. Available: http://www.sciencedirect.com/science/article/pii/S0966636217307658.

- S. Bertuletti, A. Cereatti, M. Caldara, and U. Della Croce, "A proximity

sensor for the measurement of the inter-foot distance in static and dynamic tasks", *Gait & Posture*, vol. 49, S15, 2016, SIAMOC, ISSN: 0966–6362. DOI: 10.1016/j.gaitpost.2016.07.044. [Online]. Available: http://www.sciencedirect.com/science/article/pii/S0966636216301813.

- S. Bertuletti, A. Cereatti, M. Caldara, M. Galizzi, and U. Della Croce, "Indoor distance estimated from Bluetooth low energy signal strength: Comparison of regression models", in *Proceedings of IEEE Sensors Applications Symposium (SAS)*, Apr. 2016, pp. 1–5. DOI: 10.1109/SAS.2016.7479899.

National Conference Proceedings

- S. Bertuletti, U. Della Croce, and A. Cereatti, "A wearable prototype device for direct bilateral step detection by instrumenting a single foot", in *19th Proceedings of SIAMOC*, 2018.
- S. Bertuletti, A. Cereatti, and U. Della Croce, "Inter-foot distance measurement in healthy adults during gait using a wearable prototype device: Validation on straight walking and turning for different distance sensor locations", in *19th Proceedings of SIAMOC*, 2018.
- S. Bertuletti, A. Cereatti, and U. Della Croce, "A wearable system based on Time-of-Flight technology for direct derivation of step number and step width on healthy gait", in *Proceedings of GNB*, 2018.
- S. Bertuletti, A. Cereatti, and U. Della Croce, "Detection of the turn switch during alpine skiing using a novel wearable system: A preliminary investigation", in *18th Proceedings of SIAMOC*, 2017.
- S. Bertuletti, A. Cereatti, and U. Della Croce, "Measurement of the inter-foot distance using a Time-of-Flight proximity sensor: Preliminary evaluation during leg oscillation exercises", in *Proceedings of GNB*, 2016.
- S. Bertuletti, A. Cereatti, M. Caldara, M. Galizzi, D. Comotti, and U. Della Croce, "Fall detection localization using Bluetooth low energy devices: A preliminary investigation", in *16th Proceedings of SIAMOC*, 2015.

International Conference Proceedings

- S. Bertuletti, A. Cereatti, and U. Della Croce, "A wearable system for step width measurement and step detection based on Time-of-Flight technology:

Preliminary validation on healthy subjects", in *Proceedings of 3-D Analysis of Human Movement*, 2018.

- S. Bertuletti, V. Camomilla, A. Cereatti, M. Caldara, M. Galizzi, and U. Della Croce, "Comparison of regression models for interdistance estimate between two BLE devices based on RSSI", in *Proceedings of 3-D Analysis of Human Movement*, 2016.

Patents

- A. Cereatti, S. Bertuletti, M. Caldara, and U. Della Croce, "Sistema per l'analisi dell'attività motoria di una persona e relativo metodo", pat. 102017000003986, 2017, Italy (pending).

Contents

List of Figures

List of Tables

Glossary

(M-)IMU (magneto-)inertial measurement unit. 55, 56

6MWT six-minute walking test. 76, 79, 83

AoI angle of incidence. 41–48

BLE Bluetooth low energy. 20, 85–88, 90, 91, 93, 95, 96, 101–103

BoS base of support. 56, 63, 71, 101

CT computer tablet. 87, 88

DiSC distance sensor step counter. 75, 76, 79–84, 102, 103

DS distance sensor. 55–60, 62, 63, 65–72, 75–77, 79, 81–84, 96, 103, 115, 116

E grand error. 45–47, 60, 80

e error. 46, 47, 60, 80, 82

$E_{\%}$ grand mean percentage error. 75, 82, 83

EDSS expanded disability status scale. 75, 76, 78, 81–83

FSM finite state machine. 29–31

GPS global positioning system. 4, 85

GUI graphical user interface. 29, 30, 32–34

I2C inter-integrated circuit. 17, 23, 26

IC integrated circuit. 15, 21, 22, 25, 29

IDE integrated development environment. 29, 32

IFD inter-foot distance. 56, 57, 59–63, 101

IFOD inter-foot distance. 65, 66, 68–72, 102, 103

IMU inertial measurement unit. 3, 13, 65, 66, 71, 76, 83

IN-step instrumented step. 67–71, 79–82

IP intersection point. 59, 60

IR infrared radiation. 40, 48, 56, 57, 72

IR-LI light intensity infrared. 56, 62, 63, 96

MAE grand mean absolute error. 45–48, 60, 62, 80, 91, 95

mae mean absolute error. 46, 60, 80

MAE% grand mean absolute percentage error. 45–47, 60, 80–83, 91, 95

mae% mean absolute percentage error. 46, 60, 80

MIMU magneto-inertial measurement unit. 1, 3, 13, 39, 42, 55, 59, 86–93, 96, 101, 115, 116

MS multiple sclerosis. 73–78, 83, 84

NIN-step non-instrumented step. 67–71, 79–82

ODR output data rate. 48, 56

PCB printed circuit board. 17, 20, 24

RSSI received signal strength indicator. 2, 4, 85–95, 102, 103

RTC real-time clock. 17, 18, 30, 32

SD grand standard deviation. 45–47, 60

sd standard deviation. 46, 60

SP system stereo-photogrammetric system. 57–60, 68

SPI serial peripheral interface. 17–19, 21

SW step width. 3, 41, 48, 56, 63, 101

ToF time-of-flight. 1, 13, 15, 19, 22, 23, 25–28, 30, 32, 33, 36–48, 101, 102

UART universal asynchronous receiver-transmitter. 18, 20

US ultrasound. 56, 62, 63, 96

USART universal synchronous and asynchronous receiver-transmitter. 17, 20

USB universal serial bus. 18, 21, 25, 31

1 Introduction and Background

Objectives and Outline of the thesis

The objectives of the research conducted and reported in this Ph.D. thesis regard the devise, development, validation and applications of an innovative wearable system for the human movement monitoring and analysis. This system must allow the measurement of accelerations, angular velocities and local magnetic field, but also it has to be able to detect the presence of nearby objects without any physical contact and to provide position estimates in an indoor environment due to the fact that 60 % of daily time is spent indoor. Therefore, the innovative system will have to integrate in the same system a magneto-inertial measurement unit (MIMU), at least one infrared time-of-flight (ToF) distance sensor and a Bluetooth module.

The thesis is organised as follows:

Introduction and Background reports the objectives of this thesis and its structure, and introduces the topic through the presentation of the technologies used for the analysis and monitoring of the human movement.

Part I - The SWING system presents the development of an innovative wearable system, named SWING, "from the idea to the product". Starting from the requirements that the system must comply and the selection of most suitable and performing electronic components. The circuit diagram and the printed circuit board were designed and described in Chapter 2. A description of the implemented firmware and the developed graphical user interface was provided in Chapter 3. As the system has to be worn, the enclosures of the SWING system and the infrared ToF distance sensors were designed and printed using a 3D printer. Furthermore, to make the SWING system easy to use and wear and to facilitate its calibration, a support for the SWING^{2DS} and for the calibration of the infrared ToF distance sensors were also designed and printed (Chapter 4). Finally, in Chapter 5, the

characterisation of the infrared ToF distance sensor in both static and dynamic conditions resembling those encountered when analysing human movement was provided.

Part II - Applications presents the applications in which the SWING system was tested and validated. The applications were grouped by two categories: *i*) gait analysis/clinical gait analysis (Chapter 6, 7 and 8): the SWING system was validated against a stereophotogrammetric system or video recordings to provide information about the inter-foot distance while walking on healthy subjects and step detection on both healthy and pathological subjects (multiple sclerosis patients); *ii*) indoor positioning (Chapter 9): the Bluetooth low energy module, which could be embedded in the SWING system, was used to provide distance information based on the received signal strength indicator (RSSI) reads from another SWING system (beacon node).

General results, Main contributions, and Future works summarises the achievements of the research performed during the Ph.D. program and provides an outlook for future research.

Technologies for human movement monitoring and analysis

The monitoring and analysis of the human movement aim at providing objective quantities of the musculo-skeletal system (e.g. kinetic, kinematic and muscles forces) during the execution of a motor task.

Traditionally, the measurement of these quantities is conducted under controlled conditions in laboratories by means of technologies such as cameras (e.g. motion capture systems [16]), force plates [17] and instrumented walkways [18]. These technologies provides measurements that are very accurate, highly repeatable and reproducible [19] and, since these systems are directly connected to the power source, do not have power consumption restrictions. However, their use is restricted to laboratory settings thus not allowing the assessment of the human motion during daily-life activities. Furthermore, they are costly and the measurement process must be carried out by specialised personnel.

Over the past decades, thanks to the advancement in the development of miniaturised, less power consuming and more performing electronic components, wearable technologies have gained popularity in the analysis and monitoring of the human movement [20]. Wearable technologies make it possible to analyse, monitor and

capture a wide range of information of the human movement also outside the laboratory and during activities of daily living [21]. They can provide a wide range of measurements of the human motion and related quantities: joint kinematics [22], forces and moments [23], biosignals [24] and locating, tracking and positioning [25]. However, some factors such as performance, limitations of their use, noise, interference of external factors present in the environment and power consumption restrictions due to the limited battery duration, must be taken into account.

Among wearable technologies aimed at measuring the human movement inertial measurement unit (IMU) is the most popular. IMU consist of a tri-axial accelerometer and a tri-axial gyroscope capable of measuring linear accelerations and angular velocities in the 3D components, respectively. An assembly of an IMU and a tri-axial magnetometer, which measures the local magnetic field in the 3D components, is generally referred to as a MIMU. MIMUs are tiny, light-weight, can provide both real-time data streaming and data logging depending on the application and can be connected each other wirelessly to create a synchronised network. Due to their characteristics and depending on the parameter of interest, MIMUs can be easily attached to one or more body segments (e.g. head, wrist, pelvis, shank, ankle, foot, etc.) and can be used in a large variety of applications such as clinical and health monitoring [26], sports science [27] and entertainment [28].

Although they are increasingly used, a typical problem that affect the computation and that must be taken into account refers to the single and double integration of linear accelerations and angular velocities which are both affected by noise (drift). Another problem is related to the gravity that has to be decomposed in the three components according to the IMU orientation (local reference system) and then removed before the integration. Mostly in indoor environments, the biggest limitation referred to the magnetometer is related to additional magnetic fields which can cause interferences. Interferences can be caused by ferromagnetic material or equipment nearby the magnetometer ("soft iron" and "hard iron" interferences).

To reduce/eliminate the above-mentioned problems and limitations and the need to measure new quantities which cannot be measured by MIMU such as spatial information (e.g. step width (SW) during walking, etc.) and position (e.g. human navigation) have led to the integration of MIMU with other technologies.

Video cameras and distance sensors are different technologies capable of providing spatial information. In the last few years, the technology advance of electronic devices allowed to develop always smaller and smaller video cameras that are specifically designed to be worn on the human body, for example on the chest or that can be embedded in clothes or accessories such as eyeglasses [29]. Video cameras provide a very large quantity of data. However, their use for monitoring

and to analyse the human motion is limited to the ability to develop algorithms capable of extrapolating information from the analysis of image frames which require high computational capacity and intelligence [30]. Proximity sensors are electronic devices able to detect the presence of nearby objects without any physical contact. They can be implemented based on different technologies: ultrasound, photoelectronic, inductive, capacitive and magnetic. Proximity sensors can provide several information based on their location on the human body. For instance, they can be used for obstacle avoidance [31] or in addition, when positioned on the feet, they can measure the relative foot positions [32] and foot clearance [33].

The most common technology for the estimation of the position is represented by the global positioning system (GPS). GPS is a satellite-based radionavigation system owned by the United States of America [34]. GPS provides geolocation of a GPS receiver where there is an unobstructed line of sight to four or more GPS satellites. Nowadays, since GPS is already embedded in the common wearable technologies (e.g. smartphone, smartwatch, etc.), it is very widespread and used for several applications (e.g. navigation, sports, etc.). Main limitations of GPS are due to the low position accuracy (about 5 m), low sampling rate (about 1 Hz) and obstacles such as buildings block that can affect the power of the GPS signal and therefore its accuracy. As a result, GPS cannot be used in indoor environments thus other technologies solutions must be undertaken.

An alternative solution can be the use of barometric pressure sensors which are devices that measure the atmospheric pressure. Generally, barometric pressure sensors consist of a capacitve or piezoelectric sensing element which detects absolute pressure by measuring the changes in the capacitance or thickness of the sensing element depending on the atmospheric pressure. They are used especially for indoor positioning to calculate altitude or to determine floor level in a building (z-axis) [35]. However, they cannot provide information about the position in the x-y plane.

A further and promising alternative solution for the position estimation could be provided by Bluetooth. Bluetooth is a short-range wireless communication technology that allows devices to transmit data wirelessly over a short distance [36]. Even if Bluetooth is mainly used for data transmission, it can be also used for localization in an indoor environment. Upon comparing the received signal values from Bluetooth devices, positioned in known locations of the environment (beacons), is possible to get the first, rough position estimate through the RSSI. RSSI represents a value of the power of a received radio signal. The longer the distance is, the lower the RSSI signal is. By integrating the RSSI signal from at least three different beacons is possible to determine the position by implementing trilateration algorithms [37].

Part I

The SWING system

This part will illustrate the design, development, realisation and characterisation of a novel wearable system, named SWING, aimed at monitoring and analyse the human movement.

The novel idea of the SWING system, with respect to those available on the market, is related to the integration of magneto-inertial data, Bluetooth data and distance data into a single system. At present time, MIMUs (comprising also Bluetooth) and distance sensors are sold singly, thus the quantities provided by these three technologies are not yet integrated. In the research field only few works presented the integration of MIMUs and distance sensors. Trojaniello et al. [38] used a system integrating an IMU and an infrared distance sensor. In this work, the system was used to measure the inter-foot distance during static and dynamic conditions (leg oscillation and walking) on a single healthy subject while wearing the system on a foot and a white target on the contralateral one. Weenk et al. [32] proposed a system which integrates an inertial sensor and an ultrasound transducer on each foot for the measurement of the relative foot position (e.g. step length, stride width) on three healthy adults. Duong et al. [39] presented a methodology to improve the accuracy of foot pose estimation by attaching two infrared ToF distance sensors pointing the ground on a shoe in addition to an IMU.

The main advantage of the development of a new system from scratch (white box) is that the design and implementation of the hardware and the software (e.g. algorithms) are defined and known to the developer. Not necessarily, this information are known to the end user of a commercial devise (black box). Furthermore, this integration aimed at *i*) measuring quantities that cannot be measured by MIMUs and Bluetooth alone; *ii*) directly measuring quantities (i.e. distances) instead of obtaining them indirectly by double integrating accelerations and *iii*) improving the accuracy of algorithms based only on magneto-inertial data, Bluetooth data or distance data.

2 Hardware

2.1 Requirements

The SWING system was designed to comply the following specific requirements: *i*) it has to be tiny and light-weight in order to be easily worn by a person; *ii*) it has to integrate an accelerometer, a gyroscope and a magnetometer; *iii*) it has to integrate up to three infrared ToF distance sensors; *iv*) the onboard microcontroller has to offer enough power and processing capabilities to host intensive algorithms (e.g. online Kalman Filter) and user-define application code; *v*) it has to provide real-time data streaming (i.e. integrating a Bluetooth module) and data logging (i.e. integrating a flash memory); *vi*) it has to be powered by a rechargeable battery and finally *vii*) it has to provide at least 8 h of battery life.

2.2 Block scheme

An overview of the SWING system is reported in Figure 2.1. It is composed of two different types of units: the main board and the satellite board. The main board integrates all the components aimed at processing, sensing, storing data and connecting to external devices and it integrates all integrated circuits (ICs) dedicated to the power management and I/O, while the satellite board integrates the infrared ToF distance sensor. Up to three satellite boards can be simultaneously connected to the main board. A further description of these two boards is provided in section *Design*.

The infrared ToF distance sensor was integrated in a different board in order to make the SWING system more versatile to the customer needs and to be used in a wide range of applications. This hardware configuration enables the customer to position each satellite board in a different place with respect to the other satellite board and to the main board.

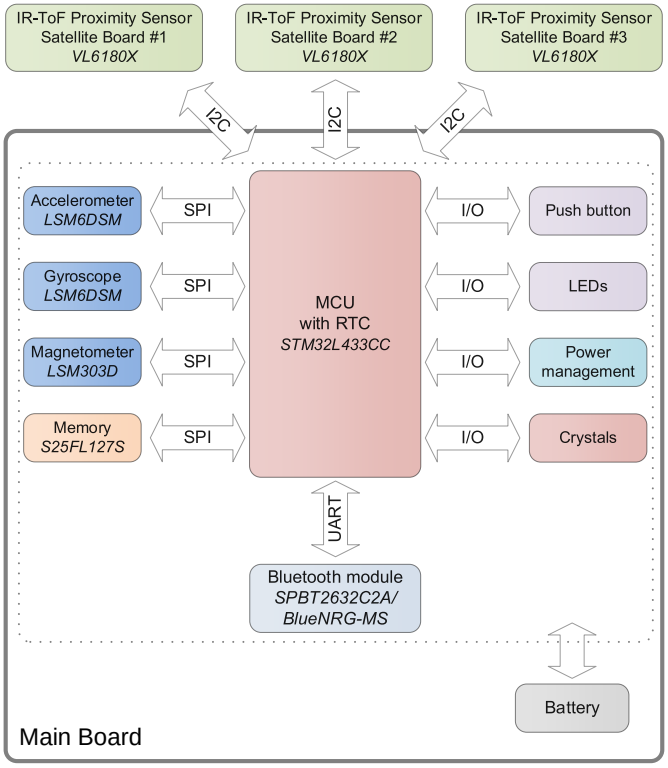

Figure 2.1 – Block scheme of the SWING system.

2.3 Configurations

The SWING system has been designed to be used in four different hardware configurations depending on the requirements of the application in which it has to be used. In Table 2.1, for each configuration, are reported all the combinations of active sensors which are automatically detected by the system by plugging in/out the satellite boards.

Table 2.1 – Active sensors combinations for each SWING system configuration. The • symbol denotes that the specific sensor is active.

Configuration	Active sensors			
	MIMU	Sat. Board #1	Sat. Board #2	Sat. Board #3
SWING	•			
SWING^{DS}	•	•		
	•		•	
	•			•
SWING^{2DS}	•	•	•	
	•	•		•
	•		•	•
SWING^{3DS}	•	•	•	•

2.4 Design

The circuit diagram of the SWING system was designed with the Autodesk EAGLE software. Autodesk EAGLE is a freeware electronic design automation software enabling printed circuit board (PCB) designers to seamlessly connect schematic diagrams, component placement, PCB routing and comprehensive library content.

2.4.1 Main board

Schematics

Processing

The core processing unit of the SWING system is the STM32L433CC (Figure 2.2) [40]. The STM32L433CC is an ultra-low-power microcontroller based on the high-performance ARM® Cortex®-M4 32-bit core operating at a frequency of up to 80 MHz. The Cortex-M4 core features a floating point unit single precision which supports all ARM single-precision data processing instructions and data types. It also implements a full set of digital signal processor instructions and a memory protection unit which enhances application security. The STM32L433CC microcontroller embeds high-speed memories (256 kB of flash memory and 64 kB of static random access memory), a low-power real-time clock (RTC) and an extensive range of enhanced I/Os and peripherals. It also features standard and advanced communication interfaces, among which: three inter-integrated circuits (I2Cs), three serial peripheral interfaces (SPIs), three universal synchronous and asynchronous

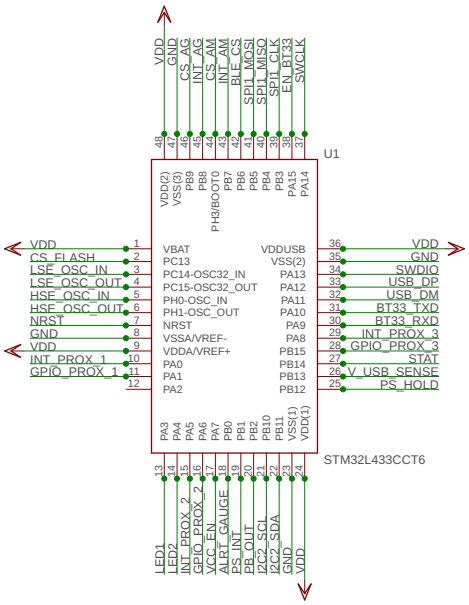

Figure 2.2 – Microcontroller.

receiver-transmitters (USARTs), one low-power universal asynchronous receiver-transmitter (UART) and a universal serial bus (USB) full-speed device crystal less. A comprehensive set of power-saving modes, such as stop mode, standby mode and shutdown mode, allows the design of low-power applications.

Instead of using the internal oscillator, a more stable clock source has been obtained by connecting an external crystal oscillator. In particular, the 8 MHz SMD crystal oscillator with a frequency tolerance of ±0.5 % was used [41] (Figure 2.3).

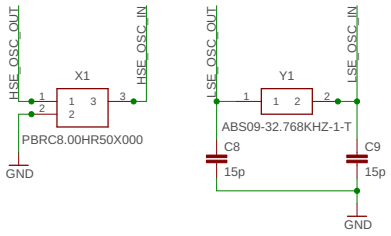

Figure 2.3 – High speed external oscillator (8 MHz) and low speed external oscillator (32.768 kHz).

The system clock used by the embedded RTC is generated internally by the STM32L433CC. However, in order to achieve a more accurate and precise timestamp, an external crystal is connected to the microcontroller (SMD crystal provided by Abracon [42]) (Figure 2.3). This component generates a clock signal of 32.768 kHz with a frequency tolerance of ±10 ppm (parts per million).

Sensing

The SWING system sensing capabilities are provided by two modules connected via SPI to the STM32L433CC microcontroller (Figure 2.4).

The first one is the LSM6DSM (STMicroelectronics) [43], which is a system-in-package featuring a 3D digital accelerometer and a 3D digital gyroscope performing at 0.65 mA in high-performance mode and enabling always-on low-power features

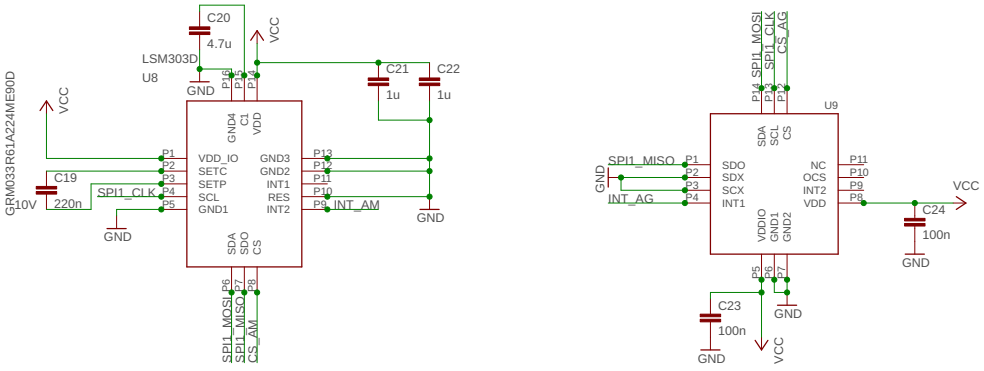

Figure 2.4 – Accelerometer, gyroscope and magnetometer.

for an optimal motion experience. The LSM6DSM has a full-scale acceleration range of $\pm 2/\pm 4/\pm 8/\pm 16\,g$ and an angular rate range of $\pm 125/\pm 250/\pm 500/\pm 1000/\pm 2000\,°/s$.

The second one is the LSM303D (STMicroelectronics) [44] which is a system-in-package featuring a 3D digital linear acceleration sensor and a 3D digital magnetic sensor. The LSM303D has linear acceleration full scales of $\pm 2/\pm 4/\pm 6/\pm 8/\pm 16\,g$ and a magnetic field full scale of $\pm 2/\pm 4/\pm 8/\pm 12$ gauss. The system can also be configured to generate an interrupt signal for free-fall, motion detection and magnetic field detection. Magnetic and accelerometer blocks can be enabled or put into power-down mode separately.

Storage

The Cypress S25FL127S [45] is a 16 MB flash non-volatile memory that is connected to the STM32L433CC microcontroller using SPI. The S25FL127S memory introduces new features to SPI category memories such as extended address for access to higher memory density, autoboot for simpler access to boot code following power up, multiple options for initial read latency (number of dummy cycles) for faster initial access time or higher clock rate read commands and advanced sector protection for individually controlling the protection of each sector. Data can be read at 6 MB/s (normal read speed) and written at 1.5 MB/s.

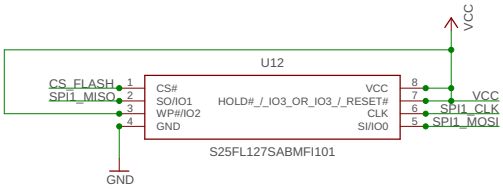

Figure 2.5 – 16 MB flash memory.

Connectivity

Two different type of data can be exchange between the SWING system and an external device. The first one refers to raw data provided by the sensors onboard the system (such as accelerations, angular velocities, magnitude of local magnetic fields, distances) or computed data (such as quaternions and eulero angles), while the second one concerns to all commands required for the configuration of the SWING system (such as the selection of the recording mode: stream or log, the selection of the output data rate, etc.) and the sensors (calibration of the accelerometer, gyroscope, magnetometer and infrared ToF distance sensors).

The first technology aimed at exchanging both type of data (raw, computed and

configuration data) is represented by the use of a Bluetooth module (Figure 2.6). The pinout of this module was specifically designed to be compliant with both a Bluetooth v3.0 and a Bluetooth low energy. The main differences between these solutions concern the power consumption and the data rate. Bluetooth v3.0 has a higher data rate and higher power consumption with respect to the Bluetooth low energy (BLE). Therefore, depending on the application, one module fits better than the other. In particular, in high data rate streaming applications is better to use the Bluetooth v3.0, while for those focused on long time monitoring with periodically data transmission the best solution is given by the Bluetooth low energy. Both Bluetooth modules are provided by STMicroelectronics: SPBT2632C2A module (Bluetooth 3.0) [46] and BlueNRG-MS (Bluetooth low energy) [47].

The SPBT2632C2A is an easy to use Bluetooth module, compliant with Bluetooth v3.0. The module is one of the smallest form factor available on the market which provides a complete radio frequency platform. It is designed for maximum performance in a minimal space including fast speed UART and seven general purpose I/O lines, several serial interface options, and up to 560 kbps transmission speed with SPP service active, 250 kbps with iAP1 service active. The SPBT2632C2A is a surface mount PCB module that provides fully embedded and ready to use Bluetooth wireless technology. In addition, the reprogrammable flash memory contains embedded firmware for serial cable replacement using the Bluetooth SPP profile. The module communicates with the STM32L433CC microcontroller using the USART protocol.

The BlueNRG-MS is a low-power Bluetooth low energy single-mode network processor compliant with Bluetooth specification v4.1. The BlueNRG-MS supports multiple roles simultaneously (master and slave) and can act at the same time as Bluetooth smart sensor and hub device. The maximum peak current is only 10 mA at 1 dBm of output power. Ultra low-power sleep modes and very short transition times between operating modes allow very low average current consumption, resulting

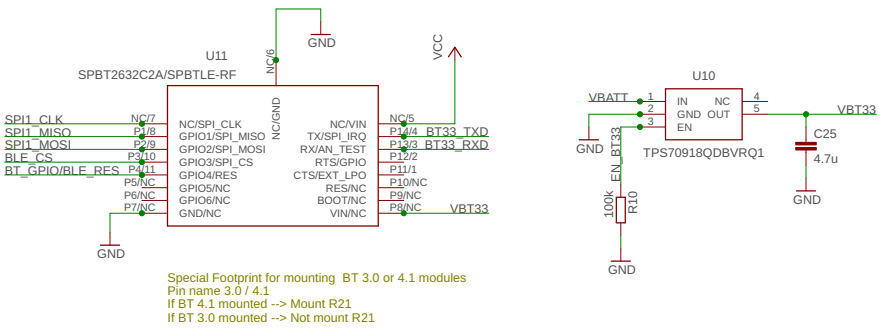

Figure 2.6 – Bluetooth module with dedicated low-dropout regulator.

in longer battery life. Since the BlueNRG-MS offers the option of interfacing with external microcontrollers using SPI transport layer, it was connected to the STM32L433CC microcontroller via SPI.

The second solution, which allows only the transmission of raw and computed data, is represented by the use of the USB which is directly connected to the STM32L433 microcontroller (Figure 2.7).

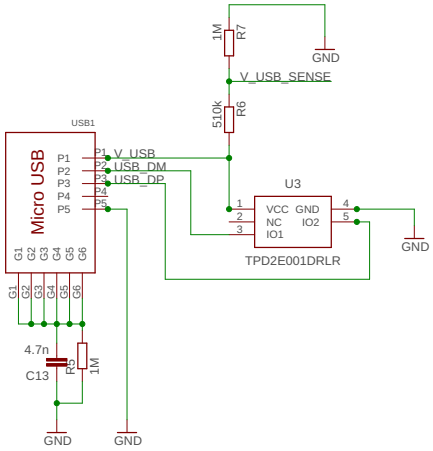

Figure 2.7 – μUSB connector.

Power Management

As the SWING system is a wearable device which includes a Li-poly battery, it requires particular ICs aimed at managing the recharge and the state of the battery. For these two purposes two different ICs were used: a battery charger (MCP73831 provided by Microchip [48]) and a fuel gauge (MAX17048X provided by Maxim Integrated [49]) (Figure 2.8).

The MCP73831 device is a highly advanced linear charge management controller for use in space limited and cost-sensitive applications. Due to its small physical size and the low number of required external components make this IC ideally suited for portable applications. The MCP73831 employs an efficient charge algorithm with selectable preconditioning and charge termination.

The MAX17048 is a tiny, micropower current fuel gauges for Li-poly batteries. The IC uses a Li-poly battery-modeling algorithm ModelGauge™ to track the battery relative state-of-charge continuously over widely varying charge and discharge conditions. The IC automatically detects when the battery enters a low-current state and enters low-power 3 µA hibernate mode, while still providing accurate fuel gauging. It automatically exit hibernate mode when the system returns to active state.

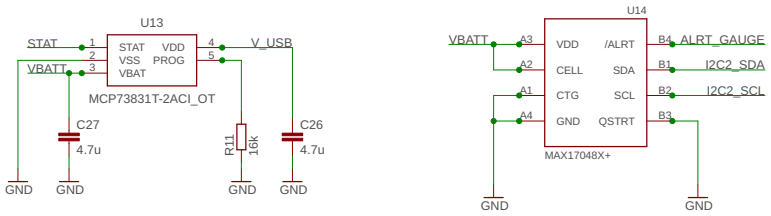

Figure 2.8 – Battery charger and fuel gauge module.

A buck regulator has been used in order to provide a fixed power supply (2.8 V) for all ICs in the board from a 3.7 V Li-poly battery. A buck regulator or step-down converter is a DC-to-DC power converter which steps down voltage from its input (i.e. Li-poly battery) to its output (ICs). The selected buck converter is the TPS62740 provided by Texas Instruments [50] which is a first step down converter featuring typical 360 nA quiescent current and operating with a tiny 2.2 µH inductor and 10µF output capacitor. The output voltage is user selectable by four VSEL pins within a range from 1.8 V to 3.3 V in 100 mV steps. For the current application the four VSEL pins were selected in order to provide an output voltage equal to 2.8 V. A very helpful feature given by the TPS62740 is related to the pin CTRL which controls the output LOAD pin. In fact, for low-power consuming strategies, all the sensing elements (accelerometer, gyroscope, magnetometer and infrared ToF distance sensors) were power supplied by the LOAD pin which was controlled by the microcontroller instead of connecting them directly to the system power supply.

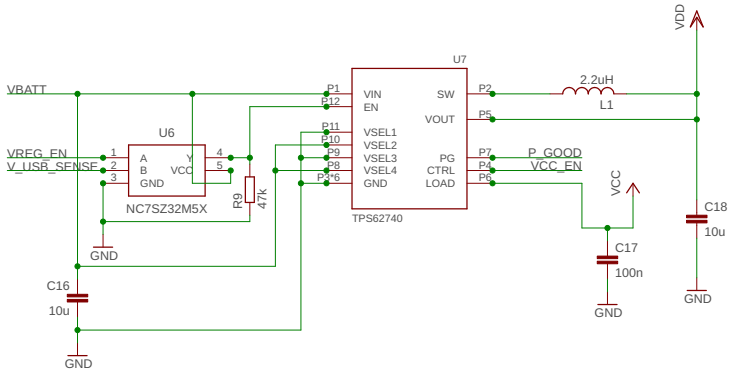

Figure 2.9 – Buck regulator.

I/O

Infrared ToF distance sensors connectors

Based on the requirements of the SWING system, three six-pins connectors were embedded in the SWING system layout which for allowing the user to connect

simultaneously via I2C up to three satellite boards/infrared ToF distance sensors.

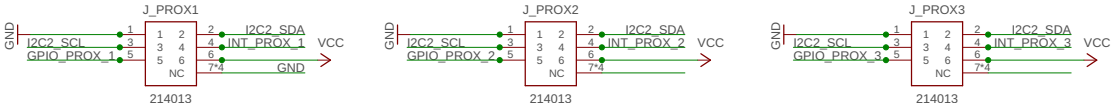

Figure 2.10 – Satellite boards/infrared ToF distance sensors connectors'.

Button and LEDs

The SWING system integrates a button and three LEDs. The button was used in combination with the smart push-button on/off controller (STM6600 provided by STMicroelectronics [51]) in order to power-up, power down, reset and change the state of the SWING system based on how long the button is pressed.

Among the three LEDs (blue, white and orange), the orange one was used only to indicate a low level battery (under a selected threshold voltage), while the remaining two LEDs (blue and white) were used to provide information to the user about the state of the SWING system (e.g. in TX state the blue LED blinks at the output data rate frequency).

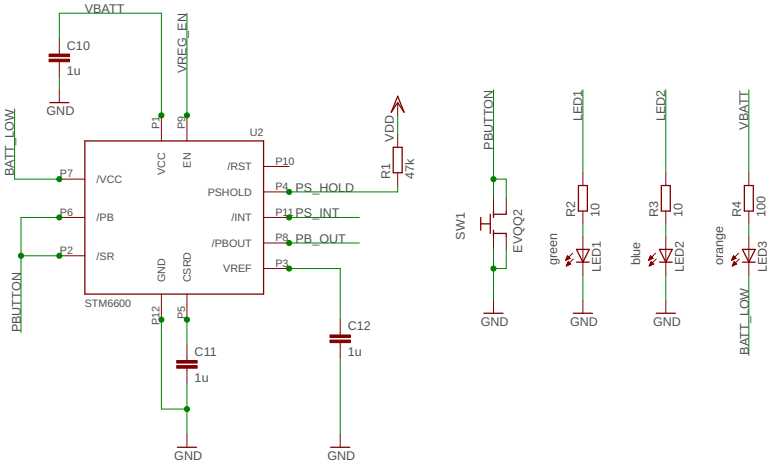

Figure 2.11 – Button with smart push-button on/off controller and LEDs.

Debug connector

Finally, a connector made of ten pins was used to enable the debugging and the flashing of the SWING system.

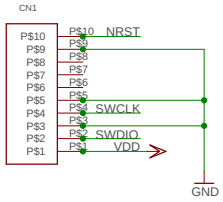

Figure 2.12 – Debug connector.

Stackup

The stackup of the SWING system has been designed in order to reduce the production costs while maintaining a small form factor. The PCB is composed of two layers: top (layer 1) and bottom (layer 16). The overall stackup achieved for the SWING system is depicted in Figure 2.13 with 0.035 mm thickness for each of the two layers and a total height of 1.57 mm.

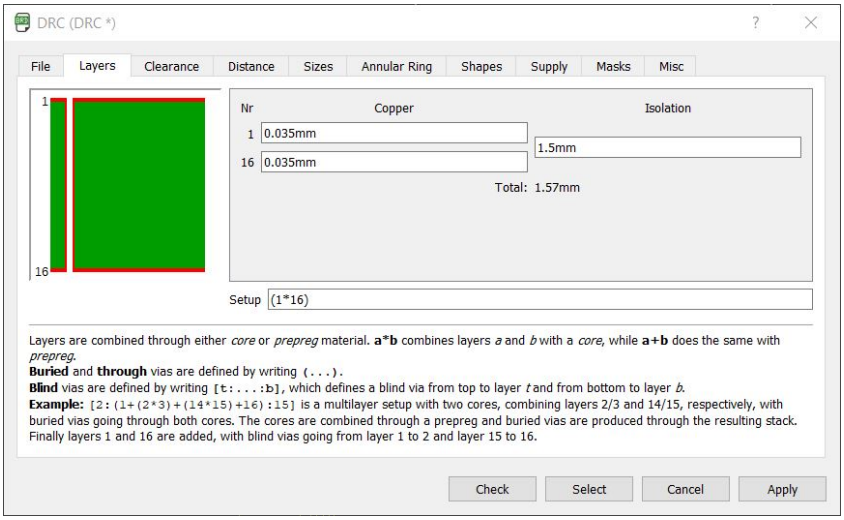

Figure 2.13 – PCB 2D build up.

Layout

The PCB of the SWING system measures $35 \times 35\,\text{mm}^2$ in which the positioning of the components has been carefully addressed. In particular:

- the magnetometer has been place away from high current traces. This expedient is mandatory to avoid distortions of the earth magnetic field measurement;
- the placement of the Bluetooth module has been made in order to guarantee the maximum compliance of the design rules imposed by the antenna manufacturer (no traces under the Bluetooth antenna).

The top layer (Figure 2.14) integrates the Bluetooth module, the flash memory, the infrared ToF distance sensors connectors, the μUSB and the debug connectors, whereas on the bottom layer (Figure 2.15) are mounted the processing unit, the sensing units and the power management ICs.

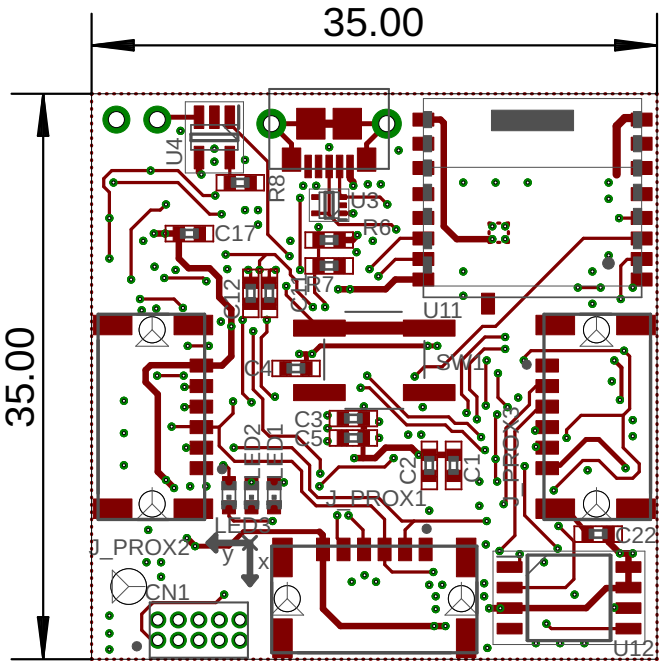

Figure 2.14 – Top view of the SWING layout (units in millimeters).

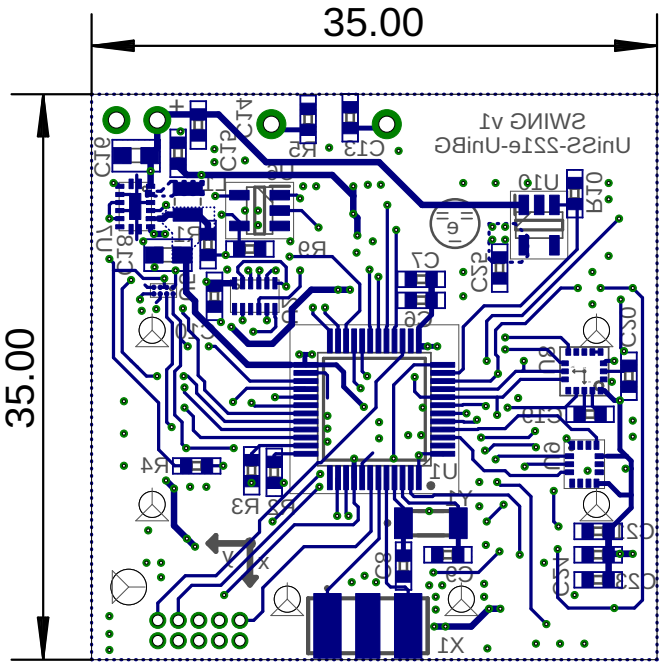

Figure 2.15 – Bottom view of the SWING layout (units in millimeters).

In Figure 2.16 are reported the top and the bottom layers of the SWING system after the fabrication and the assembly of the board.

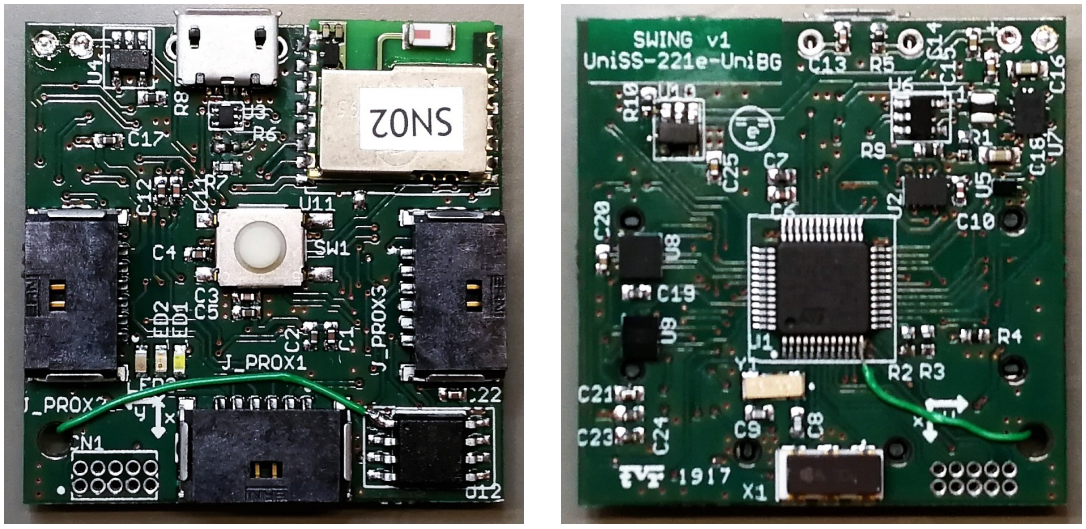

Figure 2.16 – Top and bottom views of the fabricated and assembled SWING system.

2.4.2 Infrared time-of-flight satellite board

Satellite board provided by STMicroelectronics

The satellite board VL6180X-SATEL [52], provided by STMicroelectronics, is an evaluation board which integrates the VL6180X infrared ToF distance sensor in order to makes VL6180X-SATEL easier to integrate into development and evaluation devices due to its small form factor. For 2.8 V supply applications, such as the SWING system, the VL6180X-SATEL can be divided in a "mini board" in order to only use the VL6180X distance sensor.

The VL6180X [53] is an infrared ToF distance sensor based on ST's patented FlightSense™ technology. Instead of estimating the distance by measuring the amount of light reflected back from the object (approach which is colour and surface dependent), the VL6180X measures the time that the light takes to travel to the nearest object and reflect back to the sensor. It integrates in the same chip an infrared emitter and a range sensor. The full scale range can be setted up to 200 mm, 400 mm or 600 mm with a resolution of 1 mm, 2 mm and 3 mm, respectively with a ranging frequency up to 50 Hz (depending on the full scale range). The VL6180X was connected to the STM32L433CC microcontroller using the I2C interface.

The VL6180X-SATEL "mini board" ready to be connected to the SWING system is depicted in Figure 2.17.

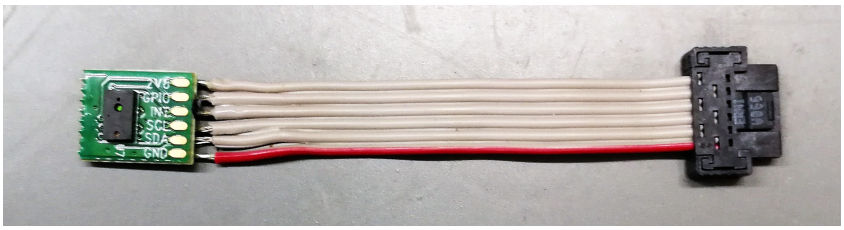

Figure 2.17 – VL6180X satellite board ready to be connected to the SWING system.

Custom satellite board

A custom satellite board, which incorporates the VL53L1X distance sensor [54] and a connector, was devised to make it more versatile than the STMicroelectronics one. In particular, the advantage of this board is that the same satellite board can be used in different applications that require different cables lengths.

The VL6180X was replaced with the VL53L1X which is the latest and updated version of the VL6180X with an incremented distance range (up to 4 m). In addition, the VL53L1X enables the user to program the region of interest size on the receiving array, allowing the sensor field of view to be reduced. The circuit diagram and the printed circuit board of the custom satellite board are reported in Figure 2.18 and Figure 2.19, respectively. Since the custom satellite board has not yet fabricated and assembled, its 3D rendering has been generated and provided in Figure 2.20.

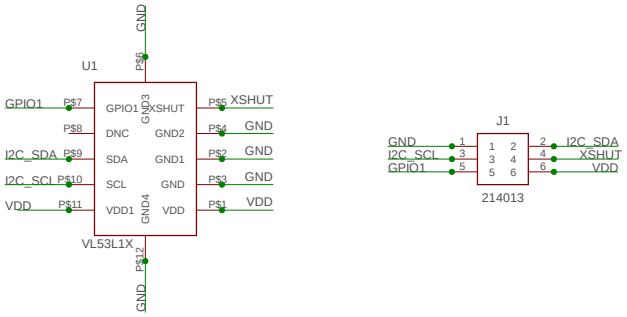

Figure 2.18 – Circuit diagram of the custom infrared ToF satellite board.

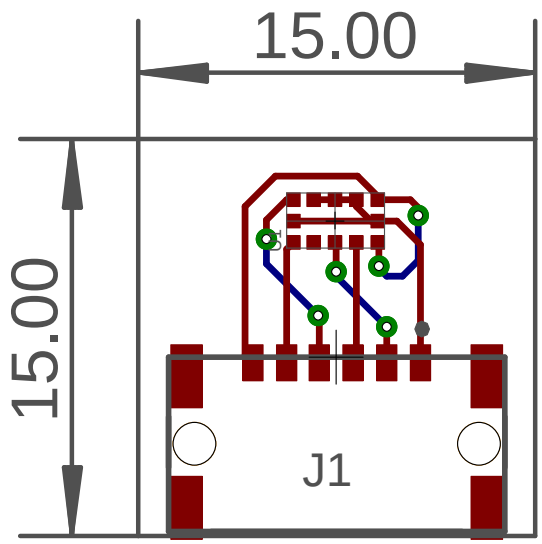

Figure 2.19 – Top and bottom views of the custom infrared ToF satellite board layout (units in millimiters).

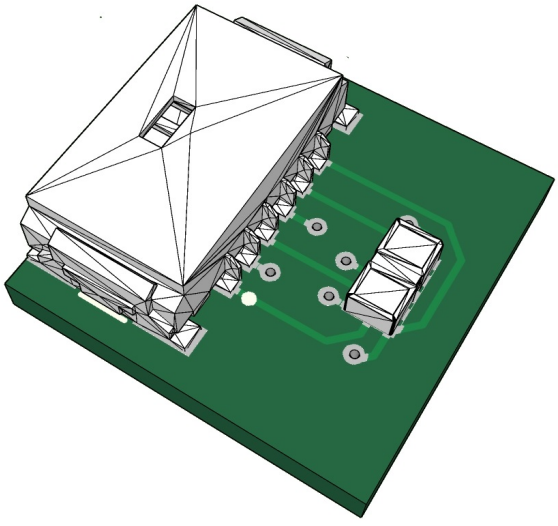

Figure 2.20 – Top view of the 3D rendering of the custom infrared ToF satellite board.

3 Software

3.1 Embedded firmware

The embedded firmware for the SWING system has been implemented with the CubeMX hardware abstraction layer and the integrated development environment (IDE) TrueSTUDIO® for STM32. A graphical and simple way to describe the functioning of a system is represented by the finite state machine (FSM). FSM is an abstract machine that can be in exactly one of a finite number of states at any given time and it can change from one state to another (transition) in response to some external inputs.

3.1.1 Finite State Machine

The SWING system can be only powered on by pressing the button. Once the system is powered on, a STARTUP routine is run for the initialisation of the system which consists of the configuration of the microcontroller (clock, timers, GPIOs, etc.) and the ICs (sensing elements, memory, Bluetooth, etc.). If the initialisation succeeds, the system enters in IDLE state. In IDLE state, depending on the configuration of the system (energy-save mode enabled or disabled), the sensing elements are powered off or powered on. In this state the system is waiting for a connection via Bluetooth to an external device. Once the connection is established, the SWING system and the external device can start a two-way communication based on a specific set of commands.

The SWING system implements two recording modes: stream (TX) and log (LOG). In this two states the system is running and the data provided by the sensing elements are recorded. In TX state data are sent via Bluetooth to the graphical user interface (GUI), while in LOG state these data are saved in the flash memory embedded onboard the system. The stream and the log mode can be

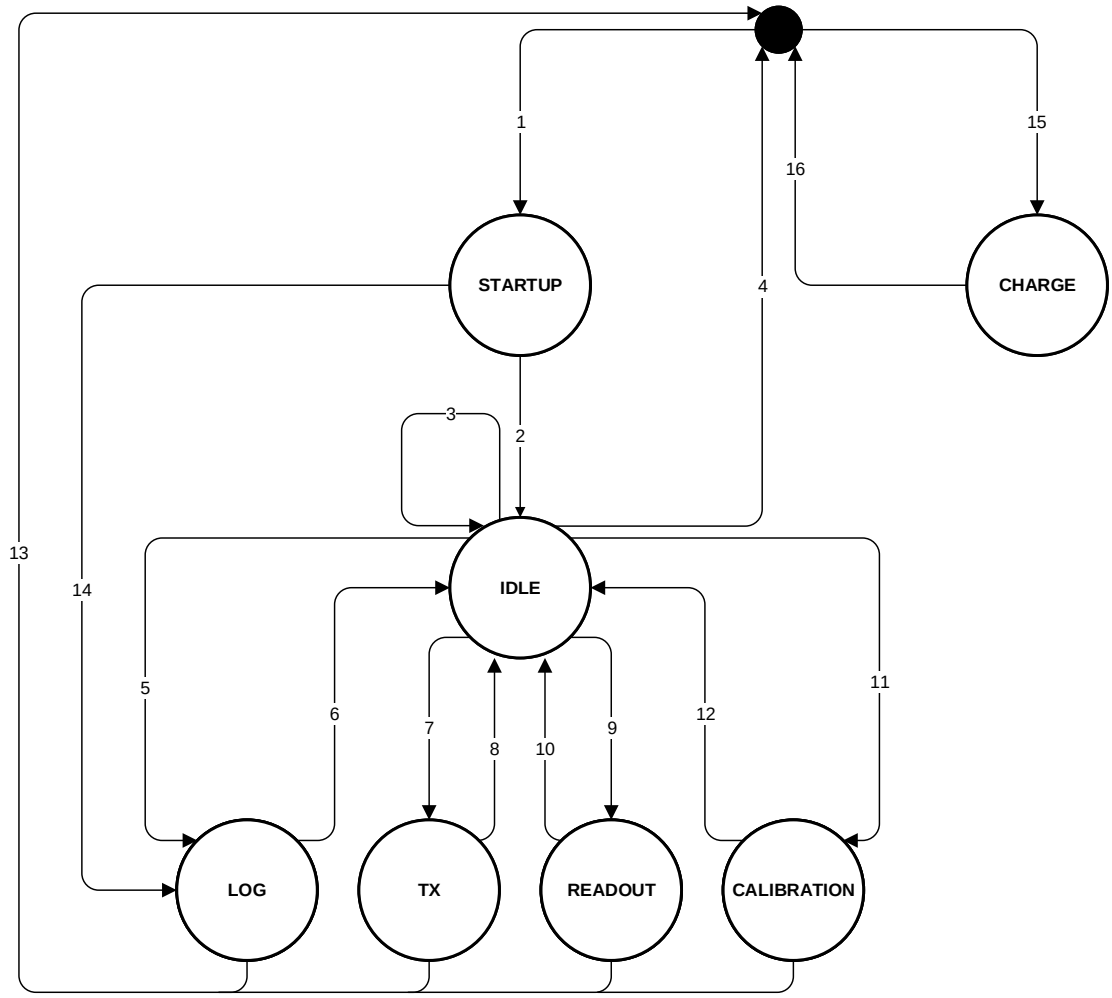

Figure 3.1 – FSM of the SWING firmware.

stopped by sending the STOP command or by pressing the button.

In IDLE state is also possible to read the data that was previously saved on the onboard flash memory by sending the READOUT command.

Finally, always from IDLE state, is possible to calibrate the accelerometer, gyroscope, magnetometer and infrared ToF distance sensors separately by sending specific CALIBRATION commands. When the calibration is completed, the system saves the calibration parameters in the flash memory and it automatically returns to IDLE state.

Additional commands can also be sent to the SWING system, while it is in IDLE state, to enable or disable the log mode, to set the output data rate of both stream and log mode, to change the name associated to the Bluetooth module and to update and verify the SWING system RTC.

The SWING system can also be configured to automatically start recording (log mode) immediately after the power up and the initialisation of the system without

passing through the IDLE state. This feature was developed in order to enable the user to use the SWING system without using the GUI and connecting an external device. The recording can be stopped and restarted simply by pressing the button.

From all states, except CHARGE state, the SWING system can be power down with a long push of the button.

The SWING system automatically starts charging the Li-poly battery when it detects current floating from the USB connector. Until the system is still in CHARGE state the white led blinks. When the charge is completed the white led stop blinking and it remains lit.

The list of the actions related to the FSM state transitions are reported in Table 3.1.

Table 3.1 – List of the FSM state transitions of the SWING system.

N.	From State	To State	Action
1	OFF	STARTUP	Device power on
2	STARTUP	IDLE	Peripherals correctly initialised
3	IDLE	IDLE	Bluetooth connection or CONFIGURATION commands
4	IDLE	OFF	DISCONNECT command or long button pressed
5	IDLE	LOG	START LOG command or button pressed (if LOG mode previously enabled)
6	LOG	IDLE	STOP command or button pressed
7	IDLE	TX	START TX command
8	TX	IDLE	Button pressed or STOP command
9	IDLE	READOUT	READ MEMORY command
10	READOUT	IDLE	Read memory finished
11	IDLE	CALIBRATION	CALIBRATION command
12	CALIBRATION	IDLE	Calibration finished
13	LOG	OFF	Long button pressed
13	TX	OFF	Long button pressed
13	READOUT	OFF	Long button pressed
13	CALIBRATION	OFF	Long button pressed
14	STARTUP	LOG	Log mode enabled
15	OFF	CHARGE	Plug-in USB
16	CHARGE	OFF	Plug-out USB

3.2 Graphical user interface

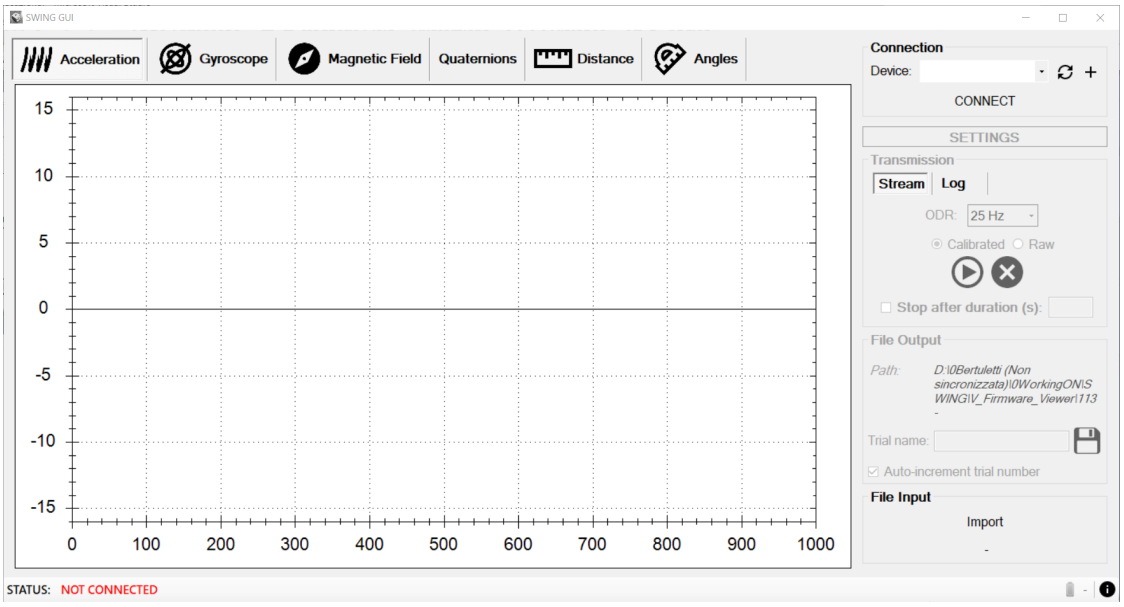

Figure 3.2 – Main window of the SWING GUI.

The SWING_GUI, developed in C# language using the Visual Studio IDE, allows the user to interact with the SWING system through graphical icons. In particular, as depicted in Figure 3.2, the main window is composed of seven main groups:

- **graphs** in which the raw/calibrated data provided by the sensing elements of the SWING system and the computed data (quaternion and angles) are shown;
- **connection** which contains all the controls aimed at the management of the connection to the SWING system such as the pairing with a new SWING system (not yet associated) and the connection/disconnection to a SWING system (already associated);
- **settings button** which enables the user to configure (log mode, energy-saving modes, update and verify the RTC and rename the Bluetooth module), calibrate (accelerometer, gyroscope, magnetometer, infrared ToF distance sensors, log mode) and manage (read data from the flash memory and erase the flash memory) the SWING system;
- the **transmission panel** aimed at starting a new acquisition by selecting stream or log mode, selecting the desired output data rate and subsequently

starting, stopping or cancelling the acquisition. Both stream and log recordings can be automatically stopped by giving a specific trial duration to the GUI;

- **file output** which enables the user to select the name and the location of the output file;
- **file input** which can be used to import and plot data from an external file;
- a **tool strip** to provide additional information to the user. In particular, a label which shown the status of the connection to the selected SWING system (connected or disconnected), a button once pressed shown the battery status and an information button that will open a new window containing additional information about the GUI and the developers.

By clicking the settings button the GUI will open a new window used for the system configuration. In particular one panel for each sensing element (accelerometer, gyroscope, magnetometer and infrared ToF distance sensors) was developed in order to calibrate, reset and set full scales (Figure 3.3). Two additional panels were developed to configure the log mode (enable/disable, selection of the output data rate, selection of which data that have to be saved) (Figure 3.4), read data from memory, erase the memory and enable/disable the energy saving mode, configure the time of the SWING system and the name of Bluetooth associated to the SWING system (Figure 3.5).

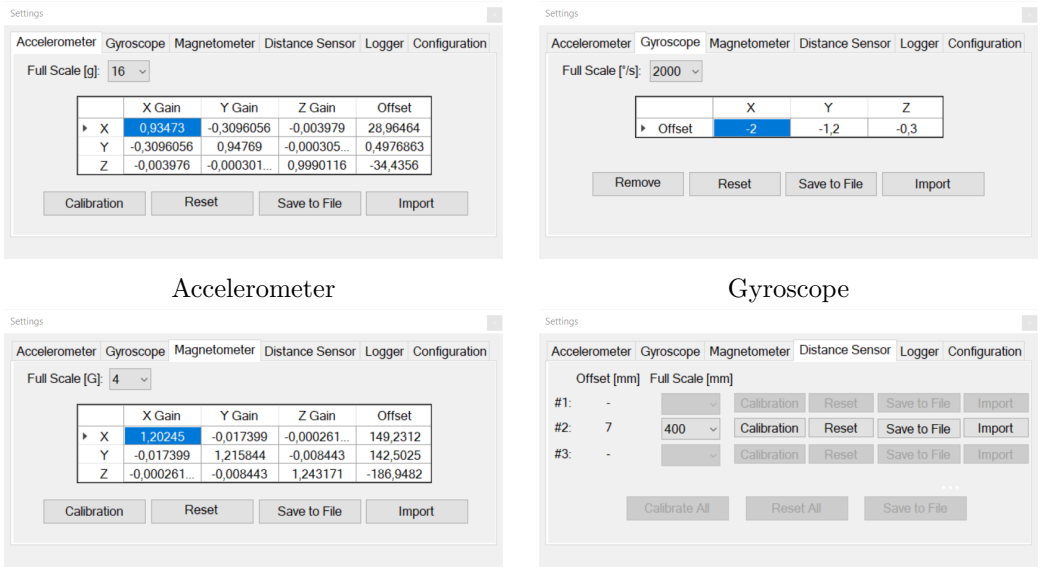

Accelerometer

Gyroscope

Magnetometer

Infrared ToF distance sensors

Figure 3.3 – Sensing units windows' in the settings of the SWING GUI.

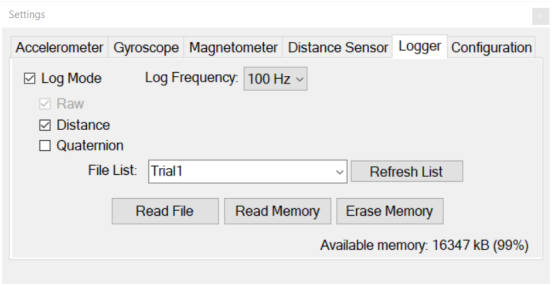

Figure 3.4 – Logger window in the settings of the SWING GUI.

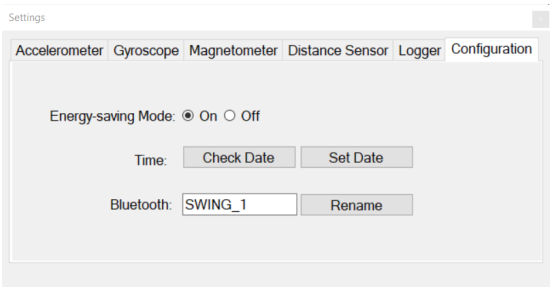

Figure 3.5 – Configuration window in the settings of the SWING GUI.

4 Enclosures and Supports

4.1 Enclosures

In addition to the development of the SWING system (circuit diagram and board), the SolidWorks software, which is a solid modeling computer-aided design, was used to design the enclosures of the SWING system. In particular, in Figure 4.1 and Figure 4.2 are depicted the enclosures of the SWING system and the STMicroelectronics satellite "mini board", respectively.

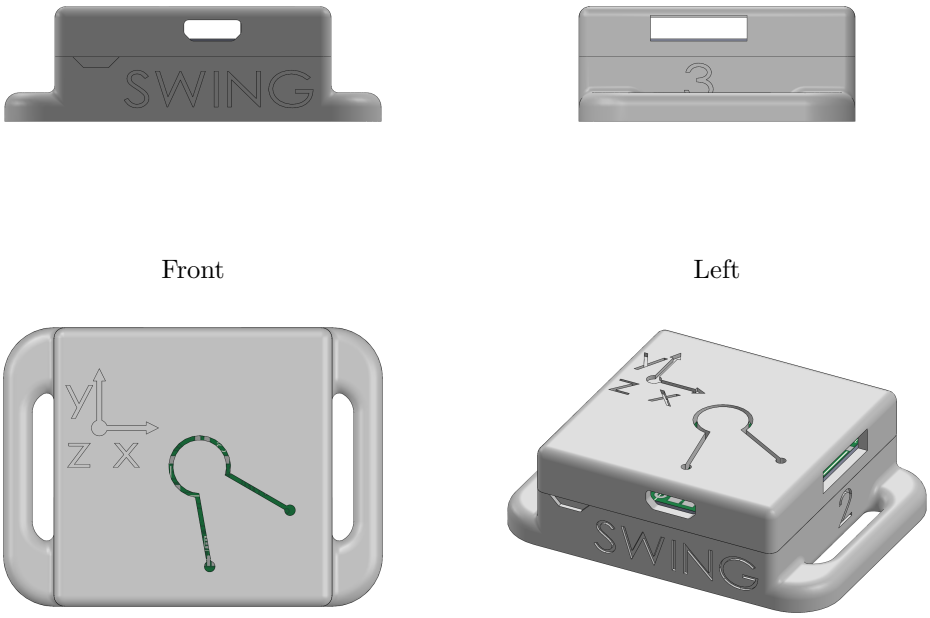

Figure 4.1 – 2D-views and 3D-view of the enclosure of the SWING system.

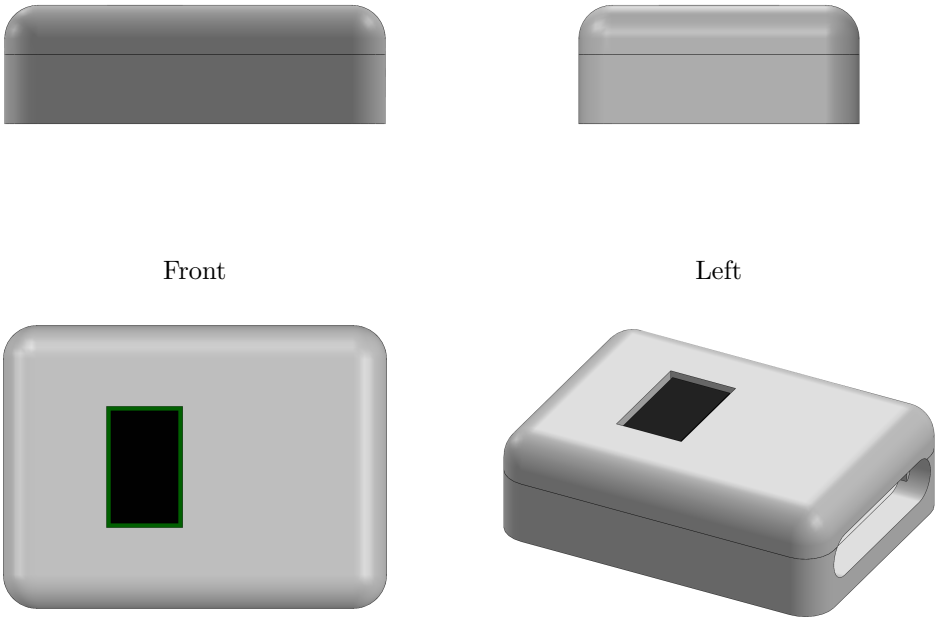

Figure 4.2 – 2D-views and 3D-view of the enclosure of the STMicroelectronics satellite "mini board".

All these 3D models were converted into GCODE format which is a language used to describe how a 3D printer should print a 3D model. In particular, it stores instructions in plain text where each line represents a different command, such as how fast the printer should print, the temperature it should be set at, and where the printing parts should move. Finally, these files were sended to a 3D printer and printed using a polylactide filament.

4.2 Supports

In addition to the enclosures of the SWING system and the STMicroelectronics satellite "mini board", the support for the SWING system in its two infrared ToF distance sensors configuration was devised and printed (Figure 4.3). This support was specifically designed to be worn by a person on the medial side of the foot by using two velcro straps. The support aimed at simultaneously measuring the distance between feet by two infrared ToF distance sensors positioned one close to the rearfoot and the other close to the forefoot while pointing the contralateral foot.

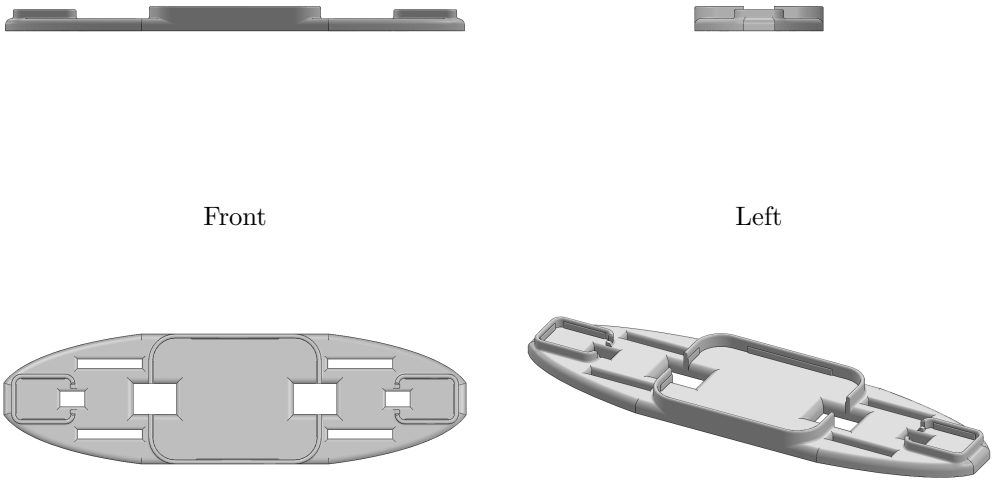

Figure 4.3 – 2D-views and 3D-view of the support specifically designed for the SWING^{2DS} which incorporates in the middle the magneto-inertial unit and two infrared ToF distance sensors by the sides of the support.

Even if the infrared ToF distance sensors are calibrated from the factory (STMicroelectronics) it is suggested, as reported in the specifications [53], to periodically check their accuracy. The calibration procedure for an infrared ToF distance sensor is the following:

1. place a white target at 50 mm away from the infrared ToF distance sensor if the range is set to 200 mm or at 100 mm if the range is set to 400 mm or 600 mm;

2. set the offset of the infrared ToF distance sensor equal to 0 mm;

3. perform a minimum of ten range measurements and compute the average range;

4. calculate the part-to-part offset as follows:

$$\text{part-to-part offset} = \text{target distance} - \text{average range} \tag{4.1}$$

5. the new offset value has to be written into a specific register of the infrared ToF distance sensor each time the device is reset.

To simplify this procedure and to reduce calibration errors due to an incorrect positioning of the target (e.g. at a distance that is not exactly 50 mm or 100 mm) or to an incorrect positioning of the infrared ToF sensor (the infrared ray must be orthogonal to the target) a calibration structure was devised and printed (Figure 4.4). The base has been designed to integrate one infrared ToF sensor while pointing orthogonally to the target surface. Since the distance from the target surface can be 50 mm or 100 mm, depending on the selected range of measurement, two sets of three pillars were devised and printed (both sets of pillars, one at a time, can be used with the same base and target).

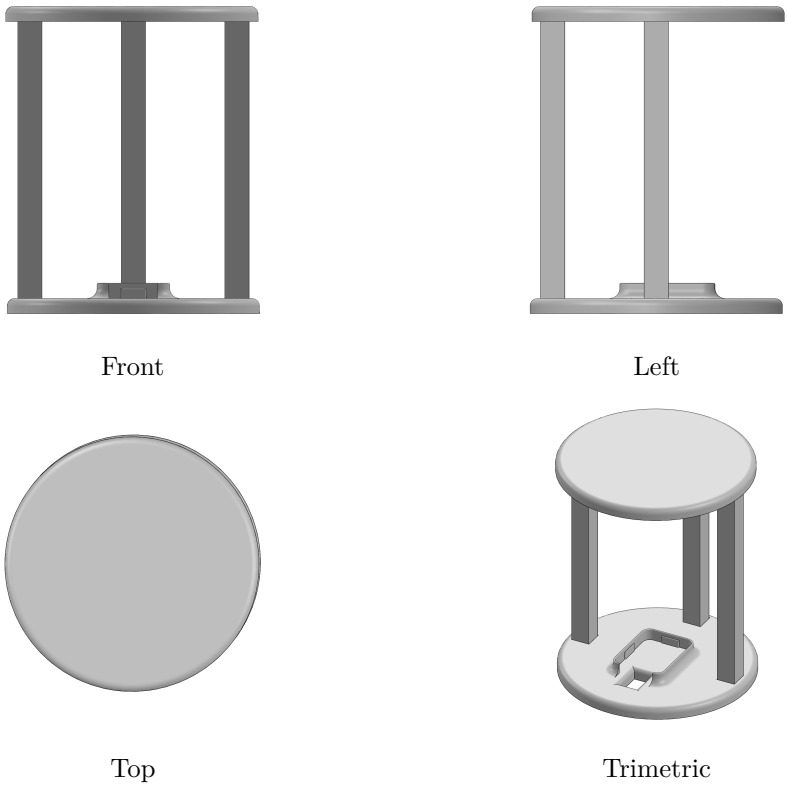

Figure 4.4 – 2D-views and 3D-view of the structure specifically designed for the calibration of the infrared ToF sensor.

5

Infrared time-of-flight sensor characterisation

The characterisation of the infrared ToF sensor [53] has been performed by using the first prototype of the SWING system, called D-MuSe. The D-Muse is a wearable system which includes a MIMU and an infrared ToF sensor. The typical range performances of the infrared ToF sensor (VL6180X), reported in the specifications [53], only refer to static conditions using a target (with different reflectances) positioned in front of the infrared ToF sensor (Figure 5.1).

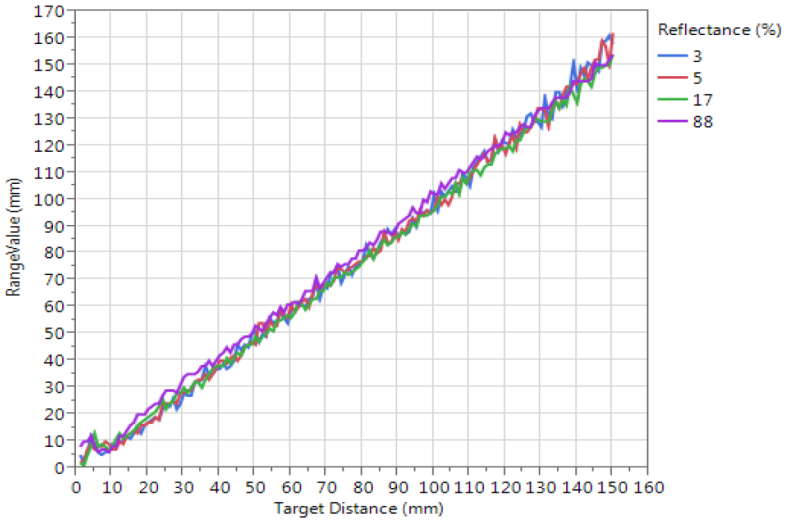

Figure 5.1 – Typical ranging performance of the VL6180X sensor, provided by STMicroelectronics (Geneva, Switzerland), for different target reflectance (3 %, 5 %, 17 % and 88 %) by varying the range from 0 to 150 mm.
Source: [53], Figure 6.

This chapter is based on:
S. Bertuletti, A. Cereatti, D. Comotti, M. Caldara, and U. Della Croce, "Static and dynamic accuracy of an innovative miniaturized wearable platform for short range distance measurements for human movement applications", *Sensors*, vol. 17, no. 7, 2017, ISSN: 1424–8220. DOI: 10.3390/s17071492. [Online]. Available: http://www.mdpi.com/1424-8220/17/7/1492.

Therefore, the applicability of this technology for human movement analysis applications has required further investigations. The present characterisation aimed at filling this gap by performing a thorough test under experimental conditions resembling those encountered when analysing human movement focused on the lower limb during walking.

5.1 Principle of functioning

A sensor that implements the infrared ToF technology provides estimates by measuring the time that the light takes to travel to the nearest object and reflect back to the sensor. Specifically, the distance is estimated by measuring the phase shift φ between the radiated *s(t)* and the reflected *r(t)* infrared radiation (IR) waves (Figure 5.2):

$$s(t) = \sin(2\pi f_m t), \tag{5.1}$$

$$r(t) = R \cdot \sin(2\pi f_m t - \varphi) = R \cdot \sin\left[2\pi f_m \left(t - \frac{2d}{c}\right)\right], \tag{5.2}$$

where R is a reflection coefficient, c is the speed of light ($3 \cdot 10^8$ m/s) and f_m is the modulation frequency of the radiated and reflected signals. Once φ is measured (e.g., phase comparator circuit), the distance d between the position of the IR emitter and the target can be calculated from Equation (5.2) as follows:

$$d = \frac{c}{4\pi f_m} \cdot \varphi. \tag{5.3}$$

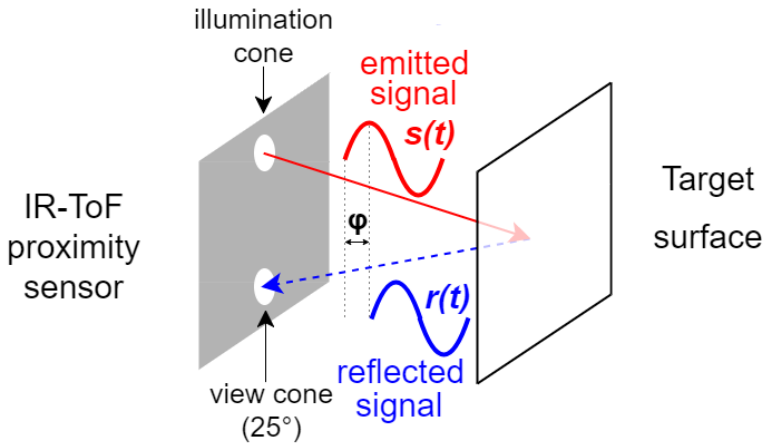

Figure 5.2 – The infrared ToF sensor provides the distance estimates from the target reflecting surface by measuring the phase shift φ between the emitted *s(t)* and the reflected *r(t)* signals.

5.2 Analysed factors

The following factors, which could potentially affect the accuracy associated with distance estimation, were analysed:

(i) colours of the target surface (red, green, blue, yellow, white and black);

(ii) distance (from 20 to 200 mm);

(iii) angle of incidence (AoI) (0 °, 30 °, −30 °, 60 ° and −60 °);

(iv) relative velocity between the infrared ToF sensor and the target.

The influence of factor (i) was tested in static conditions only, factors (ii) and (iii) were tested both in static and dynamic conditions and factor (iv) was tested only in dynamic conditions. These factors were chosen to cover the range of possible configurations occurring during both normal and pathological human gait such as different shoe colours, different internal-external rotation foot angles, different values of the SW and different foot velocities [55]–[59].

5.3 Experimental setup

The infrared ToF sensor sampling rate was set to 50 Hz (maximum frequency allowed), and, since the maximum distance between feet during gait is generally less than 200 mm [55]–[57], its measurement range was set to 0–200 mm. To improve its accuracy, an ad hoc calibration between 0 and 200 mm was performed and, when no light reflection was observed, the firmware of the D-MuSe system was programmed to return a "0" distance value.

The D-MuSe was attached to the end of a wooden pendulum (length 600 mm) simulating the oscillation of a human leg, while a stationary rectangular cuboid target, with dimensions similar to those of a shoe ($180 \times 70 \times 40\,\text{mm}^3$), was positioned in front of the pendulum (Figure 5.3). Let C be the intersection between the diagonals of the rectangular face facing the sensor, while the distances d between the infrared ToF sensor and the target were set using a ruler (gold standard, 1 mm resolution).

5.4 Experimental data acquisition

The first part of the infrared ToF sensor characterisation consisted of a series of static acquisitions using six different target colours (red, green, blue, yellow, white

and black) varying the distance in the range of 0–200 mm with an increment of 20 mm (Figure 5.4).

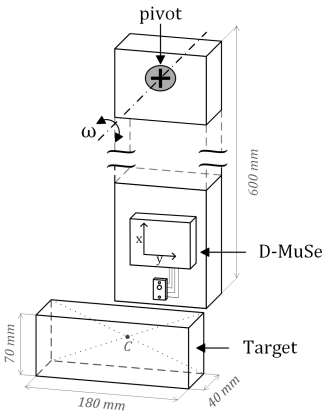

(a) Model of the experimental setup

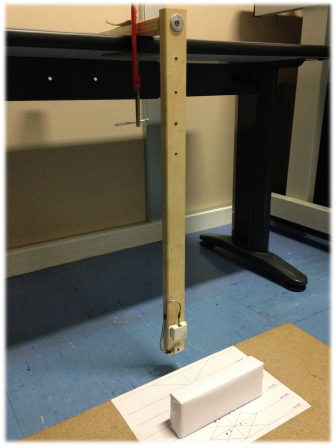

(b) Experimental setup

Figure 5.3 – A wooden pendulum with the MIMU and the infrared ToF sensor attached to its distal end. The stationary target was positioned in front of the pendulum.

Figure 5.4 – The six colours of the rectangular cuboid targets used during the static acquisitions (red, green, blue, yellow, white and black).

Based on the results provided by this preliminary investigation, only the white colour was selected for the subsequent experimental acquisitions.

In static acquisitions, the target was kept stationary in front of the infrared ToF sensor, while during dynamic acquisitions, the pendulum was kept horizontal in the starting position and then released. For both static and dynamic acquisitions, the following experimental conditions were tested:

- AoI $= 0\,^\circ$ and $d = 40$, 70, 100, 130, 160, 190 mm;
- AoI $= 30\,^\circ$ and $d = 70$, 100, 130, 160, 190 mm;
- AoI $= -30\,^\circ$ and $d = 70$, 100, 130, 160, 190 mm;
- AoI $= 60\,^\circ$ and $d = 100$, 130, 160, 190 mm;
- AoI $= -60\,^\circ$ and $d = 100$, 130, 160, 190 mm.

To avoid a collision between the target and the pendulum, for AoI = ±30 ° the minimum distance d was equal to 70 mm, whereas, for AoI = ±60 °, the minimum distance d was equal to 100 mm. A schematic representation of the experimental set-up and an example of the raw distance values measured by the infrared ToF sensor for different AoI values are reported in Figure 5.5. The distance d is measured in correspondence of the lowest point of the pendulum, which is the point with the maximum angular velocity (minimum potential energy and the maximum kinetic energy).

5.5 Data analysis

Since inertial data were acquired at 100 Hz, while distance data were acquired at 50 Hz (maximum frequency allowed), a continuous estimate of the distance at 100 Hz was necessary and therefore computed by linearly interpolating and then re-sampling the distance measurements at 100 Hz. During static acquisitions, the sensor-target distance was determined by averaging 30 readings. For each dynamic acquisition, the set of distance values d_{ToF_k} provided by the infrared ToF sensor was extracted, one for each k-th oscillation, while the angular velocity measured in correspondence of the lowest point of the pendulum varied between 1 and 6 rad/s (≈30 oscillations) (Figure 5.6).

For each dynamic acquisition, defined by specific values of AoI and d, the following quantities were computed:

$$e_{AoI,d} = \frac{1}{N}\sum_{k=1}^{N}(d_{ToF_k} - d), \tag{5.4}$$

$$sd_{AoI,d} = \sqrt{\frac{1}{N-1}\sum_{k=1}^{N}(d_{ToF_k} - d)^2}, \tag{5.5}$$

$$mae_{AoI,d} = \frac{1}{N}\sum_{k=1}^{N}|d_{ToF_k} - d|, \tag{5.6}$$

$$\text{mae}_{\%\,AoI,d} = \frac{mae_{AoI,d}}{d} \cdot 100, \tag{5.7}$$

where d_{ToF_k} is the distance estimated by the infrared ToF sensor when the gyroscope measured a peak, d is the true distance and N is the number of oscillations with angular velocity between 1 and 6 rad/s. Furthermore, for each AoI value, the average values of latter indices were computed over the different distances (grand error (E), grand standard deviation (SD), grand mean absolute error (MAE) and

grand mean absolute percentage error ($MAE_{\%}$)).

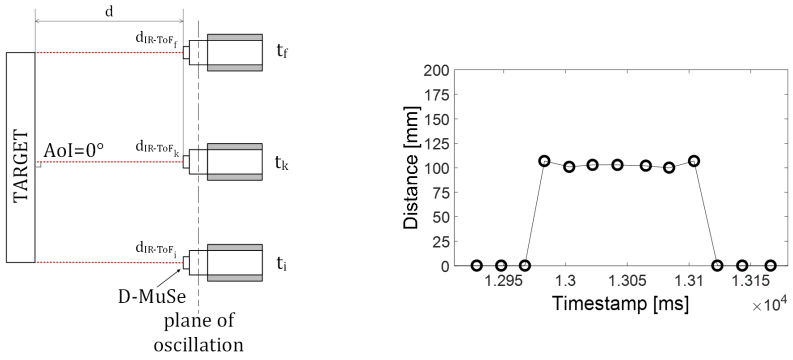

(a) AoI = 0 °

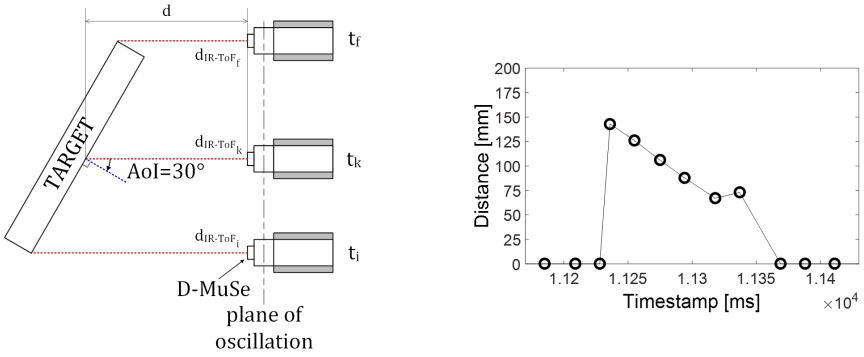

(b) AoI = 30 °

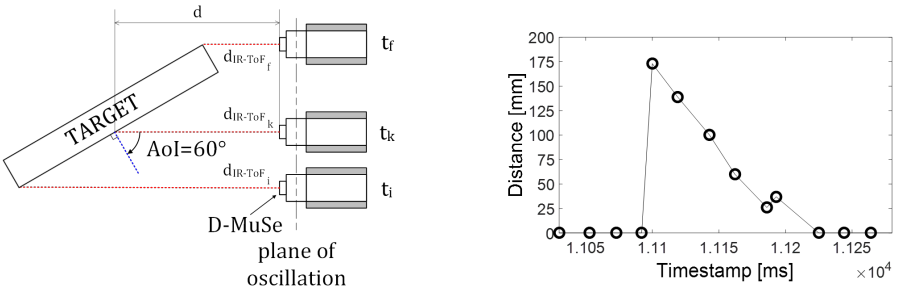

(c) AoI = 60 °

Figure 5.5 – On the left, the top view of the experimental setup for AoI = 0 ° (a), 30 ° (b) and 60 ° (c). The red dotted line represents the infrared ray emitted by the infrared ToF sensor. d is the imposed distance using a ruler, while d_{ToF_k} is the distance estimated by the infrared ToF sensor when the gyroscope measured a positive/negative peak according to the direction of the pendulum oscillation. d_{ToF_i} and d_{ToF_f} are the initial and final estimated distances, respectively. On the right, for each AoI value, an example of the distance values measured by the infrared ToF sensor at $d = 100$ mm is reported. It should be noted that, in dynamic acquisitions, when the AoI differs from zero, the sensor-target distance d_{ToF} varies with time between d_{ToF_i} and d_{ToF_f} ((b) and (c)).

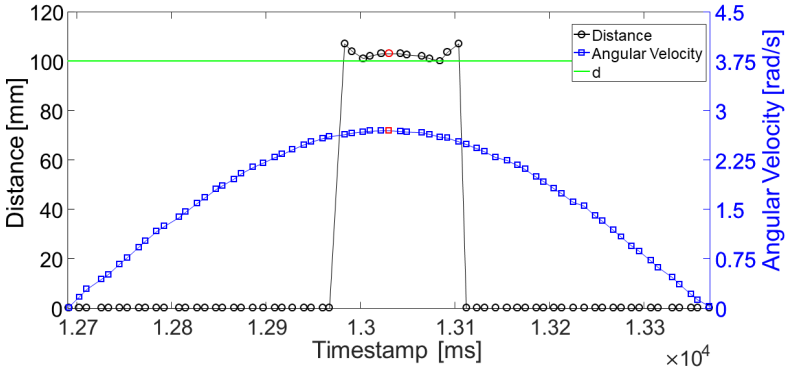

Figure 5.6 – An example of the readings, provided by the infrared ToF sensor and re-sampled at 100 Hz, is reported for an oscillation k with an angle of incidence equal to 0 ° and $d = 100$ mm. The value of d_{ToF_k}, obtained in correspondence of the angular velocity peak (red square), is reported with a red circle.

5.6 Results

The performance of the infrared ToF sensor obtained for different colours of the target are reported in Table 5.1. When the black target was used, the infrared ToF sensor could not measure distances larger than 140 mm.

Table 5.1 – Grand mean error with standard deviation (E ± SD), grand mean absolute error (MAE) and grand mean absolute percentage error ($MAE_{\%}$) of the distance for the six target colours.

Colour	E ± SD [mm]	MAE [mm]	$MAE_{\%}$ [%]
Red	1.1 ± 1.2	1.3	3.0
Green	1.5 ± 1.1	1.5	3.7
Blue	2.1 ± 1.2	2.1	4.2
Yellow	1.1 ± 1.1	1.5	3.9
White	1.6 ± 1.1	1.6	3.8
Black [I]	14.1 ± 1.2	4.1	7.2

The accuracy of the distance estimates for an AoI equal to 0 ° and $d = 40$, 70, 100, 130, 160, 190 mm using a white rectangular cuboid target are reported, for both static and dynamic acquisitions, in Table 5.2. In static acquisitions, $MAE_{\%}$ ranged from 0.8 % for d =160 mm to 2.5 % for 40 mm, while, in dynamic acquisitions, the value of $MAE_{\%}$ ranged from 0.8 % for d = 160 mm to 2.3 % for d = 40 mm.

[I] The distance range was 20–140 mm because no distance values were obtained for $d = 160$, 180 and 200 mm.

Table 5.2 – Mean error with standard deviation (e ± sd), mean absolute error (mae) and mean absolute percentage error ($mae_{\%}$) for an angle of incidence (AoI) equal to 0 ° during both static and dynamic acquisitions using a white rectangular cuboid target.

	Static			Dynamic		
d [mm]	e ± sd [mm]	mae [mm]	$mae_{\%}$ [%]	e ± sd [mm]	mae [mm]	$mae_{\%}$ [%]
40	0.7 ± 1.0	1.0	2.5	0.5 ± 1.1	0.9	2.3
70	0.2 ± 1.4	1.0	1.5	0.7 ± 1.5	1.3	1.8
100	0.6 ± 1.5	1.1	1.1	0.7 ± 1.5	1.3	1.3
130	1.6 ± 1.5	1.8	1.4	1.9 ± 1.5	2.0	1.5
160	0.5 ± 1.5	1.2	0.8	1.1 ± 1.2	1.3	0.8
190	−2.5 ± 1.2	2.5	1.3	−2.2 ± 1.7	2.3	1.2

Distance estimation errors for the different AoI values are reported, for both static and dynamic acquisitions, in Table 5.3. In static acquisitions, E ± SD ranged from 0.2 mm (1.3 mm) for AoI = 0 ° to −7.8 mm (1.7 mm) for AoI = −60 °. In dynamic acquisitions, E ± SD ranged from 0.5 mm (1.4 mm) for AoI = 0 ° and −9.9 mm (26.9 mm) for AoI = −60 °. In static acquisitions the $MAE_{\%}$ values varied from 1.4 % for AoI = 0 ° to 5 % for AoI = −60 °, whereas, in dynamic acquisitions, they varied from 1.5 % for AoI = 0 ° to 19.2 % for AoI = −60 °.

Table 5.3 – Grand mean error and standard deviation (E ± SD), grand mean absolute error (MAE) and grand mean absolute percentage error ($MAE_{\%}$) of the distance for the five conditions (angle of incidence (AoI) equal to 0 °, ±30 ° and ±60 °) using a white target.

Condition		E ± SD [mm]	MAE [mm]	$MAE_{\%}$ [%]
AoI = 0 °	Static	0.2 ± 1.3	1.4	1.4
	Dynamic	0.5 ± 1.4	1.5	1.5
AoI = 30 °	Static	2.4 ± 1.5	2.7	2.5
	Dynamic	3.1 ± 11.0	9.8	9.5
AoI = −30 °	Static	−3.4 ± 1.5	3.6	2.5
	Dynamic	−5.6 ± 12.4	11.9	10.2
AoI = 60 °	Static	0.4 ± 1.9	3.6	2.5
	Dynamic	−8.0 ± 24.2	22.8	16.3
AoI = −60 °	Static	−7.8 ± 1.7	7.8	5.0
	Dynamic	−9.9 ± 26.9	25.6	19.2

In addition, for each AoI value, the relationship between the absolute values of the errors e and the angular velocity values during all dynamic acquisitions was investigated by performing a first order polynomial regression (Figure 5.7).

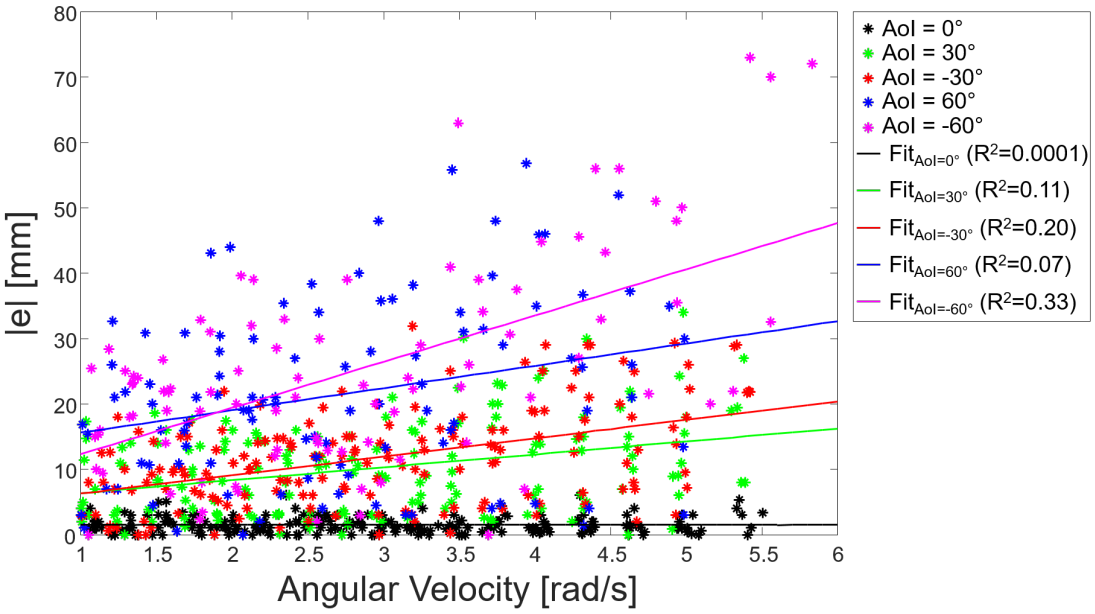

Figure 5.7 – The absolute values of the errors e computed by the infrared ToF sensor during all dynamic experiments are reported with a different colour for each angle of incidence (AoI) value. Furthermore, for each AoI value, a coloured line showed the trend of the absolute errors with respect to the angular velocity.

5.7 Accuracy evaluation

The performance of the infrared ToF sensor by changing the colour of the target showed that the infrared ToF technology is not sensitive to the variations of target colour except when black is used. In fact, the MAE varied between 1.3 mm and 2.1 mm among all target colours in the range 20–200 mm (except for black). With a black target, the infrared ToF sensor could only measure distances up to 140 mm and the accuracy of the distance estimation was lower (MAE = 4.1 mm). This finding was in accordance with the study of Lachat et al. [60] performed on a Kinect v2 sensor (Microsoft, Redmond, WA, USA) for close range 3D modelling and it revealed that caution should be paid when dark colours (i.e. dark shoes) are used. However, if strictly necessary, errors might be reduced by performing specific black-target calibration of the infrared ToF sensor and by adjusting the measurement range for larger distances (higher than 200 mm).

The device performance was tested both in static and dynamic conditions at distances in the range of 40–190 mm and sensor-target orientations between 0 ° and ±60 °. The latter values were chosen to include values of SW and foot progression angles similar to those observable during normal and pathological gait [61]. In general, for AoI equal to 0 °, the infrared ToF sensor performed equally well both in static and dynamic acquisitions among all distances, while errors increased as the AoI increased. During static acquisitions, MAE values varied between 1.4 mm and 7.8 mm when increasing the AoI up to ±60 °. The latter trend is likely to occur because the incident rays emitted by the IR illumination cone, striking the non-orthogonal target surface, are reflected with an AoI equal to the target orientation, and this would modify the phase shift once detected by the view cone. In dynamic acquisitions, MAE values varied between 1.5 mm (AoI = 0 °) to 25.6 mm (AoI = −60 °). The larger errors, observed during the dynamic acquisitions compare to the static ones, may be related to the unavoidable uncertainty associated to the correct identification of the instant of time during which the infrared ToF sensor is in front of the target (imposed known distance) (Figure 5.3). In fact, when the AoI is equal to 0 ° (pendulum oscillating parallel to the target surface), the sensor-target distance is constant (Figure 5.5a); conversely, when AoI is different from 0 °, the sensor-target distance changes with time (Figure 5.5b, 5.5c). Since the gyroscope output data rate (ODR) is 100 Hz, the time difference between two consecutive samples is 10 ms. This implies that the maximum error in the identification of the instant of time, which maximizes the angular velocity, is 5 ms. By performing simple geometrical calculation, given AoI = ±60 °, a length of the pendulum l = 600 mm and ω = 6 rad/s, a time shift of 5 ms causes an error in the estimated distance equal to ±31 mm. This hypothesis was preliminarily confirmed by the experimental results reported in Figure 5.7, which showed a weak but positive correlation between the error magnitude and the angular velocity for AoI different from zero. However, given the limitations found in the pendulum experiments (worsening of the performance for AoI values larger than 30 °, high pendulum angular velocity and black target colour), future studies under real conditions (i.e human movement) should pay attention to the effects of different gait speeds and patterns (e.g. healthy and pathological), excessive foot progression angles and different types of shoes.

Part II

Applications

6

Gait analysis - Inter-foot distance measurement on healthy adults

6.1 Abstract

The aim of this study is the validation of a novel custom-made wearable system (SWING) for the inter-foot distance estimation. The SWING system consists of a MIMU and up to three infrared time-of-flight distance sensors (DSs). The SWING system, attached to the medial side of a foot, is capable of providing distance measurements between feet during walking. Sixteen healthy adults walked on level ground along a loop (including rectilinear and curvilinear paths) at self-selected pace for two minutes in two different sessions (test and retest) with and without a target on the medial side of the contralateral foot. The SWING system showed a mean absolute error in the range of 10.5–13.2 mm with target and 9.3–12.4 mm without target.

6.2 Introduction

In the last decade, we have been witnessing an increased use of low cost wearable technologies for objective and ecological assessment of gait, stability and balance during daily life activities [26], [62]–[64]. Generally, wearable motion capture systems consist of a single or a network of (magneto-)inertial measurement units

This chapter is based on:

- S. Bertuletti, A. Cereatti, and U. Della Croce, "Inter-foot distance measurement in healthy adults during gait using a wearable prototype device: Validation on straight walking and turning for different distance sensor locations", in *19th Proceedings of SIAMOC*, 2018.
- S. Bertuletti, A. Cereatti, and U. Della Croce, "A wearable system based on Time-of-Flight technology for direct derivation of step number and step width on healthy gait", in *Proceedings of GNB*, 2018.

((M-)IMUs). These systems allow for gait cycles segmentation, initial and final contacts identification and the determination of temporal gait parameters (e.g. stride time, double support time, swing time, etc.). Spatial parameters (e.g. stride length and width, step length and width, etc.) are typically estimated by combining the temporal parameters estimates with foot kinematics information. There is a large body of literature that evaluated the performance of different methods for the estimation of the spatio-temporal gait parameters on both healthy and pathological populations (e.g. multiple sclerosis, Parkinson, stroke, etc.) [26], [62]–[64] from (M-)IMUs data. However, none of the (M-)IMU systems allow for direct measurements of the relative distance between the subject's feet, which are necessary to estimate the SW or the base of support (BoS) over time [65] which are relevant when gait instability and risk of falling are of interest [55], [56], [66]. To overcome these limitations, some researchers have combined (M-)IMU with other technologies which are able to provide information about distance such as ultrasound (US) [32] and light intensity infrared (IR-LI) [38]. US sensors estimate a distance by measuring the time required by an ultrasonic wave to travel from the transmitter to the receiver. This technology is characterised by an ODR up to 40 Hz and a power consumption up to 15–30 mA, which may limit the use of this technology for long-term monitoring applications. Furthermore, for the measurement of the SW, it requires to instrument both feet: one with the US transmitter and the contralateral one with the US receiver. Another technology, based on IR-LI sensors, determines the distance by measuring the amount of light reflected from an object. This technology allows for a higher ODR (about 60 Hz), but its accuracy is heavily dependent on experimental factors. In fact, the amount of light reflected by an object depends on its colour, reflectance and material.

Recently, a new sensor technology has been made available: infrared time-of-flight DS [67]. By using this technology, the distance is estimated by measuring the phase shift between the emitted and the reflected IR waves. The advantages of this technology are: *i*) greater robustness to the colour of the target and the environmental conditions (such as ambient light) than IR-LI; *ii*) faster response than ultrasound due to the higher wave propagation speed (ODR up to 50 Hz); *iii*) transmitter and receiver in the same small chip (i.e. VL6180X: $4.8 \times 2.8 \times 1\,\text{mm}^3$ [53]). Thus, it is not strictly required to instrument both feet such as for US (transmitter and receiver) and IR-LI (sensor and target). In a previous work [2], the performances of the DS were evaluated under experimental conditions resembling those encountered during gait by varying the colour of the target, the distance and the angle between the DS and the target. In addition, a very preliminary measurement of the inter-foot distance (IFD) on a single healthy subject during

straight gait was reported. In the current work, we present and validate a novel custom-made wearable system (SWING; patent pending) for the IFD estimation during walk on sixteen healthy subjects. The performance of the SWING system was evaluated against an optoelectronic stereo-photogrammetric system (SP system) by taking into account different DS positions on the foot, different walks and with and without a target attached to the contralateral foot.

6.3 Materials and Methods

6.3.1 Hardware description

A description of the SWING system (52L × 38W × 16H mm^3; weight 28 g) is provided in Figure 6.1 and Figure 6.2. The processing core is an ultra-low-power 32-bit controller (7 × 7 mm^2) with 100 DMIPS (dhrystone million instructions per second) peak capability and an extremely low-power consumption, scalable down to 84 µA/MHz. The SWING system integrates a 3D accelerometer (up to ±16 g), a 3D gyroscope (up to ±2000 °/s) and a 3D magnetometer (up to ±16 gauss). Zero, one, two or three DSs can be connected simultaneously to the SWING system (SWING, $SWING^{DS}$, $SWING^{2DS}$ or $SWING^{3DS}$). Each DS provides distance estimates in the range of 0–600 mm by measuring the time the IR waves take to travel to the nearest object (e.g. foot) and reflect back to the distance sensor. For this specific study, magneto-inertial data were sampled at 100 Hz and the full scales were set to

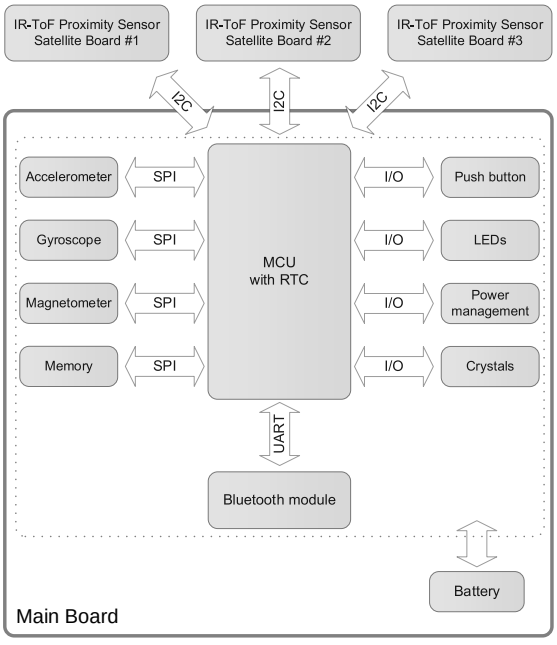

Figure 6.1 – Block diagram of the SWING system.

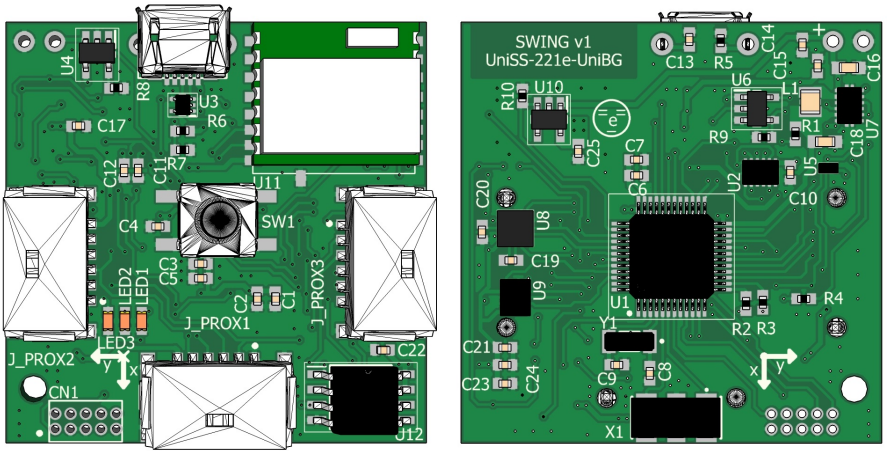

Figure 6.2 – Top and bottom view of the 3D rendering of the SWING system.

±16 g, ±2000 °/s and ±4 gauss for the accelerometer, gyroscope and magnetometer, respectively. Only two of the three available DSs were used (SWING^{2DS}). Distance data were acquired at 50 Hz (maximum frequency allowed) and the measurement range was set to 0–200 mm since the maximum distance between feet during gait in healthy subjects is generally less than 200 mm [55], [56]. To improve the DSs accuracy, for each DS, an ad hoc calibration between 0–200 mm was performed.

6.3.2 Experimental setup and Data acquisition

Data from sixteen healthy subjects (6 females and 10 males; age [mean ± sd]: 39 ± 11 years) were acquired in the AIMA Laboratory of Porto Conte Ricerche. The SWING^{2DS} system was mounted in a specifically designed plastic rigid support attached to the medial side of the right foot (Figure 6.3a). DSs were positioned close to the heel ($REAR_{DS}$) and the first metatarsophalangeal joint ($FORE_{DS}$). Experimental sessions consisted in two minutes walking on level ground at a self-selected pace along a loop (rectilinear and curvilinear walks). Two distinct sessions (test and retest) were recorded (one week apart). For each subject, gait data were collected both with and without a rectangular target ($200 \times 100\,mm^2$) attached to the medial side of the left foot (Figure 6.3b and 6.3c). The target was used to eliminate measurement uncertainties due to the irregular shape of the shoe. Subjects wore their own shoes of the colours of their choice. A cluster of three markers was placed on each foot (on the heel, on the big toe and below the ankle) and its position was recorded using a ten-camera SP system (Vicon Motion Systems,

Oxford, UK; 100 Hz).

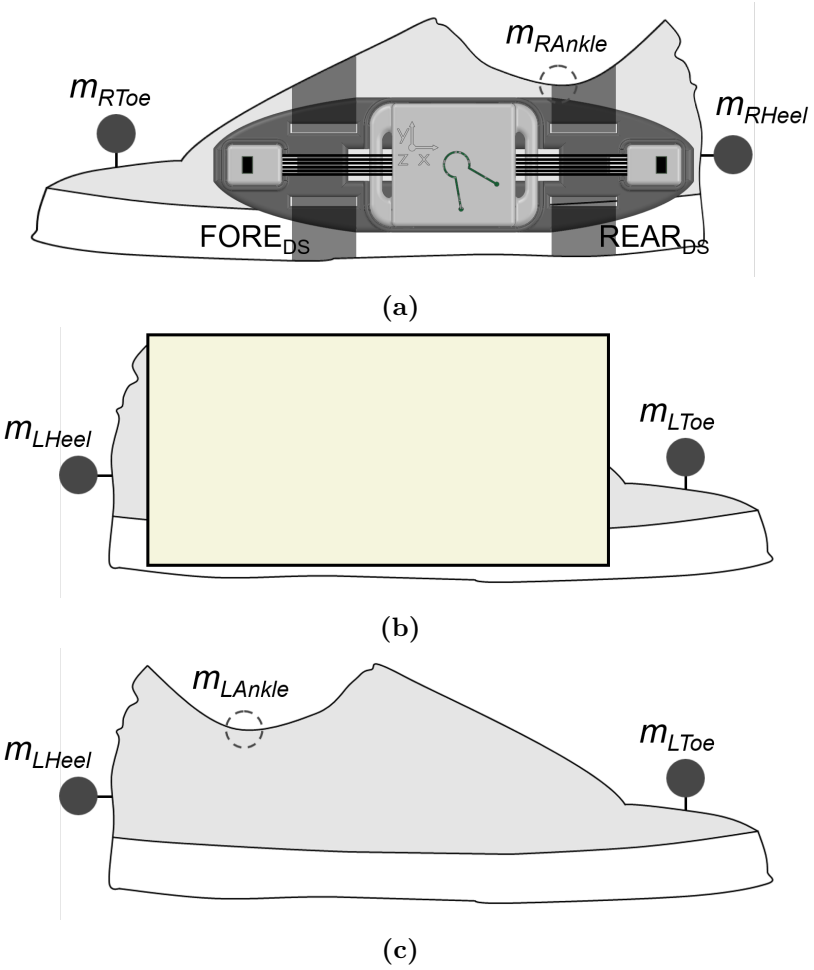

Figure 6.3 – The SWING^{2DS} system, target and markers placement on the feet: (a) instrumented right foot; (b) left foot with target; (c) left foot without target.

6.3.3 Data analysis

Each subject was asked to hit the instrumented foot on the force plate (electronically synchronised with the SP system) three times at the beginning and three times at the end of each session to synchronise the SWING^{2DS} system and the SP system.

Both clusters of three markers were used to define a foot technical coordinate system. Left foot medial surface (target/shoe) and SWING geometry (MIMU and DSs positions) were defined in the coordinate system during an initial static calibration acquisition by using ten additional markers (two on the DSs, one on the MIMU centre, three on the support and four on the target/left foot medial side) (Figure 6.4). The marker-based IFD was obtained as the distance between the marker on the DS and the intersection point (IP) between the medial surface of

the left foot and the line orthogonal to the support passing through the DS. The comparison between the IFD estimates obtained with the SWING^{2DS} system and those provided by the SP system was carried out only for those steps for which the IP fell into the polygon defining the medial foot surface (IFD-step#). For each subject, the mean and standard deviation of the IFD obtained with the SP system system ($IFD_{SP} \pm sd$) and with the SWING^{2DS} system ($IFD_{SWING} \pm sd$), the mean and standard deviation of the error ($e \pm sd$), the mean absolute error (mae) and the mean absolute percentage error ($mae_{\%}$) were computed. The mean of the latter indices were computed over gait cycles and subjects ($E \pm SD$, MAE, $MAE_{\%}$).

Figure 6.4 – Markers positioning during the initial static calibration acquisition. The marker positioned on the fifth metatarsophalangeal joint was not considered in the data analysis of this study.

6.4 Results

The total IFD-step# analysed for the measurement of the IFD for $REAR_{DS}$ was equal to 1504 (rectilinear: 792; curvilinear: 712) for test with target, 1353 (rectilinear: 755; curvilinear: 598) for retest with target, 751 (rectilinear: 389; curvilinear: 362) for test without target and 771 (rectilinear: 446; curvilinear: 325) for retest without target, while for $FORE_{DS}$ IFD-step# was equal to 2135 (rectilinear: 1233; curvilinear: 902) for test with target, 2060 (rectilinear: 1255; curvilinear: 805) for retest with target, 1803 (rectilinear: 1006; curvilinear: 797) for test without target and 1688 (rectilinear: 997; curvilinear: 691) for retest without target.

The computed indices were reported, for both DSs locations, in Table 6.1 for rectilinear walks with target, in Table 6.2 for curvilinear walks with target, in Table 6.3 for rectilinear walks without target and in Table 6.4 for curvilinear walks without target for each session (test and retest). Mean IFD values measured by $FORE_{DS}$ ($REAR_{DS}$) varied between 77.9 mm (63.7 mm) and 89.2 mm (75.5 mm)

with target and between 81.4 mm (64.0 mm) and 88.6 mm (90.2 mm) without target. When the target was used, the MAE varied in the range of 10.5–13.2 mm and 11.7–24.1 mm for $FORE_{DS}$ and $REAR_{DS}$, respectively. Without target the MAE varied between 9.3 mm and 12.4 mm for $FORE_{DS}$ and between 11.8 mm and 24.0 mm for $REAR_{DS}$.

Table 6.1 – Performance of $REAR_{DS}$ and $FORE_{DS}$ for the measurement of the inter-foot distance (IFD) during rectilinear sections of a loop for test and retest session using the target on the contralateral foot.

		$IFD_{SP} \pm SD$ [mm]	$IFD_{SWING} \pm SD$ [mm]	$E \pm SD$ [mm]	MAE [mm]	$MAE_{\%}$ [%]
$REAR_{DS}$	Test	63.2 ± 12.4	65.4 ± 11.9	2.2 ± 10.4	11.7	35.8
	Retest	59.9 ± 12.5	63.7 ± 12.3	3.8 ± 9.9	12.8	39.1
$FORE_{DS}$	Test	82.9 ± 14.6	77.9 ± 15.1	-5.0 ± 9.2	10.8	14.1
	Retest	82.7 ± 14.5	80.8 ± 16.0	-1.9 ± 10.6	10.5	15.7

Table 6.2 – Performance of $REAR_{DS}$ and $FORE_{DS}$ for the measurement of the inter-foot distance (IFD) during curvilinear sections of a loop for test and retest session using the target on the contralateral foot.

		$IFD_{SP} \pm SD$ [mm]	$IFD_{SWING} \pm SD$ [mm]	$E \pm SD$ [mm]	MAE [mm]	$MAE_{\%}$ [%]
$REAR_{DS}$	Test	71.4 ± 22.8	74.4 ± 20.4	3.0 ± 28.9	24.1	63.5
	Retest	73.5 ± 22.7	75.5 ± 20.3	2.0 ± 27.3	22.0	64.2
$FORE_{DS}$	Test	90.0 ± 27.3	83.8 ± 26.2	-6.2 ± 12.7	12.9	15.2
	Retest	92.1 ± 26.0	89.2 ± 25.2	-2.9 ± 14.5	13.2	17.2

Table 6.3 – Performance of $REAR_{DS}$ and $FORE_{DS}$ for the measurement of the inter-foot distance (IFD) during rectilinear sections of a loop for test and retest session without using the target on the contralateral foot.

		$IFD_{SP} \pm SD$ [mm]	$IFD_{SWING} \pm SD$ [mm]	$E \pm SD$ [mm]	MAE [mm]	$MAE_{\%}$ [%]
$REAR_{DS}$	Test	64.0 ± 11.5	68.9 ± 12.4	4.9 ± 10.3	11.8	20.9
	Retest	61.1 ± 10.0	64.0 ± 12.8	2.9 ± 10.2	12.7	20.9
$FORE_{DS}$	Test	80.6 ± 13.8	81.4 ± 15.4	0.8 ± 10.6	9.3	13.2
	Retest	85.1 ± 14.6	82.0 ± 15.9	-3.2 ± 11.7	11.5	15.3

Table 6.4 – Performance of $REAR_{DS}$ and $FORE_{DS}$ for the measurement of the inter-foot distance (IFD) during curvilinear sections of a loop for test and retest session without using the target on the contralateral foot.

		$IFD_{SP} \pm SD$ [mm]	$IFD_{SWING} \pm SD$ [mm]	$E \pm SD$ [mm]	MAE [mm]	$MAE_{\%}$ [%]
$REAR_{DS}$	Test	82.8 ± 22.2	90.2 ± 18.5	7.3 ± 28.1	24.0	38.7
	Retest	80.0 ± 19.7	78.6 ± 21.2	-1.4 ± 28.2	22.9	30.7
$FORE_{DS}$	Test	91.6 ± 24.7	88.6 ± 24.6	-3.0 ± 12.8	11.1	13.0
	Retest	95.1 ± 24.8	88.6 ± 24.2	-6.5 ± 12.5	12.4	13.9

6.5 Discussion

In this study, an innovative wearable custom-made system for the IFD measurement was developed, presented and validated on sixteen healthy subjects during two distinct sessions one week apart. Contextually, we compared the results obtained with and without the use of a rectangular target on the contralateral foot for two different DS locations (forefoot and rearfoot) and for two different walking paths (rectilinear and curvilinear).

The use/non-use of the target did not affect the accuracy of both DSs. In fact, the MAE obtained for $REAR_{DS}$ was in the range of 11.7–24.1 mm with target and in the range of 11.8–24.0 mm without target, while for $FORE_{DS}$ it varied between 10.5–13.2 mm with target and 9.3–12.4 mm without target. Consequently, also the colour of the shoes (four grey shoes, three white shoes, three brown shoes, two black shoes, two blue shoes and one red and one green shoe) worn by the subjects did not influence the DSs accuracy.

On the contrary, an effect of the DS location ($REAR_{DS}$ vs $FORE_{DS}$) and type of walking path (rectilinear vs curvilinear) was observed. Similar results were obtained while comparing $REAR_{DS}$ and $FORE_{DS}$ during straight walks (11.7–12.8 mm vs 9.3–11.5 mm), while larger errors were obtained for $REAR_{DS}$ during turns. In this condition, $FORE_{DS}$ (MAE between 11.1 mm and 13.2 mm) performed better than $REAR_{DS}$ (MAE in the range of 22.0–24.1 mm). Therefore, $FORE_{DS}$ performed equally well for both rectilinear and curvilinear walks, while $REAR_{DS}$ performed much better during straight walks with respect to turns.

The errors obtained using $FORE_{DS}$ (MAE in the range of 10.5–13.2 mm with target and 9.3–12.4 mm without target) were similar to those obtained using US (MAE = 12 ± 12 mm) [32] and slightly larger than those obtained using IR-LI (MAE in the range of 5.3–10.1 mm) [68]. However, it should be considered that

[68] and [32] acquired only one and three subjects, respectively. Compared to US and IR-LI sensors, which required to instrument both feet (transmitter/receiver or sensor/target), the SWING system required to instrument only one foot. This circumstance is particularly beneficial when monitoring/evaluating subjects during their daily-life activities.

6.6 Conclusion

The findings of this study confirmed that the SWING system, mounted only on one of the two feet, is a valid solution for measuring the IFD during gait in both rectilinear and curvilinear paths. Forefoot (FORE_{DS}) turned out to be the best DS location on the foot. In fact, FORE_{DS} performed better than REAR_{DS} in both conditions (with/without target and rectilinear/curvilinear paths).

However, this study was limited to the analysis of the SWING performance to healthy adults walking in a laboratory setting. In a future work, the use of the SWING system will be extended to pathological groups performing more complex walking tasks (six-minute walk test, timed up and go test, etc.). Furthermore, a sensor fusion algorithm integrating magneto-inertial and distance data will be developed to obtain SW measurements which are necessary for the estimation of the BoS.

7

Gait analysis - Direct bilateral step detection on healthy adults

7.1 Abstract

Accurate step detection is crucial for the estimation of gait spatio-temporal parameters. Although several step detection methods based on the use of inertial measurement units (IMUs) have been successfully proposed, they may not perform adequately when the foot is dragged while walking, when walking aids are used, or when walking at low speed. The aim of this study was to test an original step-detection method, the inter-foot distance step counter (inter-foot distance (IFOD)), based on the direct measurement of the distance between feet. Gait data were recorded using a wearable prototype system (SWING^{2DS}), which integrates an IMU and two time-of-flight distance sensors (DSs). The system was attached to the medial side of the right foot with one DS positioned close to the forefoot ($FORE_{DS}$) and the other close to the rearfoot ($REAR_{DS}$). Sixteen healthy adults were asked to walk over ground for two minutes along a loop, including both rectilinear and curvilinear portions, during two experimental sessions. The accuracy of the IFOD step counter was assessed using a stereo-photogrammetric system as gold standard. The best performance was obtained for $REAR_{DS}$ with an accuracy higher than 99.8 % for the instrumented foot step and 88.8 % for the non-instrumented foot step during both rectilinear and curvilinear walks. Key features of the IFOD step counter are that it is possible to detect both right and left steps by instrumenting one foot only and that it does not rely on foot impact dynamics. The IFOD step counter

This chapter is based on:
S. Bertuletti, U. Della Croce, and A. Cereatti, "A wearable solution for accurate step detection based on the direct measurement of the inter-foot distance", *Journal of Biomechanics*, vol. 84, pp. 274 –277, 2019, ISSN: 0021-9290. DOI: https://doi.org/10.1016/j.jbiomech.2018.12.039. [Online]. Available: http://www.sciencedirect.com/science/article/pii/S0021929018309382.

can be combined with existing IMU-based methods for increasing step-detection accuracy.

7.2 Introduction

The accurate detection of steps during gait is crucial for the estimation of gait parameters that are typically analysed in clinical assessments and to measure daily motor activity-related quantities, such as the distance walked, gait speed, and energy expenditure [69], [70]. During the last decade, inertial measurement units (IMUs) have been increasingly used to measure human movement both in clinical settings and in free-living conditions [26], [71]. IMU-based step detection is obtained by recording accelerations and angular velocities from various body locations and by analysing the signals features using one of several methods proposed in the literature [68], [72]–[76]. However, the performance of IMU-based methods generally deteriorates when highly abnormal gait patterns are analysed, when walking aids are used and when walking at low speed [77]–[79]. In this work, we preliminarily tested an original method for bilateral step detection based on the direct measurement of the distance between feet during gait, the inter-foot distance (IFOD) step counter. Gait data were recorded using a single miniaturised prototype system (SWING^{2DS}) attached to the foot, which incorporated two infrared time-of-flight distance sensors (DSs) [53]. The performance of the IFOD step counter was assessed on healthy subjects for two different DS locations on the foot, during two over-ground walking sessions (test and retest).

7.3 Methods

7.3.1 System description - SWING^{2DS} system

The SWING^{2DS} includes a magneto-IMU and two DSs (mod. VL6180X, STMicroelectronics, Switzerland [53]) and represents an upgraded version of the D-MuSe system in terms of hardware performance and number of connectable DSs [2]. The system was embedded on a custom 3D-printed rigid support (Figure 7.1) and attached to the medial side of the right foot with the IMU z-axis made to coincide with the medio-lateral axis of the foot (Figure 7.2a). The DSs were positioned orthogonally to the support and close to the first metatarsophalangeal joint ($FORE_{DS}$) and to the heel ($REAR_{DS}$).

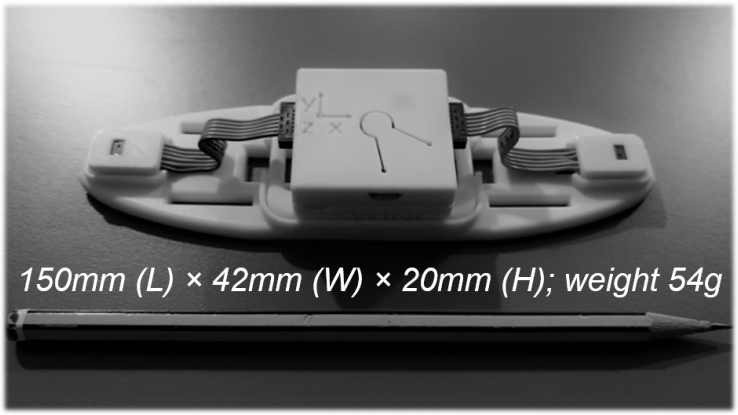

Figure 7.1 – The SWING^{2DS} system embedded on a custom 3D-printed rigid support.

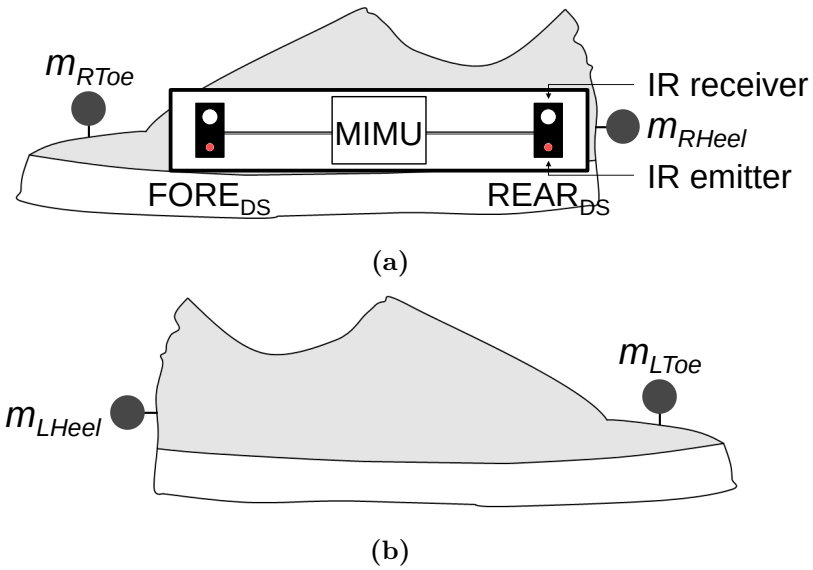

Figure 7.2 – Experimental setup: (a) right foot with the SWING^{2DS} system (instrumented foot); (b) left foot (non-instrumented foot).

7.3.2 Step detection method - IFOD step counter

During walking recordings, each DS returned a distance value when the two feet faced each other, hence twice per gait cycle, once during the swing of the instrumented foot (instrumented step (IN-step)) and once during the swing of the non-instrumented foot (non-instrumented step (NIN-step)). Bilateral step detection was performed by directly counting the number of time intervals characterised by non-zero distance values. Two non-zero distance values were considered to belong to the same time interval, and therefore identified the same step, if the time between the readings was less than 200 ms. This condition was applied to consider the potential multiple-distance readings during the same IN-foot swing (e.g. one distance reading at early-mid swing when the instrumented foot faces the contra-lateral shank and

another at late swing when facing the contralateral foot). IN-steps and NIN-steps were discriminated offline by applying a subject-specific threshold on the values of the angular velocity component around the medio-lateral axis (ω_{ML}). Specifically, a non-zero distance time interval characterised by angular velocity higher than the 30 % of the maximum ω_{ML} were labelled IN-steps and those that were lower were labelled NIN-steps.

7.3.3 Experimental data collection

SWING^{2DS} inertial data and DSs data were collected at 100 Hz and 50 Hz (DS maximum frequency) with the full scale of the gyroscope set to $\pm 2000\,^{\circ}/s$ and the DS measurement range set to 0–200 mm. For validation purposes, two markers were placed on each foot (markers on the heel and on the first metatarsal head) (Figure 7.2). Markers' trajectories were recorded using a nine-camera Vicon Bonita stereo-photogrammetric system (SP system) sampling at 100 Hz. SWING^{2DS} and SP systems were software synchronised. The number of actual steps (A-step#) was counted by visually inspecting the heel and toe markers trajectories recorded with the SP system. After providing their written informed consent, sixteen healthy adults (age [mean $\pm$ sd]: 39 ± 11 y.o.) walked on level ground at a self-selected pace for two minutes along a loop (including both curvilinear and rectilinear portions) during two sessions (test and retest, one week apart). Local ethics committee approval was previously obtained.

7.3.4 Data processing and Accuracy assessment

Rectilinear and curvilinear walking sections were identified and segmented based on the trajectory of the heel marker of the instrumented foot, expressed in the SP coordinate system. For both DS locations ($REAR_{DS}$ and $FORE_{DS}$), the IFOD step counter accuracy was evaluated under the following conditions: a) type of gait (rectilinear, curvilinear), b) side (IN-step, NIN-step), and c) session (test, retest). As the SWING^{2DS} and SP systems were synchronised, for every experiment it was possible to quantify *i*) A-step#, *ii*) the number of missed and extra steps obtained with the IFOD step counter, and *iii*) the accuracy of the IFOD step counter. The latter was computed as the ratio between the IFOD step count (IN-step# and NIN-step#) and the actual number of steps (A-step#). For each condition, the average of the accuracy values across subjects was computed.

7.4 Results

An example of synchronised time-series of raw REAR_{DS} and FORE_{DS} data and right and left heel markers z-axis trajectories during a rectilinear walk is reported in Figure 7.3.

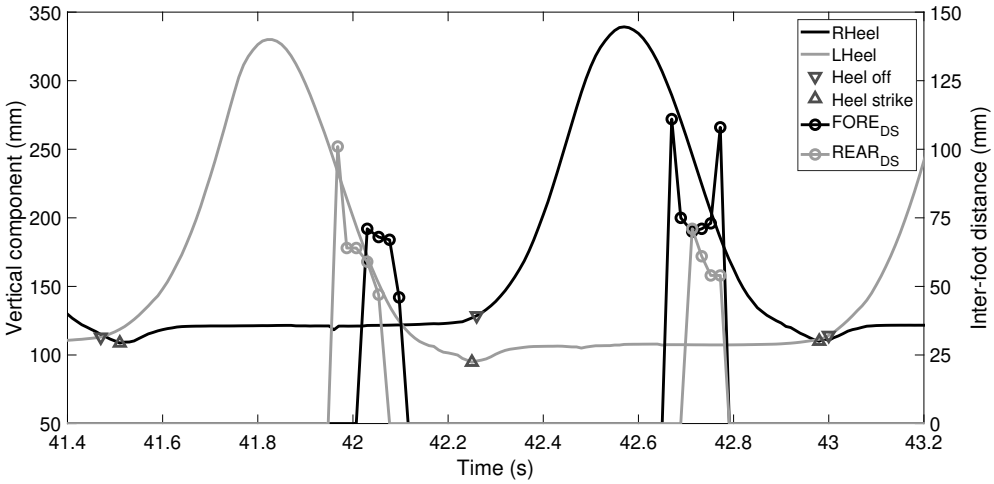

Figure 7.3 – Synchronised time-series of raw $\text{SWING}^{\text{2DS}}$ data (REAR_{DS} and FORE_{DS}) and vertical component (z-axis) of right and left heel markers (triangular markers indicate the heel strike and heel off) for the stride of a subject during a rectilinear walk.

A total of 5,077 steps were analysed: 2,763 in the rectilinear portion of the loop (IN-step#=1,390 and NIN-step#=1,373) and 2,314 in the curvilinear (IN-step#=1,151 and NIN-step#=1,163) portion of the loop. The performance of the IFOD step counter is reported for rectilinear walks in Table 7.1 and Table 7.2 and for curvilinear walks in Table 7.3 and Table 7.4. For neither DS location the IFOD step counter detected extra steps. The accuracy of REAR_{DS} (FORE_{DS}) varied in the range of 96.1–100 % (92.0–99.9 %) during rectilinear walking and between 88.8–100 % (75.8–100 %) during curvilinear walking.

Table 7.1 – Performance of the IFOD step counter for REAR_{DS} and FORE_{DS} locations and test and retest sessions for the detection of the instrumented step (IN-step) during rectilinear walking portions.

		A-step [#]	Missed [#]	Extra [#]	Accuracy [%]
REAR_{DS}	Test	684	0	0	100.0
	Retest	706	0	0	100.0
FORE_{DS}	Test	684	1	0	99.9
	Retest	706	3	0	99.6

Table 7.2 – Performance of the IFOD step counter for $REAR_{DS}$ and $FORE_{DS}$ locations and test and retest sessions for the detection of the non-instrumented step (NIN-step) during rectilinear walking portions.

		A-step [#]	Missed [#]	Extra [#]	Accuracy [%]
$REAR_{DS}$	Test	687	0	0	100.0
	Retest	686	27	0	96.1
$FORE_{DS}$	Test	687	18	0	97.4
	Retest	686	55	0	92.0

Table 7.3 – Performance of the IFOD step counter for $REAR_{DS}$ and $FORE_{DS}$ locations and test and retest sessions for the detection of the instrumented step (IN-step) during curvilinear walking portions.

		A-step [#]	Missed [#]	Extra [#]	Accuracy [%]
$REAR_{DS}$	Test	575	0	0	100.0
	Retest	576	1	0	99.8
$FORE_{DS}$	Test	575	0	0	100.0
	Retest	576	6	0	99.0

Table 7.4 – Performance of the IFOD step counter for $REAR_{DS}$ and $FORE_{DS}$ locations and test and retest sessions for the detection of the non-instrumented step (NIN-step) during curvilinear walking portions.

		A-step [#]	Missed [#]	Extra [#]	Accuracy [%]
$REAR_{DS}$	Test	576	6	0	99.0
	Retest	587	66	0	88.8
$FORE_{DS}$	Test	576	58	0	89.9
	Retest	587	142	0	75.8

7.5 Discussion

The IFOD step counter detects steps during both straight and curvilinear walks based on direct measurements of the time-variant inter-foot distance. The most effective DS location was the back of the foot ($REAR_{DS}$) which showed, for both rectilinear and curvilinear conditions, an accuracy higher than 99.8 % and 88.8 % for IN-step and NIN-step detection, respectively. The method's accuracy slightly deteriorated in the $FORE_{DS}$ configuration, and in particular for NIN-step detection during the curvilinear walking (accuracy $\geq$ 75.8 %). It is worth noting that the

lower accuracy observed during retest session was the result of the SWING^{2DS} system being positioned too close to the ground for two of the subjects. In those cases, during the stance of the instrumented foot, the DS did not detect any distance because the subjects raised the non-instrumented foot higher than DSs (Figure 7.4a). If those two subjects are excluded from the analysis, the IFOD step counter applied to the $REAR_{DS}$ detected both IN-steps and NIN-steps with a 100 % accuracy during both rectilinear and curvilinear walks.

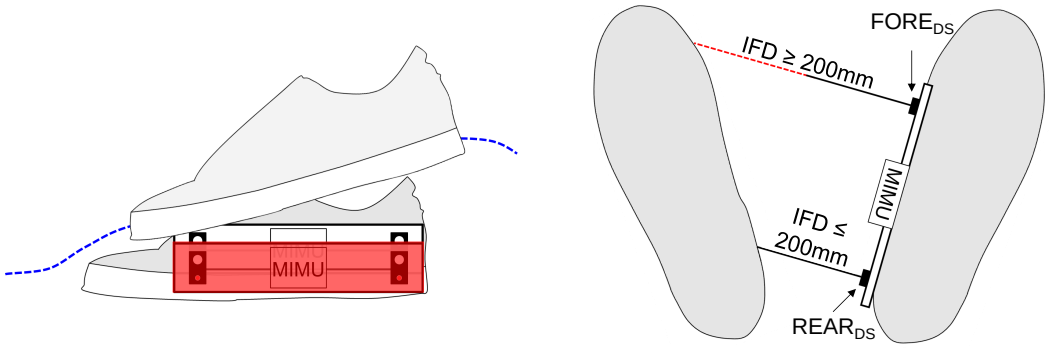

Figure 7.4 – Potential missed step scenarios: (a) distance sensor positioned too close to the ground and/or large foot clearance of the contralateral foot during swing; (b) abnormal foot external rotation during walking and/or excessively large BoS.

Key features of the IFOD step counter, compared to previously proposed IMU-based methods, are that it needs only one foot to be instrumented to detect both left and right steps, and the step detection does not rely on foot-impact dynamics or on angular velocity patterns. Indeed, the IFOD step counter relies exclusively on a single feature of walking: the feet facing each other twice in a gait cycle. For this reason, the IFOD step counter can represent an attractive solution for step detection in subjects walking with severe gait impairments (e.g. hemiparetic subjects dragging a foot) or using walking aids, although its accuracy in populations with gait disorders has not yet been assessed. Conversely, as opposed to IMU-based methods, the IFOD step counter cannot be used to determine initial and final foot contacts, which are used to identify the gait cycle phases. However, as the IFOD step counter and IMU-based methods are based on different sensor technologies, they have complementary features, and could therefore be combined and integrated within a sensor fusion framework, increasing step detection accuracy while reducing

the limitations of a single specific technology. Within the experimental setup adopted in this study, potential limitations are that *i*) a step may be missed when a subject walks with an excessive external foot rotation, causing a distance between feet larger than the maximum distance range of the DSs, *ii*) a step may be missed when a subject walks with a large foot clearance causing no reflection of the infrared (IR) waves emitted by the DSs, and *iii*) an extra step may be counted while walking on uneven ground which causes a reflection of the IR waves emitted by the DSs with something between the feet. Therefore, while implementing the IFOD step counter, precautions should be taken: the DS should not be positioned too close to the ground and its measurement range should be set high enough to consider excessive external foot rotation [80] (Figure 7.4). Since an increase of the range of measurement implies both a decrease of the DS sensor resolution and a lower sample frequency (i.e. range 0–200 mm: 1 mm resolution and 50 Hz maximum sample frequency; range 0–400 mm: 2 mm resolution and 33 Hz maximum sample frequency; range 0–600 mm: 3 mm resolution and 25 Hz maximum sample frequency), a trade-off should be pursued. Two potential solutions to increase the method's robustness are *i*) the design of a support that enables the user to adjust the orientation of the DS to compensate for excessive external foot rotation, and *ii*) the placement of the DS on the shank to reduce the effect of excessive external foot rotation and artefacts due to uneven terrain.

8

Clinical gait analysis - Direct bilateral step detection on multiple sclerosis patients

Multiple sclerosis (MS) is a chronic and progressive neurological disease of the central nervous system characterised by inflammatory demyelination and axonal damage which causes conduction delays and blockage of electrical potentials along the neuronal pathway in the central nervous system (Figure 8.1).

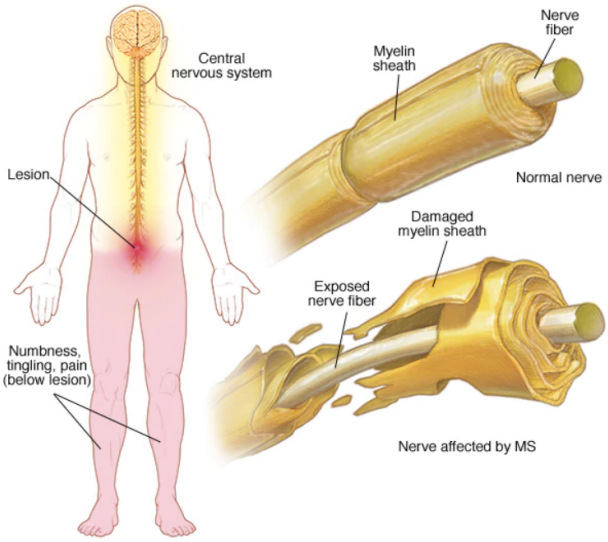

Figure 8.1 – Myelin damage and the nervous system. In multiple sclerosis, the protective coating on nerve fibers (myelin) in the central nervous system becomes detached and eventually destroyed. This creates a lesion that may cause numbness, pain or tingling in parts of the body.
Source: *Mayo Foundation for Medical Education and Research (MFMER).*

This chapter is based on:
S. Bertuletti, F. Salis, A. Cereatti, L. Angelini, E. Buckley, K. Nair, C. Mazzà, and U. Della Croce, "Inter-leg distance measurement as a tool for accurate step counting in patients with multiple sclerosis", *IEEE Engineering in Medicine and Biology Magazine (under review)*, 2019.

MS affects about 2.5–3 million adults worldwide (700.000 in Europe, of which 118.000 in Italy and 100.000 in United Kingdom) and it is diagnosed mostly between 20 and 40 years old and in women twice as many as men (Figure 8.2). The diagnosis of MS is based on the McDonald criteria (clinical, radiographic, and laboratory criteria) [81] that was revised first in 2005 [82], second in 2010 [83] and later in 2017 [84]. The causes of MS are not yet clear, but can be attributed to a combination of genetic factors, environmental and epigenetic influences.

Symptoms of MS are heterogeneous and include optic neuritis, fatigue, weakness, gait ataxia, spasticity, cognitive and bowel problems [85]. Four types of MS are named according to the way the disease acts on the body over time:

- Relapsing-Remitting MS which is the most common form of MS (about 85 %). People with Relapsing-Remitting MS have temporary periods called relapses, flare-ups or exacerbations, when new symptoms appear;
- Secondary-Progressive MS in which symptoms worsen more steadily over time, with or without the occurrence of relapses and remissions;
- Primary-Progressive MS which occur rarely (about 10 %). It is characterised by slowly worsening symptoms from the beginning, with no relapses or remissions;
- Progressive-Relapsing MS which affects only the 5 % of people with MS. It is characterised by a steadily worsening disease state from the beginning, with acute relapses but no remissions, with or without recovery.

Among mobility limitations, impairment of gait is the most common in MS. In fact, epidemiological studies have reported that 50 % of people with MS require assistance on walking after 15 years old diagnosis [87]. Furthermore, La Rocca [88] showed that, among 1011 people with MS, 41 %% reported difficulty of walk.

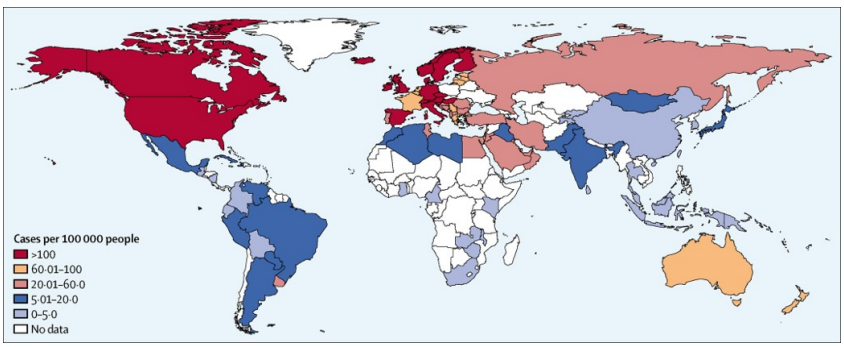

Figure 8.2 – Global number of people with multiple sclerosis.
Source: [86], Figure 1.

The most widely used outcome to measure the disability of a MS patient is the expanded disability status scale (EDSS). EDSS is a method of quantifying disability and monitoring changes in the level of disability over time based on a neurological examination. EDSS scale ranges from 0 (normal) to 10 (death due to MS), in 0.5 unit increments. EDSS steps from 1.0 to 4.5 refer to people with MS who are able to walk without any aid, while EDSS steps from 5.0 to 9.5 are defined by disability of walking [89]. Since the main limitation of the EDSS is related to the subjective nature of the neurological examination, an objective assessment of the disability and disease progression is necessary. Wearable sensors can be an attractive solution to objectively quantify the pathological conditions as well as monitoring the progression of disease or the influence of a treatment.

8.1 Abstract

Step detection is commonly performed using wearable inertial devices. However, methods based on the extraction of signals features may deteriorate their accuracy when applied to very slow walkers with abnormal gait patterns. The aim of this study is to test and validate an innovative step counter method (distance sensor step counter (DiSC)) based on the direct measurement of inter-leg distance. Data were recorded using an innovative wearable system which integrates a magneto-inertial unit and multiple time-of-flight distance sensors (DS) attached to the shank. The method allows the detection of both left and right steps using a single device and was validated on thirteen people affected by multiple sclerosis ($0 < \text{EDSS} < 6.5$) while performing a six-minute walking test. Two different measurement ranges for the distance sensor were tested (DS_{200}: 0–200 mm; DS_{400}: 0–400 mm). Accuracy was evaluated by comparing the estimates of the DiSC method against video recordings used as gold standard. Preliminary results showed a good accuracy in detecting steps with half the errors in detecting the step of the instrumented side compared to the non-instrumented (mean absolute percentage error 2.4 % vs 4.8 % for DS_{200}; mean absolute percentage error 2 % vs 5.4 % for DS_{400}. When averaging errors across patients, over and under estimation errors were compensated, and very high accuracy was achieved ($E_{\%} < 1.2\,\%$ for DS_{200}; $E_{\%} < 0.7\,\%$ for DS_{400}). DS_{400} is the suggested configuration for patients walking with a large base of support.

8.2 Introduction

MS is a chronic and progressive immune mediated neurological disorder of the central nervous system which causes conduction delays and blockage of electrical potentials along the central neuronal pathways. Although people with MS have a life expectancy similar to that of the general population, they suffer from multiple symptoms including spasticity, weakness, tremor, fatigue, cognitive disabilities and difficulties in performing daily activities. About 40 % of people with MS have difficulty in walking and 50 % requires walking assistive aids within 15 years of diagnosis [87], [88]. The most commonly used clinical scale to monitor the progress of a patient with MS is the EDSS. The EDSS ranges from 0 (normal) to 10 (death due to MS). Scores from 0 to 2 refer to people with MS who have mild disability, 3 to 5 refer to people with moderate disability, but can still walk at least 100 meters without aids, while scores above 6 refer to people with MS who require an aid to walk (severe disability) [89].

The six-minute walking test (6MWT) is also a valid and reliable test to assess walking in people with MS. Recently, the 6MWT has been better characterised with wearable inertial sensors (IMU) thus providing a finer and quantitative description of a subject's gait. The effectiveness of IMU-based analysis has already been extensively proven [26]. However, IMU-based methods may not be effective in detecting steps when gait patterns are highly abnormal (e.g. low speed walks, foot-dragging walks, use of walking aids) [79]. In such cases, alternative technological solutions are required to overcome the intrinsic limitations associated with the IMU-based methods. In this respect, time-of-flight distance sensor (DS) represents a promising technology for human movement analysis applications due to its small form factor ($4.8 \times 2.8\,\mathrm{mm}^2$), high sampling frequency (up to 50 Hz), large measurement range (up to 600 mm) and high spatial resolution (down to 1 mm) [53]. The aim of this study is to test and validate an innovative method to detect the steps of people with MS while performing a 6MWT. The method is based on the direct measurement of the inter-shank distance, using a time of flight distance sensor (DS) integrated with IMUs. The method, referred to as DiSC, is based on the use of a single wearable system (SWING), which integrates a magneto-IMU and a DS, and allows the detection of both right and left steps. In a previous study, the DiSC method was evaluated on gait data recorded on healthy adults during two different experimental sessions [1]. In the present study, we applied and validated the DiSC method on a group of subjects with MS (with moderate to severe disability) while performing a 6MWT.

8.3 Materials and Methods

8.3.1 System description – SWING system

The SWING wearable multi-sensor system developed at the Bioengineering Laboratory of the University of Sassari, integrates a triaxial accelerometer (full-scale range of $\pm 2/\pm 4/\pm 8/\pm 16$ g), a triaxial gyroscope ($\pm 125/\pm 250/\pm 500/\pm 1000/\pm 2000\,^{\circ}$/s), a triaxial magnetometer ($\pm 2/\pm 4/\pm 8/\pm 12$ gauss) and up to three time-of-flight distance sensors (mod. VL6180X, STMicroelectronics, Switzerland [53]). Each DS provides distance readings by estimating the time that an electromagnetic wave (i.e. infrared ray) takes to travel a distance or, more properly, by measuring the phase shift between the emitted and the reflected signals. Magneto-inertial measurements are sampled at a maximum frequency of 200 Hz, while DSs readings are sampled up to 50 Hz. A summary of the specifications of the time-of-flight DS are reported in Table 8.1.

Table 8.1 – Specifications of the VL6180X time-of-flight distance sensor [53].

Range [mm]	Resolution [mm]	Sampling frequency [Hz]
0 – 200	1	Up to 50
0 – 400	2	Up to 33
0 – 600	3	Up to 25

A Bluetooth module and a 128 Mbit flash non-volatile memory were integrated into the system to enable stream and log modes (e.g. 2 h data logging at 100 Hz while recording magneto-inertial data and distance data from all three DSs), respectively. Figure 8.3 shows the block diagram of the SWING system.

8.3.2 Participants

The recruitment of participants and data collection took place at the Royal Hallamshire Hospital, Sheffield, UK. The study was conducted according to the declaration of Helsinki and received ethical approval from the North of Scotland ethics committee (Protocol No. STH19739, 21-11-2017). The inclusion criteria for the participation in the study were: *i*) diagnosis of MS based on the McDonald's criteria (revised in 2017) [84], *ii*) age $>$ 18 years, *iii*) cognitive ability to give informed consent, and *iv*) ability to walk for six minutes without rest. A total number of 13 participants were recruited after obtaining an informed consent. The patient

information sheet with letter of invitation, the informed consent form, and the data collection form are reported in Appendix A. The severity of MS was measured using the EDSS [88]. Participants' demographic and clinical characteristics are shown in Table 8.2.

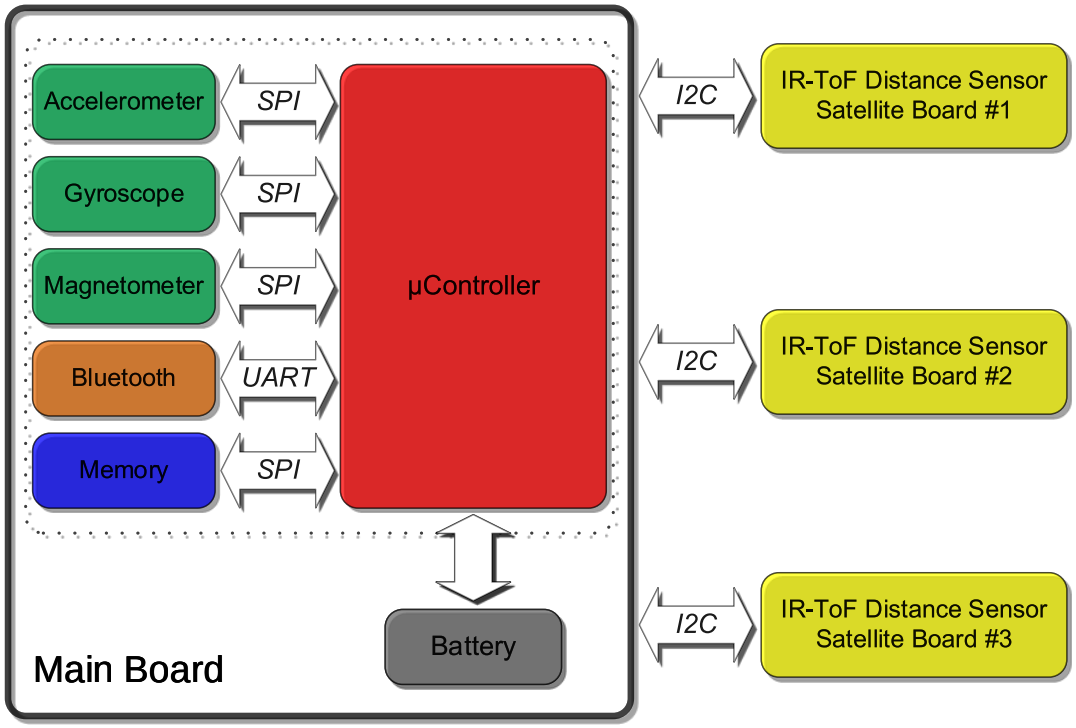

Figure 8.3 – Block diagram of the SWING system.

Table 8.2 – Demographic and clinical characteristics of patients.

Characteristics [I]	
Age (years)	42 ± 12
Sex (women:men)	5 : 8
Height (m)	1.74 ± 0.10
Weight (kg)	75 ± 20
MS type (n, %)	
RRMS	11/13 (85 %)
SPMS	2/13 (15 %)
MS duration (months)	133 ± 107
EDSS	5 ± 2

[I] All data are presented as mean ± SD unless otherwise noted; RRMS = relapsing-remitting multiple sclerosis; SPMS = secondary-progressive multiple sclerosis.

8.3.3 Equipment and protocol

To identify the most appropriate DS measurement range, the SWING system was used in the two-DSs configuration (SWING^{2DS}) with two different full scales (DS_{200}: 0–200 mm; DS_{400}: 0–400 mm). The SWING^{2DS} system was attached to the medial side of the right shank by means of a custom made support and two elastic straps (Figure 8.4). Recordings started with participants in the standing position for about 5 s with their heels aligned to the start line. Participants were asked to complete a 6MWT while walking in a corridor along a closed loop (including 10 m straight and turn portions) (Figure 8.5). Two video cameras (60 frames per second) were placed one at each turn of the loop and used as reference system.

Figure 8.4 – A patient with multiple sclerosis wearing the SWING^{2DS} system positioned above the right medial malleolus with the DS pointing to the contralateral leg.

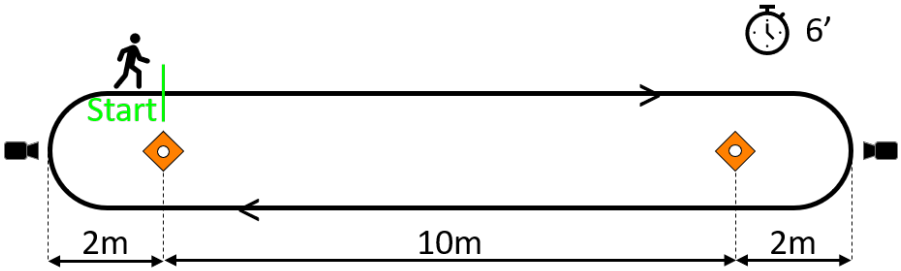

Figure 8.5 – A schematic view of the six-minute walking test performed by a patient with multiple sclerosis.

8.3.4 Data analysis

The DiSC method consisted of two phases: 1. the detection of right and left steps, and 2. the distinction between instrumented and non-instrumented steps (IN-step/NIN-step).

Bilateral step detection was performed using distance data provided from each DS by counting the number of distinct non-zero distance values intervals. Distance readings were considered to belong to the same step when separated by a time interval below 200 ms, to account for accidental multiple-distance readings during the same IN/NIN-step (early-mid swing and late swing phases).

The distinction between IN-step and NIN-step was performed offline. First, the medio-lateral component of the angular velocity (ω_{ML}) was pre-processed by removing the offset. Subsequently, the signal was low-pass filtered (cut-off frequency of 5 Hz) for reducing high frequency noise. The first IN-step was identified as the first non-zero distance data interval with a ω_{ML} value larger than a threshold ε_1 (computed as the 30 % of the mean value of ω_{ML} peaks over the trial). Six minutes of data starting from the instant of time of the initial value of the first IN-step were considered. To distinguish between IN-steps and NIN-steps, for each non-zero distance data interval of duration Δt, the local maximum of ω_{ML} (Δt) was compared with a threshold ε_2 calculated as the 20 % of the mean value of ω_{ML} peaks over the trial. Steps were labelled as IN-step when the maximum ω_{ML} value in the non-zero distance data interval was above ε_2, and as NIN-step when the latter value was below ε_2. An example of the DiSC method application on a participant is depicted in Figure 8.6. The actual number of steps was visually determined by an operator from video recordings for both instrumented and non-instrumented legs (A-IN-step and A-NIN-step). The accuracy of the DiSC method was assessed as the difference between the number of steps estimated using the DiSC method (IN-step and NIN-step, step#) and the number of steps obtained by the reference system (A-step#). Error, percentage error, absolute error and absolute percentage error were computed for each participant as follows:

$$\mathrm{e} = \mathrm{step\#} - \mathrm{A\text{-}step\#} \tag{8.1}$$

$$\mathrm{e}_{\%} = \frac{\mathrm{step\#} - \mathrm{A\text{-}step\#}}{\mathrm{A\text{-}step\#}} \cdot 100 \tag{8.2}$$

$$\mathrm{mae} = |\mathrm{step\#} - \mathrm{A\text{-}step\#}| \tag{8.3}$$

$$\mathrm{mae}_{\%} = \frac{|\mathrm{step\#} - \mathrm{A\text{-}step\#}|}{\mathrm{A\text{-}step\#}} \cdot 100 \tag{8.4}$$

The grand mean and standard deviation values of the latter indices were computed across participants ($\mathrm{E} \pm \mathrm{SD}$, $\mathrm{MAE} \pm \mathrm{SD}$, and $\mathrm{MAE}_{\%} \pm \mathrm{SD}$).

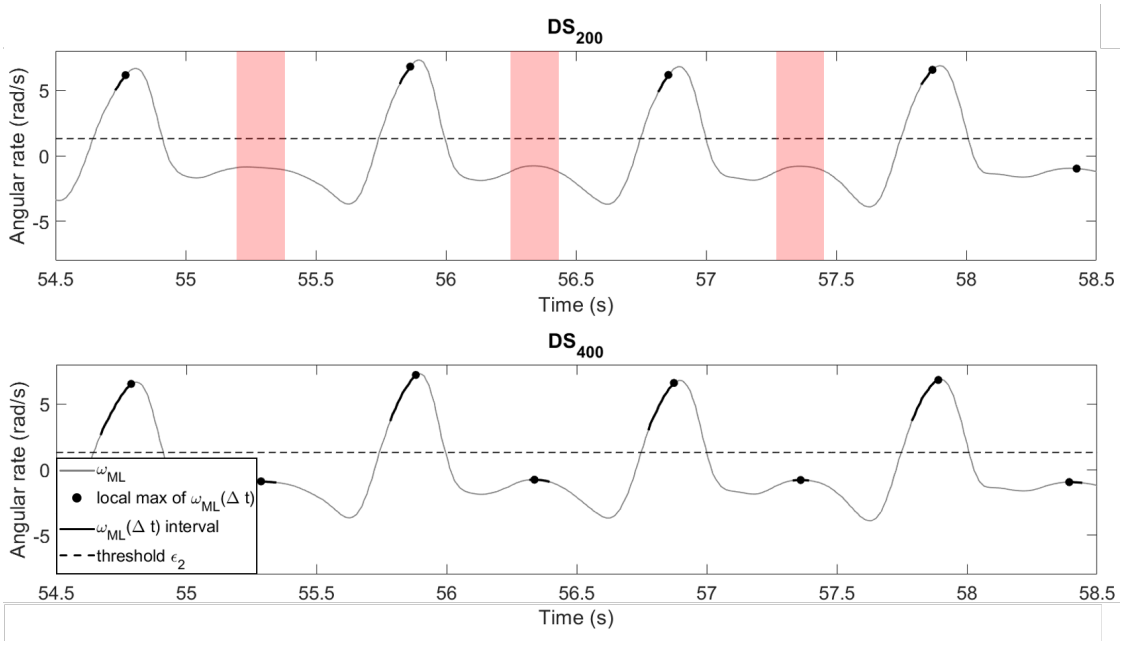

Figure 8.6 – Example of the application of the DiSC method on a participant for the DS_{200} and DS_{400} configuration. Missed NIN-steps are red highlighted.

8.4 Results

Among the total of 6,876 steps, 3,436 were IN-steps and 3,440 were NIN-steps. The overall performances of the DiSC method for both DSs configurations are shown in Table 8.3. The difference plots for IN-step and NIN-step detection are reported in Figure 8.7. In addition, Figure 8.8 shows the errors e for all the participants based on their EDSSs.

Table 8.3 – The DiSC method performance across patients for each DS configuration (DS_{200} vs DS_{400}) and instrumented/non-instrumented leg.

	IN-step		NIN-step	
	DS_{200}	DS_{400}	DS_{200}	DS_{400}
A-step $\pm$ SD (#steps)	264 ± 68		265 ± 67	
step $\pm$ SD (#steps)	263 ± 63	265 ± 65	259 ± 62	264 ± 67
E $\pm$ SD (#steps)	-1 ± 8	0 ± 7	-6 ± 18	0 ± 19
$E_{\%} \pm$ SD (%)	0.2 ± 4.2	0.6 ± 3.2	1.2 ± 8.5	0.7 ± 12
MAE $\pm$ SD (#steps)	5 ± 6	4 ± 5	11 ± 16	9 ± 16
$MAE_{\%} \pm$ SD (%)	2.4 ± 3.4	2 ± 2.5	4.8 ± 7	5.4 ± 10.7

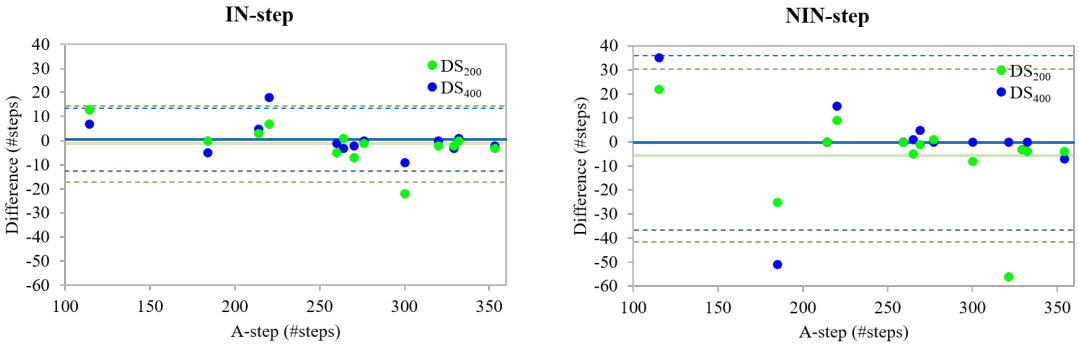

Figure 8.7 – Difference (Bland–Altman) plots for IN-step and NIN-step between DiSC method and reference system. Limits of agreement (±1.96 SD) are, respectively, 16, 13, 36, 36 steps. Bias are, respectively, -1.4, 0.5, -5.7, -0.4 steps. DS_{200} in green and DS_{400} in blue.

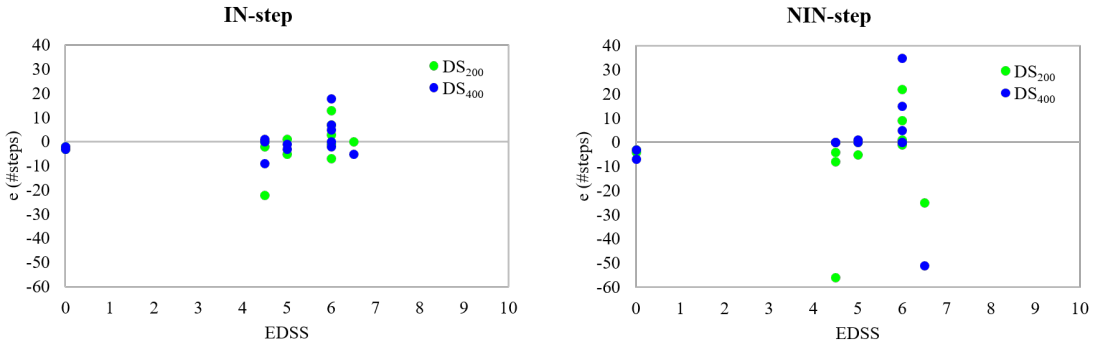

Figure 8.8 – Mean errors (e) for DS_{200} and DS_{400} are reported for each participant based on the EDSS.

8.5 Discussion

Regardless the DS range used, the DiSC method showed good accuracy in detecting steps showing half the errors for IN-steps compared to NIN-steps ($MAE_{\%200}$: 2.4 % vs 4.8 %; $MAE_{\%400}$: 2 % vs 5.4 %). When averaging errors across patients, over and under estimated errors were compensated. Indeed, extremely small mean percentage errors for both scale ranges were achieved ($E_{\%} < 1.2\,\%$ for DS_{200}; $E_{\%} < 0.7\,\%$ for DS_{400}). In general, the performance of DS_{200} and DS_{400} were similar, although for patients walking with a large base of support the DS_{200} underestimated the number of steps (Figure 8.6). In the light of this consideration, the use of DS_{400} is preferable to DS_{200} since while false positive steps can be reduced by improving the specificity of the algorithm, missed steps cannot be recovered. It is interesting to note that in the two patients walking with a cane on the contralateral side (EDSS = 6), the number of steps was overestimated due to false distance readings (35 and 16 steps for DS_{200}; 42 and 33 steps for DS_{400}). When comparing the

results of the present study with those obtained on healthy subjects [1], a slight worsening of the performance is observed ($MAE_{\%}$ in the range of 2–5.4 % vs 0 %) probably due to large inter-leg distances (larger than DS measurement range) and the use of walking aids. Several studies in the literature have discussed the validity of activity monitors/pedometers in step counts across different sensor positions (e.g. wrist, waist, ankle, foot, etc.), tasks (e.g. walking, ascending/descending stairs, running), conditions (e.g. laboratory-setting, free-living) and populations (e.g. healthy, unhealthy) with accuracy in the range of 88–100 % [69], [70], [90]–[98]. In a recent study, Sandroff and colleagues [97] compared the accuracy of two commercial IMU-based systems (StepWatch^{TM} and ActiGraph attached to the shank and waist, respectively) on 63 subjects with MS during 6MWTs at slow, comfortable and fast walking speeds. Accuracy was expressed as the percentage of the actual number of steps taken by direct observation during each of the 6MWT. The best performance was obtained with the StepWatch^{TM} with an accuracy in the range of 95.7–101.8 %, versus 87.3–100.4 % with the ActiGraph. Interestingly, the performance of both step counters worsened when analysing patients with severe disabilities (EDSS in the range of 6–6.5) walking at slow speed. A third commercial IMU-based system (MoveMonitor), positioned on the lower back, was tested and validated by Storm and colleagues [98]. 14 patients with MS (from moderate to severe disability) were recorded while walking in a laboratory setting performing four 15 m straight walks and a one minute walk (including straight walk, turn, and walking in spirals) at comfortable speed. For all the participants with moderate disability (EDSS = 5.0), walking speed above 1.0 m/s, $E_{\%}$ resulted below 4 %. Interestingly, the device accuracy decreased with increasing EDSS score with an $E_{\%}$ larger than 20 % for five participants with severe disability (EDSS = 6.5) walking at a slower speed (< 0.6 m/s). On the contrary, the DiSC method accuracy is expected to improve when analysing such patients since the number of distance readings increases when decreasing the gait speed. A limitation of the present study is that, by using video-recordings as gold standard, we could obtain information on the total number of steps but not on the step-by-step accuracy. Therefore, it was not possible to determine the number of missed and extra steps at subject level but only an aggregate description of the results.

8.6 Conclusion

The present study tested and validated a novel step counter (DiSC method), based on the measurement of the inter-leg distance, on people affected by MS (moderate to

severe disability). The DiSC method showed promising results in terms of accuracy for both tested DS configurations (recommended distance sensor measurement range: 0–400 mm). To improve the overall method accuracy the integration of distance and inertial data in a sensor fusion algorithm can be explored. As future development, the proposed method will be tested on a larger sample of MS patients.

9 Indoor positioning - Distance estimated from Bluetooth low energy signal strength

9.1 Abstract

Bluetooth low energy (BLE) is a wireless technology for exchanging data, over short distances, designed for the Internet-of-Things era. As widely supported by wearable devices (such as smartphones, smartwatches and tablets), BLE has the potential to become an alternative solution for indoor-localisation and proximity sensing. The aim of this work was to perform a thorough characterisation of the RSSI-distance relationship under controlled conditions using two BLE devices. Four calibration models underwent to a comparative evaluation analysis. The best results were obtained using a polynomial model with a mean distance percentage error equal to 25.7 % (0.4 m) in the range of 0–3 m. An overall improvement of 14.3 % (0.24 m) in the distance estimate, compared to the exponential model commonly adopted in the literature, was reported.

9.2 Introduction

The knowledge of the position of an individual during daily-life activities is essential in several applications, such as pedestrian navigation, fall localisation, guidance with handheld devices [99]. GPS is a very effective technology for outdoor localisation [34], [100], however it cannot be used for indoor-applications due to weak penetration into buildings. Since a large part of our day is spent indoor, alternative solutions must be pursued. Localisation using wireless network technologies such as WiFi,

This chapter is based on:
S. Bertuletti, A. Cereatti, M. Caldara, M. Galizzi, and U. Della Croce, "Indoor distance estimated from Bluetooth low energy signal strength: Comparison of regression models", in *Proceedings of IEEE Sensors Applications Symposium (SAS)*, Apr. 2016, pp. 1–5. DOI: 10.1109/SAS.2016.7479899.

Radio Frequency Identification, Ultra Wide Band and MIMU, has been widely investigated [101], [102]. Very recently, Bluetooth technology has been further optimised to minimize the power consumption and cost (BLE) [103]. Its maximum range can be up to 100 m depending on the class of the antenna used. For these reasons, BLE has become the "de facto" radio standard for the Internet-of-Things and it is now embedded in the majority of the wearable devices (mobile phones, tablets, etc.). An important feature of BLE technology is that the Received Signal Strength Indicator (RSSI), defined as the ratio between power of the transmitter and that of the receiver, is available to the users (IEEE 802.11 standard). Since the RSSI decreases as the distance between transmitter and receiver increases, some researchers explored the use of BLE RSSI for distance estimation [104]–[108]. The majority of the studies have modelled the RSSI-distance relationship through an exponential model [104]–[106]. The model calibration is generally based on two calibration points which are used to determine the propagation coefficient of the specific indoor environment and the RSSI offset [105]. However, the BLE signal can be highly unstable and its strength is influenced by a number of experimental factors [109]. These circumstances may limit the overall accuracy level of the distance estimates obtained from "general purpose" BLE wearable devices. In this respect, a thorough characterisation of the RSSI-distance relationship under controlled conditions is a fundamental prerequisite for any localisation applications using BLE devices.

The aim of this study is to address the following specific research questions:

1. What is the best model to represent the relationship between RSSI and distance within a given range?

2. What is the influence of calibration data set size on the estimated distance accuracy?

3. Does the orientation between receiver and transmitter influence the RSSI-distance relationship?

9.3 Materials and Methods

9.3.1 Distance estimation based on RSSI measurement

The relationship between the RSSI and the distance d is generally described by an exponential model [105]:

$$RSSI_{dBm} = -10 \cdot n \cdot log_{10}(d) + A \tag{9.1}$$

where n is a real number between 2 and 4, which depends on the specific environmental conditions and A is the RSSI value reads at an arbitrary selected distance.

By isolating d from (9.1):

$$d = 10^{\frac{-RSSI+A}{10n}} \tag{9.2}$$

The latter exponential model (EXP10) was compared with the following regressive models:

- Exponential (EXPE):

$$d = a \cdot exp^{b \cdot RSSI} \tag{9.3}$$

- Power (POW):

$$d = a \cdot RSSI^b + c \tag{9.4}$$

- Polynomial (POL):

$$d = a \cdot RSSI^2 + b \cdot RSSI + c \tag{9.5}$$

where a, b and c are the parameters that have to be estimated.

9.3.2 Hardware architecture

The system used is composed of two MIMUs and a computer tablet (CT). The devices are connected via BLE as shown in Figure 9.1. The two MIMUs have been programmed to work as a receiver (Master) and a transmitter (Slave) simultaneously. When a device is working as receiver, it can start a connection and read the RSSI from the transmitter. The CT is only used as a support to acquire, store and visualise real-time data from the MIMUs.

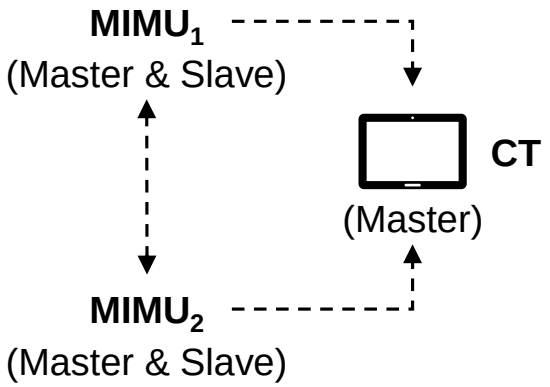

Figure 9.1 – System connection overview.

The hardware architecture consists of two different devices:

- The main component is a small ($13 \times 13\,\text{mm}^2$) and low-power MIMU. The device includes a 3D accelerometer, a 3D gyroscope, a 3D magnetometer, a complete Bluetooth low energy radio with a class two chip antenna (coverage range up to 10 m) [47], [110], an ARM Cortex-M4-based microcontroller and the power supply stage for a Li-poly battery (Figure 9.2).

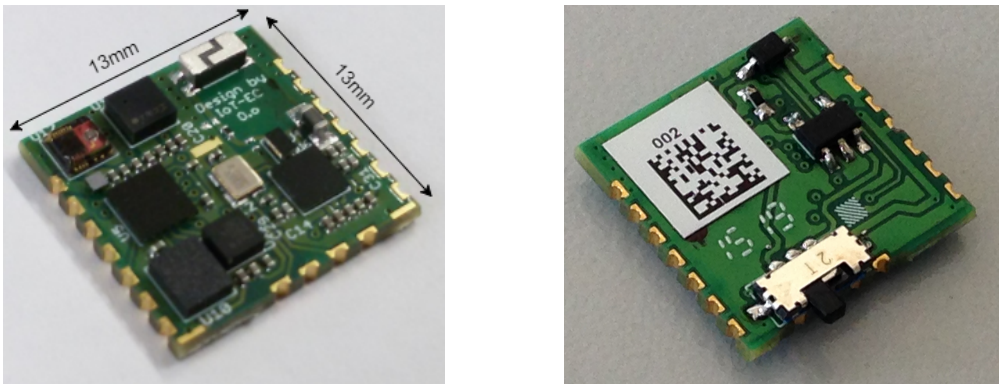

Figure 9.2 – Top and bottom view of the MIMU.

- The second component is a CT Samsung Galaxy Tab 3 Lite equipped with a BLE module (Android KitKat v.4.4.4 operating system). An Android App was developed to acquire data from the MIMUs in real-time. The RSSI acquisition rate was set to 10 Hz. An example of RSSI data read from the MIMU_1 at a distance of 0.5 m is reported in Figure 9.3.

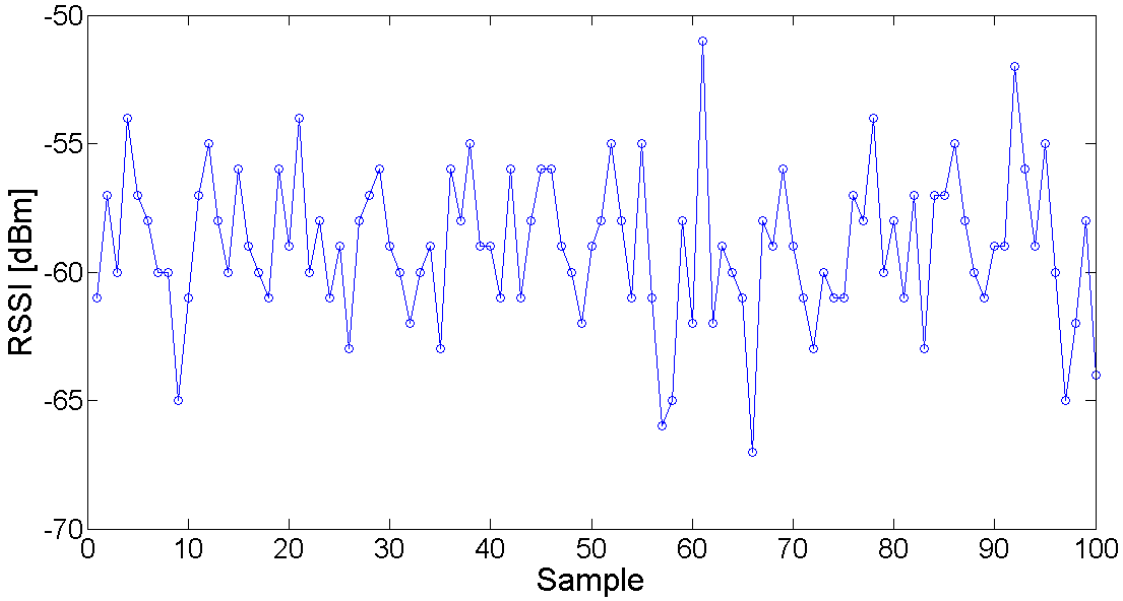

Figure 9.3 – RSSI 10 s acquisition data example.

9.3.3 Experimental setup

$MIMU_1$ was positioned with the z-axis of the antenna pointing vertically and was kept stationary, while $MIMU_2$ was moved to different positions with the x-axis vertical and the z-axis pointing to the $MIMU_1$. According to the antenna datasheet (Figure 9.4) [110], the relative orientation change during the acquisition should have no effect.

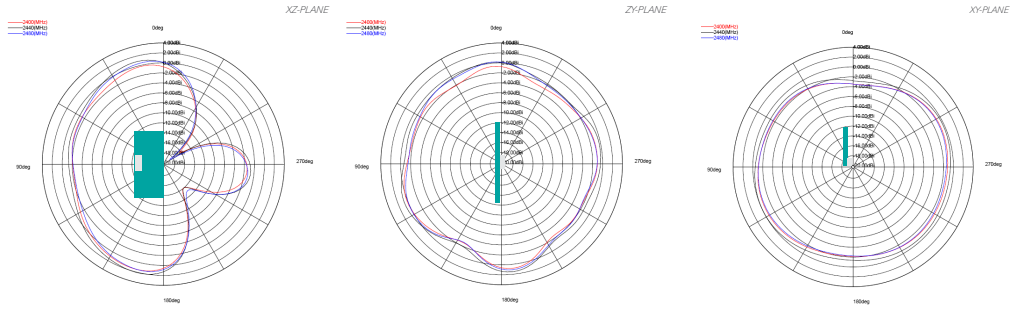

xz-plane zy-plane xy-plane

Figure 9.4 – Typical free space radiation patterns of the W3008C radio antenna.
Source: [110], Page 5.

The experimental data consisted in 10 s static acquisitions (100 RSSI samples) at four different distances (0.5 m, 1 m, 2 m, 3 m) and at different angles (from 0 ° to 180 °, angular increment 15 °) (Figure 9.5). A total of 52 (4×13) positions were explored. For each position, the mean value over the 100 RSSI samples was calculated (experimental data point). Since $MIMU_1$ and $MIMU_2$ have been programmed to work simultaneously as receiver and transmitter, a separate and independent experimental data set was recorded by each MIMU during the abovementioned experimental acquisition protocol.

9.3.4 Model parameters calibration

The determination of the model parameters requires a number of experimental data points equal or higher than the number of parameters. Among the calibration models selected for comparative analysis, the simplest ones are EXP10 and EXPE, which are described by only two parameters. The values of n and A are generally determined using the RSSI values recorded at 1 m and 3 m [105]:

$$n = -\frac{RSSI_{3m} - RSSI_{1m}}{10 \cdot log_{10}(3-1)} \tag{9.6}$$

$$A = RSSI_{1m} \tag{9.7}$$

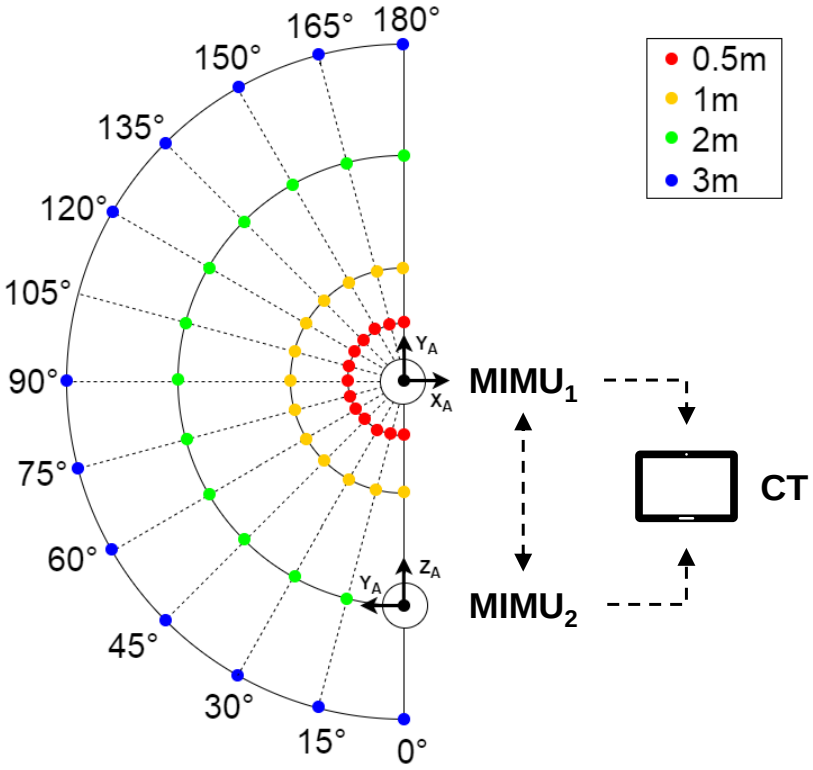

Figure 9.5 – Experimental indoor scenario.

Please note that the latter equations are derived for EXP10, but equivalent solutions can easily obtained for EXPE. However, when more than two experimental data points are available, this redundancy can be exploited to improve the calibration procedure. To investigate the effect of the number of data points, on the distance estimation using two BLE devices, we performed the calibration of the models parameters using three calibration data sets of different size. The first data set (DS_{28}) included the data recorded in 4×7 positions (angular increment 30 °), the second data set (DS_{16}) the data recorded in 4×4 positions (angular increment 60 °) and the third one (DS_{12}) the data recorded in 4×3 positions (angular increment 90 °). Curve fitting were performed on the mean RSSI values, recorded by each MIMU while working as receiver, using the *cftool* provided by MathWorks.

9.3.5 Data analysis

The performance of the four regressive models (EXP10, EXPE, POW and POL), were tested using a validation data set. This was composed by the experimental data points recorded in the 4×6 positions which have not been used for the calibration (from 15 ° to 165 °, angular increment 30 °). For each position i, three inter-MIMUs estimated distances ($\hat{d}_i^{MIMU_1}$, $\hat{d}_i^{MIMU_2}$, $\hat{d}_i^{MIMU_{1,2}}$) were computed. In detail, $\hat{d}_i^{MIMU_1}$ and $\hat{d}_i^{MIMU_2}$ are the estimates provided by $MIMU_1$ and $MIMU_2$

while working as receiver, and $\hat{d}_i^{MIMU_{1,2}}$ is the average value between the latter values. For each estimated distance, the error $e_i = \hat{d}_i - d_i$ was computed. The overall model accuracy was evaluated in terms of grand mean absolute error (MAE) and its percentage value ($\text{MAE}_{\%}$):

$$\text{MAE} = \frac{1}{24}\sum_{i=1}^{24}|e_i| \tag{9.8}$$

$$\text{MAE}_{\%} = \frac{1}{24}\sum_{i=1}^{24}\left|\frac{e_i}{d_i}\right| \cdot 100 \tag{9.9}$$

with $d_i = 0.5\,\text{m}, 1\,\text{m}, 2\,\text{m}, 3\,\text{m}$.

In the ideal case, two BLE devices working simultaneously as receiver and transmitter should read the same RSSI values. To take into account the non-ideal behavior of the sensors, due to the imperfections of the electronics, the RSSI difference between the two BLE devices was evaluated:

$$\Delta_i = |RSSI_{MIMU_1,i} - RSSI_{MIMU_2,i}| \tag{9.10}$$

where $RSSI_{MIMU_1,i}$ and $RSSI_{MIMU_2,i}$ are the mean of the value over the 100 RSSI samples at position i acquired by MIMU_1 and MIMU_2, respectively.

9.4 Results

9.4.1 RSSI-distance relationship

As an example, the relationship between the RSSI data recorded by the MIMU_1 and the tested distances is reported in Figure 9.6. The RSSI values varied from $-61.1\,\text{dBm}$ and $-43.0\,\text{dBm}$ for $0.5\,\text{m}$, $-64.6\,\text{dBm}$ and $-55.0\,\text{dBm}$ for $1\,\text{m}$, $-69.1\,\text{dBm}$ and $-61.5\,\text{dBm}$ for $2\,\text{m}$, $-71.0\,\text{dBm}$ and $-65.7\,\text{dBm}$ for $3\,\text{m}$ (the outlier at $150\,^\circ$ was discharged). The red ellipses indicate the overlapping observed in the RSSI values between two consecutive tested distances. A similar trend was observed for the MIMU_2.

An alternative graphical representation of the RSSI values recorded by the MIMU_1 is depicted in Figure 9.7. The RSSI mean values were $-49.4\,\text{dBm}$ for $0.5\,\text{m}$, $-61.3\,\text{dBm}$ for $1\,\text{m}$, $-64.9\,\text{dBm}$ for $2\,\text{m}$ and $-67.5\,\text{dBm}$ for $3\,\text{m}$. A similar trend was observed for the MIMU_2.

The RSSI differences between the two BLE devices is reported in Table 9.1.

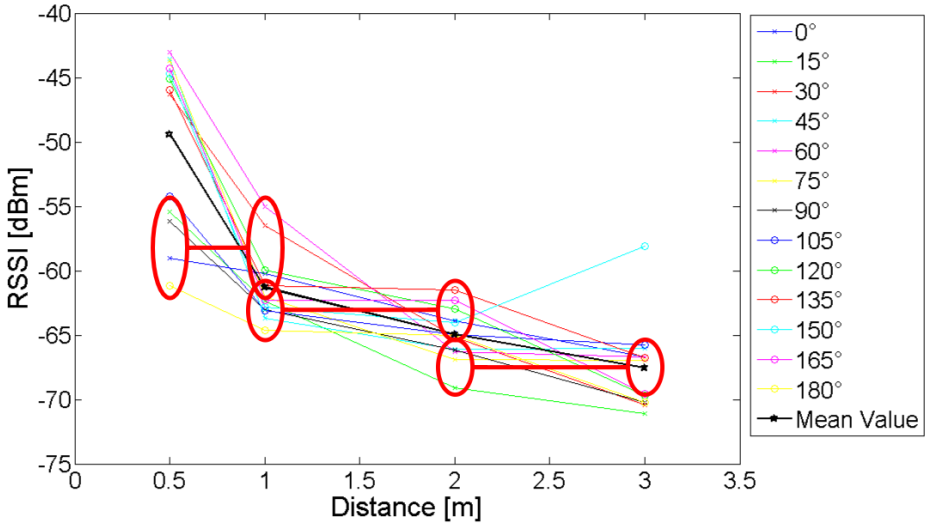

Figure 9.6 – RSSI-distance relationship obtained for the $MIMU_1$ working as receiver.

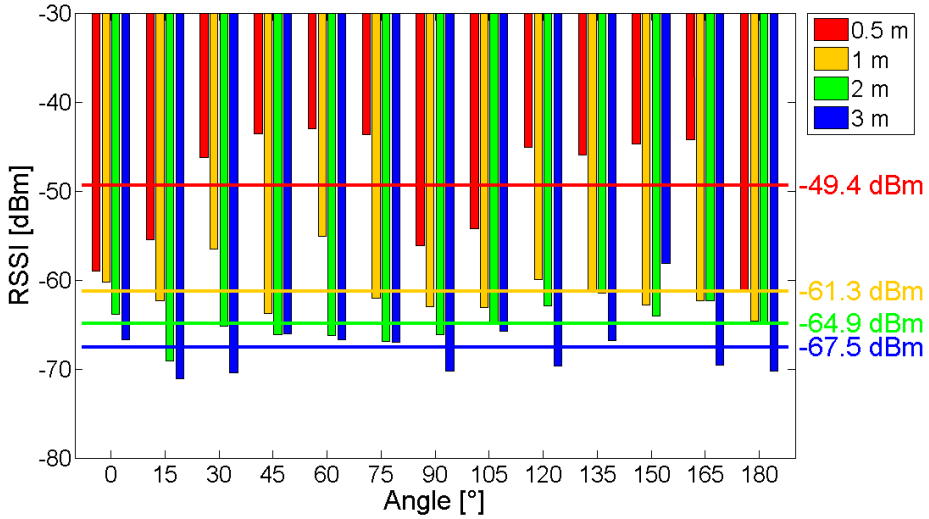

Figure 9.7 – RSSI-angle relationship obtained for the $MIMU_1$ working as receiver.

Table 9.1 – Comparison between $MIMU_1$ and $MIMU_2$ RSSI recorded data.

Distance [m]	Δ [dBm]
0.5	2.0
1	1.4
2	1.2
3	1.0

9.4.2 Regressive model

For sake of comparison with previous studies [104]–[106], [111], [112], the results obtained for EXP10 model using two calibration points, are reported in Table 9.2.

Table 9.2 – EXP10 model results, for $MIMU_1$, $MIMU_2$ and $MIMU_{1,2}$, with two calibration points.

	$MIMU_1$		$MIMU_2$		$MIMU_{1,2}$	
Distance [m]	MAE [m]	$MAE_{\%}$ [%]	MAE [m]	$MAE_{\%}$ [%]	MAE [m]	$MAE_{\%}$ [%]
0.5	0.25	50	0.33	65.5	0.27	54.7
1	0.16	16.4	0.28	28.0	0.20	20.1
2	0.77	38.7	0.86	43.0	0.81	40.8
3	1.39	46.2	1.18	39.3	1.28	42.7
Mean	0.64	37.8	0.66	43.9	0.64	39.6

In general, by assuming that the variance of the RSSI readings is identical for both MIMUs, the estimated distance error is minimised by considering, for each position, the average of the distance estimates provided by $MIMU_1$ and $MIMU_2$ ($MIMU_{1,2}$). Therefore, only the estimated errors $\hat{d}^{MIMU_{1,2}}$ has been reported for the different models and calibration data sets (DS_{28}, DS_{16} and DS_{12}) (Table 9.3, Table 9.4, Table 9.5). The results obtained for EXP10 were not shown because they were identical to those obtained with the EXPE model. The best performance was obtained with the POL model. The average improvements with respect to the EXPE and POW models were equal to 0.04 m and 0.06 m, respectively. No clear trends were observed between the magnitude of the errors and the number of calibration points used. Overall, the magnitude of the errors increased with the distance for all models.

9.5 Discussion

The aim of the present study was to provide a characterisation of the RSSI-distance relationship between two BLE devices in an indoor environment in the absence of obstacles. Looking at Figure 9.6, it is evident that the RSSI values greatly varied changing the relative angle between sensors for a constant distance thus causing overlapping between the RSSI values observed between two consecutive distances. Interestingly, by reorganizing the RSSI values according to the angle values (Figure 9.7), the RSSI consistently decreased by increasing the distance

Table 9.3 – POL model distance estimated errors, for validation data set, using 28, 16 and 12 calibration points.

	Polynomial Model (POL)					
	DS_{28}		DS_{16}		DS_{12}	
Distance [m]	MAE [m]	$MAE_{\%}$ [%]	MAE [m]	$MAE_{\%}$ [%]	MAE [m]	$MAE_{\%}$ [%]
0.5	0.11	21.5	0.06	12.8	0.12	24.4
1	0.64	64.0	0.57	57.2	0.33	33.4
2	0.34	17.0	0.40	20.2	0.45	22.6
3	0.54	17.9	0.57	18.9	0.67	22.3
Mean	0.41	30.1	0.40	27.3	0.39	25.7

Table 9.4 – EXPE model distance estimated errors, for validation data set, using 28, 16 and 12 calibration points.

	Exponential Model (EXPE)					
	DS_{28}		DS_{16}		DS_{12}	
Distance [m]	MAE [m]	$MAE_{\%}$ [%]	MAE [m]	$MAE_{\%}$ [%]	MAE [m]	$MAE_{\%}$ [%]
0.5	0.20	39.9	0.22	43.7	0.27	54.7
1	0.64	63.9	0.57	57.5	0.32	32.5
2	0.33	16.6	0.38	19.1	0.45	22.7
3	0.56	18.5	0.61	20.2	0.75	24.9
Mean	0.43	34.7	0.45	35.1	0.45	33.7

Table 9.5 – POW model distance estimated errors, for validation data set, using 28, 16 and 12 calibration points.

	Power Model (POW)					
	DS_{28}		DS_{16}		DS_{12}	
Distance [m]	MAE [m]	$MAE_{\%}$ [%]	MAE [m]	$MAE_{\%}$ [%]	MAE [m]	$MAE_{\%}$ [%]
0.5	0.12	24.5	0.17	34.1	0.65	129.7
1	0.61	61.0	0.58	57.7	0.34	34.4
2	0.35	17.3	0.38	19.2	0.44	22.1
3	0.58	19.3	0.60	20.1	0.68	22.6
Mean	0.41	30.5	0.43	32.8	0.53	52.2

(the only exception was observed for 45 ° and 3 m; 150 ° and 3 m and 165 ° and 2 m). This is probably due to the effects of the antennas directionality although, according to the BLE antenna datasheet, the antennas should be omnidirectional for the XY and ZY planes [110].

Due to unavoidable differences in the BLE antennas mounted in different devices (Table 9.1), the RSSI values measured for a given distance varied between the two BLE devices. To compensate possible under/over estimation errors, the "optimal guess" was obtained by averaging the distance values provided by each device while working as receiver. This "countermeasure approach" improved the distance estimation, obtained with the best calibration model (POL model), up to 40 % (mean improvement over distances, angles and calibration data points equal to 4.6 %). This simple method can be applied to any device by programming the firmware.

The worst results were obtained for EXP10 using two calibration points (MAE = 0.64 m; $MAE_{\%}$ = 40 %). The best performing calibration model was, irrespective of the calibration data set used, the POL model (Table 9.3). On average, the mean absolute error was about 0.4 m, which correspond to percentage errors between 25.7 % and 30.1 % depending on the number of data points used for the calibration (from 12 to 28). As expected, because EXPE and EXP10 differ only for the base of the exponential function, identical results were obtained. The performance of the different methods showed minor variations for the different calibration data sets used (28, 16, 12 points). In this respect, 12 calibration points seems to assure a good accuracy while reducing the calibration time. A further decrease of the number of data points caused an increase of the errors. The errors reported in this study were obtained by averaging 100 distance estimates (10 s at 10 Hz). However, we verified that by decimating the number of data points from 100 to 10, an average worsening of the POL model performance of 1.8 % (maximum percentage error equal to 3.8 % (0.11 m) at 3 m) was obtained. Furthermore, we programmed the firmware for a RSSI acquisition rate equal to 10 Hz, but, if required, this can be easily set up to 20 Hz.

9.6 Conclusion

The findings of this study confirm that miniaturised system, based on BLE technology, can be proficiently used to provide inter-distance estimates in a $6 \times 3\,m^2$ room with an average percentage error equal to 25.7 % (0.4 m). These performances were obtained using a polynomial model under controlled conditions (absence of

obstacles between transmitter and receiver, no other BLE devices in the environment). For those localisation applications requiring an higher accuracy, a further improvement could be obtained by increasing the number of BLE devices following a "fingerprinting" or trilateration approaches [113]–[115]. However, for proximity sensing applications which require very high accuracy (resolution down to 0.1 m), BLE cannot be proficiently used, while other technologies such as time-of-flight DS, IR-LI or US can. These approaches exploit the information provided by a redundant number of nodes to optimize the final position estimate. It is quite evident that the performance of the latter optimisation methods would benefit from a reduction of the errors affecting the estimate of each inter-nodes distance. Furthermore, sensor fusion algorithms based on the use of MIMU may benefit by the additional information provided by BLE unit to improve the position estimate [116]. This approach has great potential for monitoring human behavior in indoor environment and it opens interesting applications in various fields, such as fall detection, depression monitoring and rescuers navigation.

10

General results, Main contributions, and Future works

The research presented in this thesis consisted in the design and development of an innovative wireless wearable system (SWING, patent pending) consisting of a magneto-inertial measurement unit, a wireless technology for exchanging data (i.e. Bluetooth) and up to three infrared time-of-flight distance sensors.

The performance of the SWING system first were evaluated in static and dynamic conditions similar to those encountered in a real scenario, second were assessed for the measurement of the IFD in healthy people and then were evaluated for the measurement of the steps taken among healthy adults and persons affected by multiple sclerosis. Finally, an alternative way of using the wireless module on-board the system (BLE module) for estimating the position in an indoor environment was reported.

The main results, contributions and future works of this research project are summarised in the following sections.

Development of the SWING system

The SWING system is the result of a design aimed at providing a wireless system-on-board processing capabilities integrating a MIMU and a Bluetooth module (main board) and up to three infrared ToF distance sensors (satellite boards). It was specifically devised to take advantage of the positive points of MIMUs, which are capable of measuring the human movement with an high level of accuracy for a long period of time and during daily life activities, but also to overcome some of their limitations (e.g. drift, ferromagnetic interferences) and to allow the measurement of quantities such as IFD, SW and BoS which could not have been measured when only MIMUs were used.

The advantages of using the infrared ToF technology over other technologies (ultrasound and light intensity infrared) are that the same performance can be obtained with a simpler experimental setup (only one foot instrumented) and with a higher robustness to the changing of the experimental/environmental conditions (e.g. colour of the shoe, ambient light).

Inter-foot distance measurement

From the studies "Inter-foot distance measurement in healthy adults during gait using a wearable prototype device: validation on straight walking and turning for different distance sensor locations" and "A wearable system based on Time-of-Flight technology for direct derivation of step number and step width on healthy gait" (Chapter *Gait analysis - Inter-foot distance measurement on healthy adults*), it was concluded that the SWING system provides reliable and accurate estimates of the inter-foot distance while walking. In particular, the infrared ToF distance sensor positioned on the forepart of the foot ($\mathrm{FORE_{DS}}$) performed equally well during both rectilinear and curvilinear sections and better than that positioned close to the rearfoot ($\mathrm{REAR_{DS}}$) with a mean absolute error (mean absolute percentage error) in the range of 9.3–12.4 mm (13.0–15.3 %).

Step detection

A new method for quantifying the number of steps (IFOD/DiSC method), based on distance measurements (between feet/between lower limbs), was proposed and validated during healthy gait in the study "A wearable solution for accurate step detection based on the direct measurement of the inter-foot distance" (Chapter *Gait analysis - Direct bilateral step detection on healthy adults*) and in people affected by multiple sclerosis in the study "Inter-leg distance measurement as a tool for accurate step counting in patients with Multiple Sclerosis" (Chapter *Clinical gait analysis - Direct bilateral step detection on multiple sclerosis patients*).

The accuracy achieved by the presented method during both rectilinear and curvilinear walks was equal to 100 % for healthy gait (without considering two subjects in which the SWING system was incorrectly positioned), while for pathological gait the overall mean absolute percentage across patients was in the range of 2–5.4 %.

Indoor positioning

Nowadays, the BLE module is embedded in the majority of the smart electronic devices. In "Indoor distance estimated from Bluetooth low energy signal strength: comparison of regression models" (Chapter *Indoor positioning - Distance estimated from Bluetooth low energy signal strength*) a thorough characterisation of the BLE RSSI-distance relationship, under controlled conditions, was performed.

The best results were obtained using a polynomial model with a mean distance percentage error equal to 25.7 % in the range of 0–3 m (compared to the exponential model, commonly adopted in the literature, an improvement of 14.3 % was observed).

BLE shown promising results for indoor-localisation, whereas for distance sensing the accuracy was unsatisfactory due mainly to the fluctuation of the RSSI.

Future works

The SWING system, thanks to the wide spectrum of integrated motion and environmental sensors, can be suitable for a large variety of applications (e.g. sports science, health monitoring, etc.).

A very preliminary test for the detection of the turn switch during an alpine skiing was conducted and reported in Appendix B.

As future development, the proposed methods (IFOD and DiSC) which are mainly based on data provided by time-of-flight DSs and gyroscope will be integrated in a more complex sensor fusion algorithm. The purpose of the integration of accelerations, angular velocities, local magnetic field and distance data is to improve the overall methods accuracy and robustness while recording walks from different pathological groups (e.g. persons affected by chronic obstructive pulmonary disease, Parkinson's disease, multiple sclerosis, proximal femoral fracture, congestive heart failure).

A

Patient Information Sheet and Letter of Invitation, Informed Consent Form and Data Collection Form

Dr K P S Nair

Consultant in Neurology

Royal Hallamshire Hospital

SHEFFIELD

S10 2JF

Secretary: 0114 2712769

e-mail: siva.nair@sth.nhs.uk

Participant Information Sheet and letter of invitation for Persons with Multiple Sclerosis to participate in a Research Study

Version-3 Date 22-11-2017

Ref: **STH19739**

Study Title: **Effect of Ischemic Preconditioning on exercise tolerance in people with Multiple Sclerosis: A feasibility study**

Short title: MSIPC

Principal Investigator: **Dr KPS Nair**

Introduction

You are invited to take part in a research study. Before you decide if you would like to take part it is important to understand why the research is taking place and what it will involve. Please take time to read this information sheet carefully. It provides the purpose of this study and what participation in the study will involve. The procedures will be explained to you by the research staff. Please take the time to read the following information carefully and discuss it with friends, relatives and your GP if you wish. Ask the research staff if there is anything that is not clear or if you would like more information. Take time to decide whether or not you wish to be involved.

1. What is the purpose of the study?

Research has shown that regular physical activity improves physical fitness, fatigue, quality of life, gait and reduce progression of the disability in people with MS. Research has also shown that people with MS are less physically active than the general population. Lack of physical activity increases the risk of obesity, diabetes, and cardiovascular disease. Decreased physical activity is also associated with physical deconditioning, depression and apathy.

Ischaemic preconditioning (IPC) is when parts of the body are exposed to brief periods of blood supply disruption followed by restarting the blood supply. Recent studies have also shown that IPC improves exercise performance. The aim of this study is to see whether it is feasible to use IPC to improve exercise performance in people with MS.

This project forms part of the MSc in Clinical Neurology course. The project will be written up as the student's dissertation.

2. Why have I been chosen?

We are inviting you to participate in this research as our records show that you have Multiple sclerosis

3. Do I have to take part?

No. It is up to you to decide whether or not to take part. If you do, you will be asked to sign a consent form. You will be free to withdraw at any time and without giving a reason. A decision to withdraw at any time, or a decision not to take part, will not affect the standard of care you receive.

4. What will happen to me if I take part?

If you agree to participate in this trial, you will be asked to sign a consent form.

5. What do I have to do during the study period?

The study will take place at The Royal Hallamshire Hospital, Sheffield. If you decide to participate you will spend around two hours with a researcher for a one-off visit. If you decide to participate informed consent will be taken. A copy of this will be given to you, a copy will be filed within your patient notes and the other will be kept with the research team.

Once informed consent has been obtained the researcher will ensure that you meet the relevant criteria to be entered into the study. This will involve reviewing your medical notes and asking some questions regarding your health and medical conditions. Once eligibility has been assessed you will be randomly allocated to the intervention group or

the dummy intervention, known as Sham. You will not be told which group you have been allocated.

Study procedure:

- Your resting blood pressure and heart rate will be measured.
- You will be asked to wear an activity monitor around your waist. This is a small device, around the size of a mobile phone which will be attached to a belt. This will record the speed of the walk, the number of steps taken and the length of your stride. You will be asked to walk for six minutes with the researcher, they will measure the distance covered in 6 minutes. The researcher will then ask you to grade the exertion you experienced using a scale called Rating of Perceived Exertion.
- The researcher will then measure your blood pressure and heart rate again.
- After the six-minute walk test you will be asked to remain sitting for 10 minutes. Your blood pressure and heart rate will be measured again after 10 minutes.
- The researcher will then inflate the blood pressure cuff around your arm to particular pressure. This inflation will be maintained for a period of 5 minutes, followed by 5 minutes of rest. This will be repeated three times. The researcher will ask you to grade any pain or discomfort experienced during the procedures on a scale of 0 (no pain or discomfort) to 10 (worst pain or discomfort every experienced).
- You will once again be asked to remain sitting for 10 minutes, after which your blood pressure and heart rate will be measured once again.
- You will be asked once again to wear the activity monitor and walk for six minutes with the researcher. The researcher will measure the distance covered and will ask you to grade the exertion you experienced using the Rating of Perceived Exertion.
- Your blood pressure and heart rate will be measured for a final time.

6. What are the other possible disadvantages and risks of taking part?

This study requires around an extra two hours during your next scheduled visit to the hospital or an additional hospital visit for two hours.

The Ischaemic Preconditioning is a safe and well tolerated procedure in patients with heart diseases, neurological disorders and in healthy volunteers. We therefore do not anticipate any significant adverse effect from the procedure.

If you feel any pain or discomfort during the study, please inform the researcher. If required, the researcher will get an opinion from the on call neurology team. We will also inform your general practitioner. Please remember that you are free to stop the study at any point without giving any reason.

7. What are the possible benefits of taking part?

There are no direct benefits from taking part in this research. The information we get might help in understanding whether ischaemic preconditioning is a safe and tolerable intervention for people with Multiple Sclerosis.

8. What happens when the research study stops?

Your ongoing treatment will be continued.

9 What if there is a problem?

9.1 Complaints

If you have any concerns regarding this study, you should contact Dr Nair who will do his best to answer your questions. If you remain unhappy and wish to complain formally, you can do this through the NHS Complaints Procedure. Details can be obtained from the Royal Hallamshire Hospital.

You can also contact the Patient Services Team on 0114 271 2400 or via email: PST@sth.nhs.uk

9.2. Harm

In the event that something does go wrong and you are harmed during the research study there are no special compensation arrangements.

The NHS Trust which employs the study doctors and other researchers working under his/her supervision provide insurance cover against claims for negligence (including injury sustained by not following the protocol).

If you sustained an injury due to the negligence of the study doctor or someone working under his/her supervision, procedures are in place to enable you to make a claim for your injury. If you are harmed and this is due to someone's negligence, then you may have grounds for a legal action for compensation against Sheffield Teaching Hospitals NHS foundation Trust but you may have to pay your legal costs.

The normal National Health Service complaints mechanisms will still be available to you. You have the right to withdraw from the study at any time you wish. Should you have any complaints regarding this study, please contact your study doctor.

10. Will my taking part in the study be kept confidential?

All the information about your participation in this study will be kept confidential. The information collected will be anonymised and you will be allocated a study number. Your data will be collected using a study form. There will be no identifiable information on the data form. We will keep a record with your hospital number and the study number, so that we can identify you if required. Only the researchers will have access to this. If the results of the study are published your identity will remain confidential.

Anonymous data collected from you during the study will be electronically stored and processed using computers in Royal Hallamshire Hospital, Glossop Road, Sheffield, S10 2JF. The computers will be password protected and only the research team will be able to access this data. This data will be retained for a period of 15 years and then destroyed. The forms used to collect your data will be stored in lockable filling cabinets in a locked room with restricted access. Under the Data Protection Act of 1998, you have the right to control the use of your medical information and can request to access all information processed about you and have any wrong data about yourself corrected. You can do this through your study doctors.

The information collected will be available to the Sheffield Teaching Hospitals Research and Development department for audit and monitoring purposes.

11. What if relevant new information becomes available?

Sometimes new information becomes available during the course of a research project. If this happens, one of the research doctors involved in this study will tell you about it and discuss whether you want to or should continue in the study. If you decide not to carry on, your research doctor will make arrangements for your care to continue. If you decide to continue in the study you will be asked to sign an updated consent form. Equally, on receiving new information, your research doctor might consider it to be in your best interests to withdraw you from the study. They will explain the reasons and arrange for your care to continue. If the study is stopped for any other reason, you will be told why and your continuing care will be arranged.

12. What will happen if I don't want to carry on with the study?

You can withdraw from the study at any time. Information already collected will be used with your permission.

13. Will my General Practitioner/Family doctor (GP) be informed?

We will inform your general practitioner in case any aspect of this study causes you any distress.

14. What will happen to any samples I give?

This study does not involve taking any samples from you**.**

15. Will any genetic tests be done?

This study does not involve any genetic testing.

16. What will happen to the results of the research study?

We intend to publish these results in medical journal. You will not be identified in any report/publication without your consent. We will also inform you about the results of the trial as and when they are available.

17. Who has reviewed the study?

The North of Scotland Research Ethics Committee (2) has reviewed the study.

Contact Details

Dr KPS Nair

Royal Hallamshire Hospital

Glossop Road

Sheffield S10 2JF

Tel: 0114 2712769

Sheffield Teaching Hospitals NHS
NHS Foundation Trust

Royal Hallamshire Hospital
Glossop Road
Sheffield S10 2JF
e-mail: siva.nair@sth.nhs.uk

INFORMED CONSENT FORM
Version- 2,22-11-2017

Protocol No: **STH19739**

Study Title: **Effect of Ischemic Preconditioning on exercise tolerance in people with Multiple Sclerosis: A feasibility study**

Short title: MSIPC

Investigator: Dr Sivaraman Nair

Please initial box

1) I confirm that I have read and understood the information sheet dated ……version…….. I have had the opportunity to consider the information, ask questions and have had these answered satisfactorily. ☐

2) I understand that my participation is voluntary and that I am free to withdraw at any time without giving a reason, without my medical care or legal rights being affected. ☐

3) I understand that relevant sections of the data collected during the study may be looked at by responsible individuals from the University of Sheffield, from regulatory authorities, or from the NHS Trust, where it is relevant to my taking part in this research. I give permission for these individuals to have access to my records ☐

4) I understand that some personally identifiable information (my name, address, date of birth and telephone number) will be collected but these data will be stored in a locked office in the hospital and be kept separate from responses given during the interview or any medical information. ☐

5) I understand that information will be collected by an MSc Neurology student under the supervision of Dr Nair ☐

6) I agree to allow the team to notify my GP of my participation ☐

7) I agree to take part in the above study ☐

_____	_____	_____
Name of Patient	Date	Signature
_____	_____	_____
Name of Person taking consent (if different from researcher)	Date	Signature
_____	_____	_____
Researcher	Date	Signature

Data Collection Form

Subject No: Hospital No: Group:

Age: Duration since MS diagnosis in Months:

Type of MS:

1- Remitting and Relapsing
2- Secondary Progressive
3- Primary Progressive

EDSS:

10 minutes rest sitting: Yes/No

Resting BP: Resting Heart rate

Timed walk: Distance walked:

Completed 6 minutes: Yes/No If no time walked in minutes

Borg's perceived exertion scale:

Activity monitor data:

BP: Heart rate

10 minute rest- sitting: Yes\No

BP: Hear rate:

Intervention: Group-1/ Group-2

Timed walk: Distance walked:

Completed 6 minutes: Yes/No If no time walked in minutes

Borg’s perceived exertion scale:

Activity Monitor data

Discomfort due to intervention: Please circle a number
0 No discomfort- 10 worst discomfort possible

0 1 2 3 4 5 6 7 8 9 10

BP:

Heart rate:

10 minute rest:

BP:

Heart rate:

Distance walked -2 – Distance walked-1/Distance walked-1 X 100

Adverse events:

B

Sports applications: Alpine skiing

Miniaturised MIMUs have been widely used for sports performance evaluation during both training and competition [27]. Among winter sports, alpine skiing is one of the most popular practiced and studied. In literature, several works analysed the biomechanical aspect of the ski turns [117]–[120]. Yu et al. [119] proposed a method, based on a MIMU sensor, for the analysis of the turn performance to be used by professional skiers while training. Fasel et al. [120] adapted an algorithm designed for the diagonal stride in classical cross-country skiing to compute spatio-temporal parameters for uphill ski mountaineering using a ski-fixed inertial sensor. The aim of this preliminary experiment is to test the applicability of the SWING system to detect the ski turn during a series of rides of an amateur skier based on the boots relative position by using an infrared time-of-flight distance sensor. As depicted in Figure B.1, the SWING^{DS} was attached to the right boot and positioned about 200 mm above the medial malleolus with the DS outer-pointing.

Figure B.1 – Experimental setup: right boot with the SWING^{DS} system.

This appendix is based on:
S. Bertuletti, A. Cereatti, and U. Della Croce, "Detection of the turn switch during alpine skiing using a novel wearable system: A preliminary investigation", in *18th Proceedings of SIAMOC*, 2017.

Despite the very preliminary stage of the present test, the SWING^{DS} system can be used to provide complementary information to those measured by MIMUs. Interestingly, as reported in Figure B.2, the consistent correspondence can be noted between the peaks of the AP-component of the angular velocity and the instant of times when the two boots are facing each other and the DS computed the inter-boot distance. However, further investigations on a large number of subjects and on the effect of the experimental conditions, such as weather, temperature and snow reflections of the infrared ray emitted by the DS must be pursued.

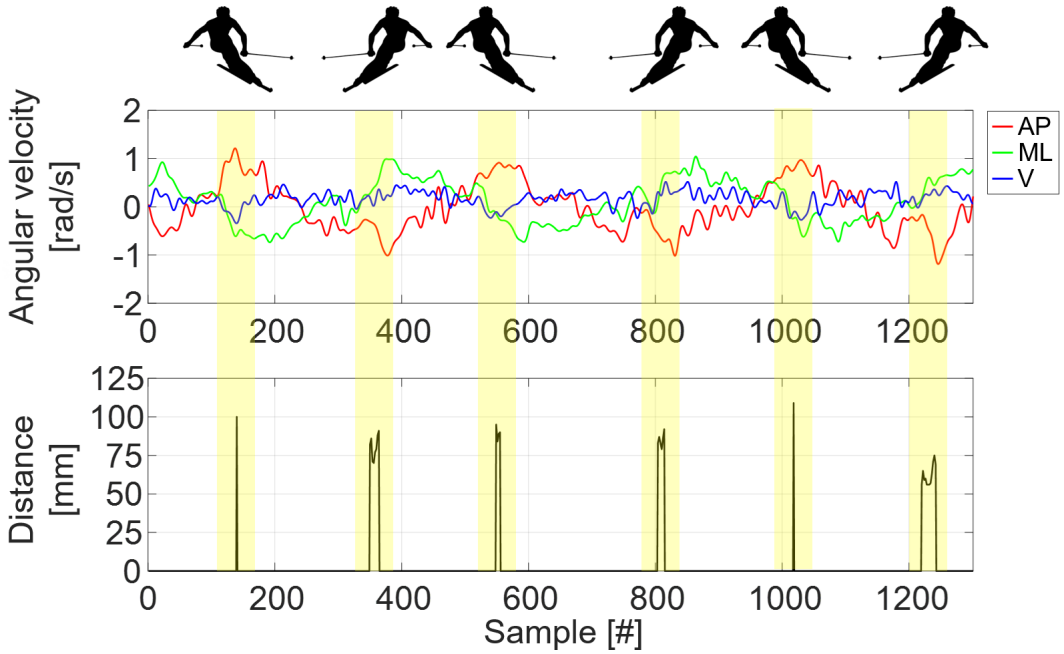

Figure B.2 – Angular velocities (@100 Hz) and DS (@50 Hz) signals acquired during a free ride. The detected ski turns switch are yellow highlighted.

Bibliography

[1] S. Bertuletti, U. Della Croce, and A. Cereatti, "A wearable solution for accurate step detection based on the direct measurement of the inter-foot distance", *Journal of Biomechanics*, vol. 84, pp. 274 –277, 2019, ISSN: 0021-9290. DOI: https://doi.org/10.1016/j.jbiomech.2018.12.039. [Online]. Available: http://www.sciencedirect.com/science/article/pii/S0021929018309382.

[2] S. Bertuletti, A. Cereatti, D. Comotti, M. Caldara, and U. Della Croce, "Static and dynamic accuracy of an innovative miniaturized wearable platform for short range distance measurements for human movement applications", *Sensors*, vol. 17, no. 7, 2017, ISSN: 1424–8220. DOI: 10.3390/s17071492. [Online]. Available: http://www.mdpi.com/1424-8220/17/7/1492.

[3] S. Bertuletti, F. Salis, A. Cereatti, L. Angelini, E. Buckley, K. Nair, C. Mazzà, and U. Della Croce, "Inter-leg distance measurement as a tool for accurate step counting in patients with multiple sclerosis", *IEEE Engineering in Medicine and Biology Magazine (under review)*, 2019.

[4] S. Bertuletti, A. Cereatti, and U. Della Croce, "Development of a novel wearable system for real-time measurement of the inter-foot distance during gait", *Gait & Posture*, vol. 57, pp. 6–7, 2017, SIAMOC, ISSN: 0966–6362. DOI: 10.1016/j.gaitpost.2017.07.054. [Online]. Available: http://www.sciencedirect.com/science/article/pii/S0966636217307658.

[5] S. Bertuletti, A. Cereatti, M. Caldara, and U. Della Croce, "A proximity sensor for the measurement of the inter-foot distance in static and dynamic tasks", *Gait & Posture*, vol. 49, S15, 2016, SIAMOC, ISSN: 0966–6362. DOI: 10.1016/j.gaitpost.2016.07.044. [Online]. Available: http://www.sciencedirect.com/science/article/pii/S0966636216301813.

[6] S. Bertuletti, A. Cereatti, M. Caldara, M. Galizzi, and U. Della Croce, "Indoor distance estimated from Bluetooth low energy signal strength: Comparison of regression models", in *Proceedings of IEEE Sensors Applications Symposium (SAS)*, Apr. 2016, pp. 1–5. DOI: 10.1109/SAS.2016.7479899.

[7] S. Bertuletti, U. Della Croce, and A. Cereatti, "A wearable prototype device for direct bilateral step detection by instrumenting a single foot", in *19th Proceedings of SIAMOC*, 2018.

[8] S. Bertuletti, A. Cereatti, and U. Della Croce, "Inter-foot distance measurement in healthy adults during gait using a wearable prototype device: Validation on straight walking and turning for different distance sensor locations", in *19th Proceedings of SIAMOC*, 2018.

[9] S. Bertuletti, A. Cereatti, and U. Della Croce, "A wearable system based on Time-of-Flight technology for direct derivation of step number and step width on healthy gait", in *Proceedings of GNB*, 2018.

[10] S. Bertuletti, A. Cereatti, and U. Della Croce, "Detection of the turn switch during alpine skiing using a novel wearable system: A preliminary investigation", in *18th Proceedings of SIAMOC*, 2017.

[11] S. Bertuletti, A. Cereatti, and U. Della Croce, "Measurement of the inter-foot distance using a Time-of-Flight proximity sensor: Preliminary evaluation during leg oscillation exercises", in *Proceedings of GNB*, 2016.

[12] S. Bertuletti, A. Cereatti, M. Caldara, M. Galizzi, D. Comotti, and U. Della Croce, "Fall detection localization using Bluetooth low energy devices: A preliminary investigation", in *16th Proceedings of SIAMOC*, 2015.

[13] S. Bertuletti, A. Cereatti, and U. Della Croce, "A wearable system for step width measurement and step detection based on Time-of-Flight technology: Preliminary validation on healthy subjects", in *Proceedings of 3-D Analysis of Human Movement*, 2018.

[14] S. Bertuletti, V. Camomilla, A. Cereatti, M. Caldara, M. Galizzi, and U. Della Croce, "Comparison of regression models for interdistance estimate between two BLE devices based on RSSI", in *Proceedings of 3-D Analysis of Human Movement*, 2016.

[15] A. Cereatti, S. Bertuletti, M. Caldara, and U. Della Croce, "Sistema per l'analisi dell'attività motoria di una persona e relativo metodo", pat. 102017000003986, 2017, Italy (pending).

[16] A. Cappozzo, U. Della Croce, A. Leardini, and L. Chiari, "Human movement analysis using stereophotogrammetry. Part 1: Theoretical background", *Gait & Posture*, vol. 21, no. 2, pp. 186–196, 2005, ISSN: 0966–6362. DOI: 10.1016/j.gaitpost.2004.01.010. [Online]. Available: http://www.sciencedirect.com/science/article/pii/S0966636204000256.

[17] C. Ekdahl, G. Jarnlo, and S. Andersson, "Standing balance in healthy subjects. Evaluation of a quantitative test battery on a force platform", *Scandinavian*, vol. 21, no. 4, pp. 187–195, 1989, ISSN: 0036–5505. [Online]. Available: http://europepmc.org/abstract/MED/2631193.

[18] B. Bilney, M. Morris, and K. Webster, "Concurrent related validity of the GAITRite® walkway system for quantification of the spatial and temporal parameters of gait", *Gait & Posture*, vol. 17, no. 1, pp. 68–74, 2003, ISSN: 0966–6362. DOI: 10.1016/S0966-6362(02)00053-X. [Online]. Available: http://www.sciencedirect.com/science/article/pii/S096663620200053X.

[19] L. Chiari, U. Della Croce, A. Leardini, and A. Cappozzo, "Human movement analysis using stereophotogrammetry: Part 2: Instrumental errors", *Gait & Posture*, vol. 21, no. 2, pp. 197–211, 2005, ISSN: 0966–6362. DOI: 10.1016/j.gaitpost.2004.04.004. [Online]. Available: http://www.sciencedirect.com/science/article/pii/S0966636204000682.

[20] S. C. Mukhopadhyay, "Wearable sensors for human activity monitoring: A review", *IEEE Sensors Journal*, vol. 15, no. 3, pp. 1321–1330, Mar. 2015, ISSN: 1530–437X. DOI: 10.1109/JSEN.2014.2370945.

[21] L. C. Benson, C. A. Clermont, E. Bošnjak, and R. Ferber, "The use of wearable devices for walking and running gait analysis outside of the lab: A systematic review", *Gait & Posture*, vol. 63, pp. 124–138, 2018, ISSN: 0966–6362. DOI: 10.1016/j.gaitpost.2018.04.047. [Online]. Available: http://www.sciencedirect.com/science/article/pii/S0966636218304715.

[22] P. Picerno, A. Cereatti, and A. Cappozzo, "Joint kinematics estimate using wearable inertial and magnetic sensing modules", *Gait & Posture*, vol. 28, no. 4, pp. 588–595, 2008, ISSN: 0966–6362. DOI: 10.1016/j.gaitpost.2008.04.003. [Online]. Available: http://www.sciencedirect.com/science/article/pii/S0966636208001008.

[23] T. Liu, Y. Inoue, and K. Shibata, "A wearable ground reaction force sensor system and its application to the measurement of extrinsic gait variability", *Sensors*, vol. 10, no. 11, pp. 10 240–10 255, 2010, ISSN: 1424–8220. DOI: 10.3390/s101110240. [Online]. Available: http://www.mdpi.com/1424-8220/10/11/10240.

[24] A. Rainoldi, G. Melchiorri, and I. Caruso, "A method for positioning electrodes during surface EMG recordings in lower limb muscles", *Journal of Neuroscience Methods*, vol. 134, no. 1, pp. 37–43, 2004, ISSN: 0165–

0270. DOI: 10.1016/j.jneumeth.2003.10.014. [Online]. Available: http://www.sciencedirect.com/science/article/pii/S0165027003003522.

[25] H. Liu, H. Darabi, P. Banerjee, and J. Liu, "Survey of wireless indoor positioning techniques and systems", *IEEE Transactions on Systems, Man, and Cybernetics, Part C (Applications and Reviews)*, vol. 37, no. 6, pp. 1067–1080, 2007, ISSN: 1094–6977. DOI: 10.1109/TSMCC.2007.905750.

[26] M. Iosa, P. Picerno, S. Paolucci, and G. Morone, "Wearable inertial sensors for human movement analysis", *Expert Review of Medical Devices*, vol. 13, no. 7, pp. 641–659, 2016, PMID: 27309490. DOI: 10.1080/17434440.2016.1198694.

[27] V. Camomilla, E. Bergamini, S. Fantozzi, and G. Vannozzi, "In-field use of wearable magneto-inertial sensors for sports performance evaluation", in *Proceedings of 33rd International Conference on Biomechanics in Sports*, 2015.

[28] @ONLINE. (2018). Xsens MVN animate, [Online]. Available: https://www.xsens.com/products/xsens-mvn-animate/.

[29] S. Ishimaru, K. Kunze, K. Kise, J. Weppner, A. Dengel, P. Lukowicz, and A. Bulling, "In the blink of an eye: Combining head motion and eye blink frequency for activity recognition with Google glass", in *Proceedings of 5th Augmented Human International Conference*, 2014, 15:1–15:4, ISBN: 978-1-4503-2761-9. DOI: 10.1145/2582051.2582066.

[30] H. Pirsiavash and D. Ramanan, "Detecting activities of daily living in first-person camera views", in *Proceedings of IEEE Conference on Computer Vision and Pattern Recognition*, Jun. 2012, pp. 2847–2854. DOI: 10.1109/CVPR.2012.6248010.

[31] D. Trojaniello, A. Cereatti, and U. Della Croce, "Foot clearance estimation during overground walking and vertical obstacle passing using shank-mounted MIMUs in healthy and pathological subjects", in *Proceedings of 37th Annual International Conference of the IEEE Engineering in Medicine and Biology Society (EMBC)*, Aug. 2015, pp. 5505–5508. DOI: 10.1109/EMBC.2015.7319638.

[32] D. Weenk, D. Roetenberg, B. J. F. van Beijnum, H. J. Hermens, and P. H. Veltink, "Ambulatory estimation of relative foot positions by fusing ultrasound and inertial sensor data", *IEEE Transactions on Neural Systems and Rehabilitation Engineering*, vol. 23, no. 5, pp. 817–826, Sep. 2015, ISSN: 1534–4320. DOI: 10.1109/TNSRE.2014.2357686.

[33] A. Arami, N. S. Raymond, and K. Aminian, "An accurate wearable foot clearance estimation system: Toward a real-time measurement system", *IEEE Sensors Journal*, vol. 17, no. 8, pp. 2542–2549, 2017, ISSN: 1530–437X. DOI: 10.1109/JSEN.2017.2665624.

[34] @ONLINE. (2018). Global Positioning System (GPS), [Online]. Available: https://www.gps.gov.

[35] S. Venkatraman, "Indoor positioning using pressure sensors", pat. US9234965B2, 2010.

[36] @ONLINE. (2018). Bluetooth, [Online]. Available: https://www.bluetooth.com/.

[37] V. Cantón Paterna, A. Calveras Augé, J. Paradells Aspas, and M. A. Pérez Bullones, "A Bluetooth low energy indoor positioning system with channel diversity, weighted trilateration and Kalman filtering", *Sensors*, vol. 17, no. 12, 2017, ISSN: 1424–8220. DOI: 10.3390/s17122927. [Online]. Available: http://www.mdpi.com/1424-8220/17/12/2927.

[38] D. Trojaniello, A. Cereatti, A. Bourke, K. Aminian, and U. Della Croce, "A wearable system for the measurement of the inter-foot distance during gait", in *Proceedings of 20th IMEKO TC4 International Symposium*, Sep. 2014, pp. 765–769.

[39] P. D. Duong and Y. S. Suh, "Foot pose estimation using an inertial sensor unit and two distance sensors", *Sensors*, vol. 15, no. 7, pp. 15 888–15 902, 2015, ISSN: 1424–8220. DOI: 10.3390/s150715888. [Online]. Available: http://www.mdpi.com/1424-8220/15/7/15888.

[40] STMicroelectronics, *STM32L433xx*, 2018. [Online]. Available: https://www.st.com/resource/en/datasheet/stm32l433cc.pdf.

[41] Kyocera, *PBRC8*, 2018. [Online]. Available: https://media.digikey.com/pdf/Data%20Sheets/Optrex%20PDFs/Cermic-Res_Cat.pdf.

[42] Abracon, *ABS09*, 2018. [Online]. Available: https://abracon.com/Resonators/ABS09.pdf.

[43] STMicroelectronics, *LSM6DSM*, 2017. [Online]. Available: https://www.st.com/resource/en/datasheet/lsm6dsm.pdf.

[44] STMicroelectronics, *LSM303D*, 2013. [Online]. Available: https://www.st.com/resource/en/datasheet/lsm303d.pdf.

[45] Cypress, *S25FL127S*, 2017. [Online]. Available: http://www.cypress.com/file/177961/download.

[46] STMicroelectronics, *SPBT2632C2A*, 2017. [Online]. Available: https://www.st.com/resource/en/datasheet/spbt2632c2a.pdf.

[47] STMicroelectronics, *BlueNRG-MS*, 2017. [Online]. Available: https://www.st.com/resource/en/datasheet/bluenrg-ms.pdf.

[48] Microchip, *MCP73831T*, 2017. [Online]. Available: http://ww1.microchip.com/downloads/en/DeviceDoc/20001984g.pdf.

[49] Maxim Integrated, *MAX17048*, 2016. [Online]. Available: https://datasheets.maximintegrated.com/en/ds/MAX17048-MAX17049.pdf.

[50] Texas Instruments, *TPS62740*, 2014. [Online]. Available: http://www.ti.com/lit/ds/symlink/tps62740.pdf.

[51] STMicroelectronics, *STM6600*, 2014. [Online]. Available: https://www.st.com/resource/en/datasheet/stm6600.pdf.

[52] STMicroelectronics, *VL6180X-SATEL*, 2015. [Online]. Available: https://www.st.com/resource/en/data_brief/vl6180x-satel.pdf.

[53] STMicroelectronics, *VL6180X*, 2016. [Online]. Available: https://www.st.com/resource/en/datasheet/vl6180x.pdf.

[54] STMicroelectronics, *VL53L1X*, 2018. [Online]. Available: https://www.st.com/resource/en/datasheet/vl53l1x.pdf.

[55] B. Maki, "Gait changes in older adults: Predictors of falls or indicators of fear?", *Journal of the American Geriatrics Society*, vol. 45, no. 3, 2015. DOI: 10.1111/j.1532-5415.1997.tb00946.x.

[56] T. M. Owings and M. Grabiner, "Variability of step kinematics in young and older adults", *Gait & Posture*, vol. 20, no. 1, pp. 26–29, 2004. DOI: 10.1016/S0966-6362(03)00088-2.

[57] J. C. Menant, J. R. Steele, H. B. Menz, B. J. Munro, and S. R. Lord, "Effects of walking surfaces and footwear on temporo-spatial gait parameters in young and older people", *Gait & Posture*, vol. 29, no. 3, pp. 392–397, 2009. DOI: 10.1016/j.gaitpost.2008.10.057.

[58] H. Stolze, J. Kuhtz-Buschbeck, C. Mondwurf, A. Boczek-Funcke, K. Jöhnk, G. Deuschl, and M. Illert, "Gait analysis during treadmill and overground locomotion in children and adults", *Electroencephalography and Clinical Neurophysiology/Electromyography and Motor Control*, vol. 105, no. 6, pp. 490–497, 1997, ISSN: 0924–980X. DOI: 10.1016/S0924-980X(97)00055-6. [Online]. Available: http://www.sciencedirect.com/science/article/pii/S0924980X97000556.

[59] C.-S. Ho, C.-J. Lin, Y.-L. Chou, F.-C. Su, and S.-C. Lin, "Foot progression angle and ankle joint complex in preschool children", *Clinical Biomechanics*, vol. 15, no. 4, pp. 271–277, 2000. DOI: 10.1016/S0268-0033(99)00068-6.

[60] E. Lachat, H. Macher, and M.-A. Mittet, "First experiences with Kinect V2 sensor for close range 3D modelling", in *Proceedings of International Archives of the Photogrammetry, Remote Sensing and Spatial Information Sciences*, vol. XL-5/W4, Feb. 2015.

[61] D. Trojaniello, A. Cereatti, E. Pelosin, L. Avanzino, A. Mirelman, J. Hausdorff, and U. Della Croce, "Estimation of step-by-step spatio-temporal parameters of normal and impaired gait using shank-mounted magneto-inertial sensors: Application to elderly, hemiparetic, parkinsonian and choreic gait", *Journal of NeuroEngineering and Rehabilitation*, vol. 11, 2014. DOI: 10.1186/1743-0003-11-152.

[62] W. Tao, T. Liu, R. Zheng, and H. Feng, "Gait analysis using wearable sensors", *Sensors*, vol. 12, no. 2, pp. 2255–2283, 2012, ISSN: 1424–8220. DOI: 10.3390/s120202255. [Online]. Available: http://www.mdpi.com/1424-8220/12/2/2255.

[63] G. Ciuti, L. Ricotti, A. Menciassi, and P. Dario, "MEMS sensor technologies for human centred applications in healthcare, physical activities, safety and environmental sensing: A review on research activities in Italy", *Sensors*, vol. 15, no. 3, pp. 6441–6468, 2015, ISSN: 1424–8220. DOI: 10.3390/s150306441. [Online]. Available: http://www.mdpi.com/1424-8220/15/3/6441.

[64] A. Muro-de-la-Herran, B. Garcia-Zapirain, and A. Mendez-Zorrilla, "Gait analysis methods: An overview of wearable and non-wearable systems, highlighting clinical applications", *Sensors*, vol. 14, no. 2, pp. 3362–3394, 2014, ISSN: 1424–8220. DOI: 10.3390/s140203362. [Online]. Available: http://www.mdpi.com/1424-8220/14/2/3362.

[65] J. R. Rebula, L. V. Ojeda, P. G. Adamczyk, and A. D. Kuo, "Measurement of foot placement and its variability with inertial sensors", *Gait & Posture*, vol. 38, no. 4, pp. 974–980, 2013, ISSN: 0966–6362. DOI: 10.1016/j.gaitpost.2013.05.012. [Online]. Available: http://www.sciencedirect.com/science/article/pii/S0966636213002427.

[66] O. Beauchet, G. Allali, C. Annweiler, S. Bridenbaugh, F. Assal, R. Kressig, and F. Herrmann, "Gait variability among healthy adults: Low and high stride-to-stride variability are both a reflection of gait stability", *Gerontology*, 2009. DOI: 10.1159/000235905.

[67] M. Hansard, S. Lee, O. Choi, and R. Horaud, *Time of Flight Cameras: Principles, Methods, and Applications*, Springer, Ed. 2013. DOI: 10.1007/978-1-4471-4658-2.

[68] D. Trojaniello, A. Cereatti, and U. Della Croce, "Accuracy, sensitivity and robustness of five different methods for the estimation of gait temporal parameters using a single inertial sensor mounted on the lower trunk", *Gait & Posture*, vol. 40, no. 4, pp. 487–492, 2014, ISSN: 0966–6362. DOI: 10.1016/j.gaitpost.2014.07.007. [Online]. Available: http://www.sciencedirect.com/science/article/pii/S0966636214006432.

[69] C.-C. Yang and Y.-L. Hsu, "A review of accelerometry-based wearable motion detectors for physical activity monitoring", *Sensors*, vol. 10, no. 8, pp. 7772–7788, 2010, ISSN: 1424–8220. DOI: 10.3390/s100807772. [Online]. Available: http://www.mdpi.com/1424-8220/10/8/7772.

[70] S. E. R. Lim, K. Ibrahim, A. A. Sayer, and H. C. Roberts, "Assessment of physical activity of hospitalised older adults: A systematic review", *The Journal of Nutrition, Health & Aging*, vol. 22, no. 3, pp. 377–386, 2018, ISSN: 1760–4788. DOI: 10.1007/s12603-017-0931-2.

[71] D. T.-P. Fong and Y.-Y. Chan, "The use of wearable inertial motion sensors in human lower limb biomechanics studies: A systematic review", *Sensors*, vol. 10, no. 12, pp. 11 556–11 565, 2010, ISSN: 1424–8220. DOI: 10.3390/s101211556. [Online]. Available: http://www.mdpi.com/1424-8220/10/12/11556.

[72] M. Bertoli, A. Cereatti, D. Trojaniello, L. Avanzino, E. Pelosin, S. Del Din, L. Rochester, P. Ginis, E. M. J. Bekkers, A. Mirelman, J. M. Hausdorff, and U. Della Croce, "Estimation of spatio-temporal parameters of gait from magneto-inertial measurement units: Multicenter validation among parkinson, mildly cognitively impaired and healthy older adults", *BioMedical Engineering OnLine*, vol. 17, no. 1, p. 58, 2018, ISSN: 1475-925X. DOI: 10.1186/s12938-018-0488-2. [Online]. Available: https://doi.org/10.1186/s12938-018-0488-2.

[73] R. Caldas, M. Mundt, W. Potthast, F. B. de Lima Neto, and B. Markert, "A systematic review of gait analysis methods based on inertial sensors and adaptive algorithms", *Gait & Posture*, vol. 57, pp. 204–210, 2017, ISSN: 0966–6362. DOI: 10.1016/j.gaitpost.2017.06.019. [Online]. Available: http://www.sciencedirect.com/science/article/pii/S0966636217302424.

[74] F. A. Storm, C. J. Buckley, and C. Mazzà, "Gait event detection in laboratory and real life settings: Accuracy of ankle and waist sensor based methods", *Gait & Posture*, vol. 50, pp. 42–46, 2016, ISSN: 0966–6362. DOI: 10.1016/j.gaitpost.2016.08.012. [Online]. Available: http://www.sciencedirect.com/science/article/pii/S096663621630488X.

[75] K. Aminian, B. Najafi, C. Büla, P.-F. Leyvraz, and P. Robert, "Spatio-temporal parameters of gait measured by an ambulatory system using miniature gyroscopes", *Journal of Biomechanics*, vol. 35, no. 5, pp. 689–699, 2002, ISSN: 0021–9290. DOI: 10.1016/S0021-9290(02)00008-8. [Online]. Available: http://www.sciencedirect.com/science/article/pii/S0021929002000088.

[76] M. Pham, M. Elshehabi, L. Haertner, S. Del Din, K. Srulijes, T. Heger, M. Synofzik, M. Hobert, G. Faber, C. Hansen, D. Salkovic, J. Ferreira, D. Berg, Sanchez-Ferro, J. van Dieën, C. Becker, L. Rochester, G. Schmidt, and W. Maetzler, "Validation of a step detection algorithm during straight walking and turning in patients with Parkinson's disease and older adults using an inertial measurement unit at the lower back", *Frontiers in Neurology*, vol. 8, p. 457, 2017. DOI: 10.3389%2Ffneur.2017.00457.

[77] R. W. Motl, E. M. Snook, and S. Agiovlasitis, "Does an accelerometer accurately measure steps taken under controlled conditions in adults with mild multiple sclerosis?", *Disability and Health Journal*, vol. 4, no. 1, pp. 52–57, 2011, ISSN: 1936-6574. DOI: https://doi.org/10.1016/j.dhjo.2010.02.003. [Online]. Available: http://www.sciencedirect.com/science/article/pii/S1936657410000294.

[78] B. M. Sandroff, R. W. Motl, L. A. Pilutti, Y. C. Learmonth, I. Ensari, D. Dlugonski, R. E. Klaren, S. Balantrapu, and B. J. Riskin, "Accuracy of stepwatch™ and actigraph accelerometers for measuring steps taken among persons with multiple sclerosis", *PLOS ONE*, vol. 9, no. 4, pp. 1–7, Apr. 2014. DOI: 10.1371/journal.pone.0093511. [Online]. Available: https://doi.org/10.1371/journal.pone.0093511.

[79] D. Trojaniello, A. Ravaschio, J. M. Hausdorff, and A. Cereatti, "Comparative assessment of different methods for the estimation of gait temporal parameters using a single inertial sensor: Application to elderly, post-stroke, Parkinson's disease and Huntington's disease subjects", *Gait & Posture*, vol. 42, no. 3, pp. 310–316, 2015, ISSN: 0966–6362. DOI: 10.1016/j.gaitpost.2015.06.008. [Online]. Available: http://www.sciencedirect.com/science/article/pii/S096663621500510X.

[80] M. Simic, T. Wrigley, R. Hinman, M. Hunt, and K. Bennell, "Altering foot progression angle in people with medial knee osteoarthritis: The effects of varying toe-in and toe-out angles are mediated by pain and malalignment", *Osteoarthritis and Cartilage*, vol. 21, no. 9, pp. 1272–1280, 2013, Pain in Osteoarthritis, ISSN: 1063–4584. DOI: 10.1016/j.joca.2013.06.001. [Online]. Available: http://www.sciencedirect.com/science/article/pii/S1063458413008376.

[81] W. I. McDonald, A. Compston, G. Edan, D. Goodkin, H.-P. Hartung, F. D. Lublin, H. F. McFarland, D. W. Paty, C. H. Polman, S. C. Reingold, M. Sandberg-Wollheim, W. Sibley, A. Thompson, S. Van Den Noort, B. Y. Weinshenker, and J. S. Wolinsky, "Recommended diagnostic criteria for multiple sclerosis: Guidelines from the international panel on the diagnosis of multiple sclerosis", *Annals of Neurology*, vol. 50, no. 1, pp. 121–127, DOI: 10.1002/ana.1032. eprint: https://onlinelibrary.wiley.com/doi/pdf/10.1002/ana.1032. [Online]. Available: https://onlinelibrary.wiley.com/doi/abs/10.1002/ana.1032.

[82] C. H. Polman, S. C. Reingold, G. Edan, M. Filippi, H.-P. Hartung, L. Kappos, F. D. Lublin, L. M. Metz, H. F. McFarland, P. W. O'Connor, M. Sandberg-Wollheim, A. J. Thompson, B. G. Weinshenker, and J. S. Wolinsky, "Diagnostic criteria for multiple sclerosis: 2005 revisions to the "McDonald criteria"", *Annals of Neurology*, vol. 58, no. 6, pp. 840–846, DOI: 10.1002/ana.20703. eprint: https://onlinelibrary.wiley.com/doi/pdf/10.1002/ana.20703. [Online]. Available: https://onlinelibrary.wiley.com/doi/abs/10.1002/ana.20703.

[83] C. H. Polman, S. C. Reingold, B. Banwell, M. Clanet, J. A. Cohen, M. Filippi, K. Fujihara, E. Havrdova, M. Hutchinson, L. Kappos, F. D. Lublin, X. Montalban, P. O'Connor, M. Sandberg-Wollheim, A. J. Thompson, E. Waubant, B. Weinshenker, and J. S. Wolinsky, "Diagnostic criteria for multiple sclerosis: 2010 revisions to the McDonald criteria", *Annals of Neurology*, vol. 69, no. 2, pp. 292–302, DOI: 10.1002/ana.22366. eprint: https://onlinelibrary.wiley.com/doi/pdf/10.1002/ana.22366. [Online]. Available: https://onlinelibrary.wiley.com/doi/abs/10.1002/ana.22366.

[84] A. J. Thompson, B. L. Banwell, F. Barkhof, *et al.*, "Diagnosis of multiple sclerosis: 2017 revisions of the McDonald criteria", *The Lancet Neurology*, vol. 17, no. 2, pp. 162–173, 2018, ISSN: 1474–4422. DOI: 10.1016/S1474-4422(17)30470-2. [Online]. Available: http://www.sciencedirect.com/science/article/pii/S1474442217304702.

[85] R. W. Motl, E. M. Snook, and R. T. Schapiro, "Symptoms and physical activity behavior in individuals with multiple sclerosis", *Research in Nursing & Health*, vol. 31, no. 5, pp. 466–475, DOI: 10.1002/nur.20274. eprint: https://onlinelibrary.wiley.com/doi/pdf/10.1002/nur.20274. [Online]. Available: https://onlinelibrary.wiley.com/doi/abs/10.1002/nur.20274.

[86] A. J. Thompson, S. E. Baranzini, J. Geurts, B. Hemmer, and O. Ciccarelli, "Multiple sclerosis", *The Lancet*, vol. 391, no. 10130, pp. 1622–1636, 2018, ISSN: 0140–6736. DOI: 10.1016/S0140-6736(18)30481-1. [Online]. Available: http://www.sciencedirect.com/science/article/pii/S0140673618304811.

[87] B. G. Weinshenker, B. Bass, G. P. A. Rice, J. Noseworthy, W. Carriere, J. Baskerville, and G. C. Ebers, "The natural history of multiple sclerosis: A geographically based study: 2 predictive value of the early clinical course", *Brain*, vol. 112, no. 6, pp. 1419–1428, 1989. DOI: 10.1093/brain/112.6.1419. eprint: /oup/backfile/content_public/journal/brain/112/6/10.1093/brain/112.6.1419/2/112-6-1419.pdf. [Online]. Available: http://dx.doi.org/10.1093/brain/112.6.1419.

[88] N. G. LaRocca, "Impact of walking impairment in multiple sclerosis", *The Patient: Patient-Centered Outcomes Research*, vol. 4, no. 3, pp. 189–201, 2011, ISSN: 1178–1661. DOI: 10.2165/11591150-000000000-00000.

[89] J. F. Kurtzke, "Rating neurologic impairment in multiple sclerosis", *Neurology*, vol. 33, no. 11, pp. 1444–1444, 1983, ISSN: 0028-3878. DOI: 10.1212/WNL.33.11.1444. eprint: http://n.neurology.org/content/33/11/1444.full.pdf. [Online]. Available: http://n.neurology.org/content/33/11/1444.

[90] M. H. Pham, M. Elshehabi, L. Haertner, S. Del Din, K. Srulijes, T. Heger, M. Synofzik, M. A. Hobert, G. S. Faber, C. Hansen, D. Salkovic, J. J. Ferreira, D. Berg, l. Sanchez-Ferro, J. H. van Dieën, C. Becker, L. Rochester, G. Schmidt, and W. Maetzler, "Validation of a step detection algorithm during straight walking and turning in patients with parkinson's disease and older adults using an inertial measurement unit at the lower back", *Frontiers in Neurology*, vol. 8, p. 457, 2017, ISSN: 1664-2295. DOI: 10.3389/fneur.2017.00457. [Online]. Available: https://www.frontiersin.org/article/10.3389/fneur.2017.00457.

[91] R. C. Foster, L. M. Lanningham-Foster, C. Manohar, S. K. McCrady, L. J. Nysse, K. R. Kaufman, D. J. Padgett, and J. A. Levine, "Precision and accuracy of an ankle-worn accelerometer-based pedometer in step counting and energy expenditure", *Preventive Medicine*, vol. 41, no. 3, pp. 778–783,

2005, ISSN: 0091–7435. DOI: 10.1016/j.ypmed.2005.07.006. [Online]. Available: http://www.sciencedirect.com/science/article/pii/S009174350500109X.

[92] H.-S. An, G. C. Jones, S.-K. Kang, G. J. Welk, and J.-M. Lee, "How valid are wearable physical activity trackers for measuring steps?", *European Journal of Sport Science*, vol. 17, no. 3, pp. 360–368, 2017, PMID: 27912681. DOI: 10.1080/17461391.2016.1255261.

[93] F. A. Storm, B. W. Heller, and C. Mazzà, "Step detection and activity recognition accuracy of seven physical activity monitors", *PLOS ONE*, vol. 10, no. 3, pp. 1–13, Mar. 2015. DOI: 10.1371/journal.pone.0118723. [Online]. Available: https://doi.org/10.1371/journal.pone.0118723.

[94] C. G. Ryan, P. M. Grant, W. W. Tigbe, and M. H. Granat, "The validity and reliability of a novel activity monitor as a measure of walking", *British Journal of Sports Medicine*, vol. 40, no. 9, pp. 779–784, 2006, ISSN: 0306–3674. DOI: 10.1136/bjsm.2006.027276. eprint: https://bjsm.bmj.com/content/40/9/779.full.pdf. [Online]. Available: https://bjsm.bmj.com/content/40/9/779.

[95] M. Karabulut, S. E. Crouter, and D. R. Bassett, "Comparison of two waist-mounted and two ankle-mounted electronic pedometers", *European Journal of Applied Physiology*, vol. 96, no. 3, pp. 334–335, 2006, ISSN: 1439–6327. DOI: 10.1007/s00421-005-0120-6.

[96] P. Grant, P. Dall, S. Mitchell, and M. Granat, "Activity-monitor accuracy in measuring step number and cadence in community-dwelling older adults", *Journal of Aging and Physical Activity*, vol. 16, no. 2, pp. 201–214, 2008.

[97] B. M. Sandroff, R. W. Motl, L. A. Pilutti, Y. C. Learmonth, I. Ensari, D. Dlugonski, R. E. Klaren, S. Balantrapu, and B. J. Riskin, "Accuracy of StepWatch™ and ActiGraph accelerometers for measuring steps taken among persons with multiple sclerosis", *PLOS ONE*, vol. 9, no. 4, pp. 1–7, Apr. 2014. DOI: 10.1371/journal.pone.0093511. [Online]. Available: https://doi.org/10.1371/journal.pone.0093511.

[98] F. A. Storm, K. P. S. Nair, A. J. Clarke, J. M. Van der Meulen, and C. Mazzà, "Free-living and laboratory gait characteristics in patients with multiple sclerosis", *PLOS ONE*, vol. 13, no. 5, pp. 1–15, May 2018. DOI: 10.1371/journal.pone.0196463. [Online]. Available: https://doi.org/10.1371/journal.pone.0196463.

[99] A. Köse, A. Cereatti, and U. Della Croce, "Bilateral step length estimation using a single inertial measurement unit attached to the pelvis", *Journal of NeuroEngineering and Rehabilitation*, vol. 9, no. 1, p. 9, 2012, ISSN: 1743–0003. DOI: 10.1186/1743-0003-9-9. [Online]. Available: 10.1186/1743-0003-9-9.

[100] B. Hofmann-Wellenhof, H. Lichtenegger, and J. Collins, *Global Positioning System: theory and practice*, SpringerVerlag, Ed. 1997.

[101] H. Liu, H. Darabi, P. Banerjee, and J. Liu, "Survey of wireless indoor positioning techniques and systems", *IEEE Transactions on Systems, Man, and Cybernetics, Part C (Applications and Reviews)*, vol. 37, no. 6, pp. 1067–1080, 2007, ISSN: 1094–6977. DOI: 10.1109/TSMCC.2007.905750.

[102] D. Zhang, F. Xia, Z. Yang, L. Yao, and W. Zhao, "Localization technologies for indoor human tracking", in *Proceedings of 5th International Conference on Future Information Technology*, 2010, pp. 1–6. DOI: 10.1109/FUTURETECH.2010.5482731.

[103] @ONLINE. (2018). Bluetooth low energy, [Online]. Available: https://en.wikipedia.org/wiki/Bluetooth_low_energy.

[104] S. Zhou and J. K. Pollard, "Position measurement using Bluetooth", *IEEE Transactions on Consumer Electronics*, vol. 52, no. 2, pp. 555–558, 2006, ISSN: 0098–3063. DOI: 10.1109/TCE.2006.1649679.

[105] E.-e.-l. Lau, B.-g. Lee, S.-c. Lee, and W.-y. Chung, "Enhanced RSSI-based high accuracy real-time user location tracking system for indoor and outdoor environments", *International Journal on Smart Sensing and Intelligent Systems*, vol. 1, no. 2, pp. 534–548, 2008. DOI: 10.1.1.665.4875.

[106] M. E. Rida, F. Liu, Y. Jadi, A. A. A. Algawhari, and A. Askourih, "Indoor location position based on Bluetooth signal strength", in *Proceedings of 2nd International Conference on Information Science and Control Engineering*, 2015, pp. 769–773. DOI: 10.1109/ICISCE.2015.177.

[107] L. Pei, R. Chen, J. Liu, T. Tenhunen, H. Kuusniemi, and Y. Chen, "Inquiry-based Bluetooth indoor positioning via RSSI probability distributions", in *Proceedings of 2nd International Conference on Advances in Satellite and Space Communications*, 2010, pp. 151–156. DOI: 10.1109/SPACOMM.2010.18.

[108] P. Vorst, J. Sommer, C. Hoene, P. Schneider, C. Weiss, T. Schairer, W. Rosenstiel, A. Zell, and G. Carle, "Indoor positioning via three different RF technologies", in *Proceedings of 4th European Workshop on RFID Systems and Technologies*, 2008, pp. 1–10.

[109] K. Heurtefeux and F. Valois, "Is RSSI a good choice for localization in wireless sensor network?", in *Proceedings of IEEE 26th International Conference on Advanced Information Networking and Applications*, 2012, pp. 732–739. DOI: 10.1109/AINA.2012.19.

[110] PulseElectronics, *W3008C*, 2010. [Online]. Available: http://productfinder.pulseeng.com/product/W3008C.

[111] A. N. Raghavan, H. Ananthapadmanaban, M. S. Sivamurugan, and B. Ravindran, "Accurate mobile robot localization in indoor environments using Bluetooth", in *Proceedings of IEEE International Conference on Robotics and Automation*, 2010, pp. 4391–4396. DOI: 10.1109/ROBOT.2010.5509232.

[112] M. Rodriguez, J. P. Pece, and C. J. Escudero, "In-building location using Bluetooth", in *Proceedings of International Workshop on Wireless Ad Hoc Networks*, 2005.

[113] R. Faragher and R. Harle, "An analysis of the accuracy of Bluetooth low energy for indoor positioning applications", in *Proceedings of 27th International Technical Meeting of The Satellite Division of the Institute of Navigation (ION GNSS+ 2014)*, Sep. 2014.

[114] B. Wang, S. Zhou, W. Liu, and Y. Mo, "Indoor localization based on curve fitting and location search using received signal strength", *IEEE Transactions on Industrial Electronics*, vol. 62, no. 1, pp. 572–582, 2015, ISSN: 0278–0046. DOI: 10.1109/TIE.2014.2327595.

[115] G. Zanca, F. Zorzi, A. Zanella, and M. Zorzi, "Experimental comparison of RSSI-based localization algorithms for indoor wireless sensor networks", in *Proceedings of Workshop on Real-world Wireless Sensor Networks*, ser. REALWSN '08, Glasgow, Scotland: ACM, 2008, pp. 1–5, ISBN: 978-1-60558-123-1. DOI: 10.1145/1435473.1435475. [Online]. Available: http://doi.acm.org/10.1145/1435473.1435475.

[116] P. K. Yoon, S. Zihajehzadeh, B. Kang, and E. J. Park, "Adaptive Kalman filter for indoor localization using Bluetooth low energy and inertial measurement unit", in *Proceedings of 37th Annual International Conference of the IEEE Engineering in Medicine and Biology Society (EMBC)*, 2015, pp. 825–828. DOI: 10.1109/EMBC.2015.7318489.

[117] E. Müller and H. Schwameder, "Biomechanical aspects of new techniques in alpine skiing and ski-jumping", *Journal of Sports Sciences*, vol. 21, no. 9, pp. 679–692, 2003, PMID: 14579866. DOI: 10.1080/0264041031000140284.

[118] B. Fasel, “Drift reduction for inertial sensor based orientation and position estimation in the presence of high dynamic variability during competitive skiing and daily-life walking”, PhD, Ecole Polytechnique federale de Lausanne, 2017.

[119] G. Yu, Y. J. Jang, J. Kim, J. H. Kim, H. Y. Kim, K. Kim, and S. B. Panday, “Potential of IMU sensors in performance analysis of professional alpine skiers”, *Sensors*, vol. 16, no. 4, 2016, ISSN: 1424–8220. DOI: 10.3390/s16040463. [Online]. Available: http://www.mdpi.com/1424-8220/16/4/463.

[120] B. Fasel, C. Praz, B. Kayser, and K. Aminian, “Measuring spatio-temporal parameters of uphill ski-mountaineering with ski-fixed inertial sensors”, *Journal of Biomechanics*, vol. 49, no. 13, pp. 3052–3055, 2016, ISSN: 0021–9290. DOI: 10.1016/j.jbiomech.2016.06.017. [Online]. Available: http://www.sciencedirect.com/science/article/pii/S0021929016306893.